An Analytic Model to Predict Detection Threshold and Performance Data for Misconvergence on a Shadow-Mask CRT

by

Carita Allene DeVilbiss

Dissertation submitted to the Faculty of the
Virginia Polytechnic Institute and State University
in partial fulfillment of the requirements for the degree of

DOCTOR OF PHILOSOPHY

in

Industrial Engineering and Operations Research

APPROVED:

H. L. Snyder, Co-chairman

R. J. Beaton, Co-chairman

G. J. Buhyoff

J. G. Casali

P. T. Kemmerling, Jr.

April, 1990

Blacksburg, Virginia

(ABSTRACT)

An Analytic Model to Predict Detection Threshold and Performance Data for Misconvergence on a Shadow-Mask CRT

by

Carita Allene DeVilbiss

This research was conducted to achieve four objectives. The first objective was to develop an analytic model to predict the expected luminance distribution through the shadow-mask structure on a color CRT display system. The model incorporates functions to describe the unique features of a color CRT, that is, the discrete sampling imposed by the shadow-mask/phosphor-dot arrangement as well as the electron beam phase relationships. The model also includes a flexible beam profile which allows the user to specify the desired shape of the beam profile, that is, whether the profile is described with a Gaussian, leptokurtic, or platykurtic distribution. This objective was fully satisfied with a computer program written in Lightspeed C which runs efficiently on Macintosh computers.

The second objective was to determine detection thresholds for various levels of misconvergence of the three electron guns. When the three guns are properly registered, the luminance profiles converge and one perceives a color combination rather than the separate red, green, and blue luminances. Misconvergence is perceived by a change in the overall color or by color fringes, for example, a red edge to a yellow line. Past research has shown that threshold detection of misconvergence occurs when the primary beams are misconverged by 1 to 2 visual arcminutes of separation. This finding was replicated in this research for the two-color beam combinations which have previously been investigated, as well as for a white pixel, which involves all three guns.

The third objective was to demonstrate the effect of misconvergence on the performance of a visual task and on subjective estimates of image quality. While subjective quality and threshold detection have previously been investigated for some color combinations, the three tasks (i.e., threshold detection, visual task performance, and subjective estimates) have not been systematically combined within the same data set for a variety of misconvergence conditions. This research provides such a composite data set. The subjective quality estimates were significantly correlated with the threshold detection data. In other words, as misconvergence of the display image increased, the probability of detection of misconvergence increased and the subjective quality rating decreased. However, the selected visual task (a short reading task with average reading time of 6.5 s) was not significantly affected by very large levels of misconvergence. Rather than conclude that the levels of misconvergence used in this research do not affect reading task performance, a more comprehensive visual task (e.g., a longer editing task, a random search task, or a map reading task) should be evaluated.

The final objective was to evaluate the ability of selected image quality metrics which are computed from the model to predict threshold detection, subjective quality ratings, or visual task performance. The three metrics computed in this model (MTF Area, MTFA, and SQRI) are all based upon the modulation transfer function (MTF) of the display. These three computed metrics were for all practical purposes constant across the range of misconvergence. While this result was unexpected, it does suggest (1) that a model based only on luminance may be deficient because of the omission of chromaticity, and (2) that MTF-based metrics may not be an appropriate representation because misconvergence does not change the display's ability to transmit information, but is a phase shift along the shadow mask.

As summarized, this research successfully met three of the stated objectives. Further, it points toward future research opportunities to further this type of modelling effort and to successfully develop image quality metrics for color displays.

ACKNOWLEDGEMENTS

This research would not have happened without the support of the United States Air Force Humans Systems Division which provided the time and resources for me to pursue this academic endeavor. Within that organization, I am deeply indebted to my supervisor and friend, Colonel Terry A. Benline, for his faith, encouragement, and leadership in pointing out this opportunity and helping make it a reality. I am also grateful to Dr. Billy Welch, for his personal support and encouragement during my time at Virginia Tech. Additionally, I wish to thank Lt. Col. Ron Hill and Mrs. Sue Douthit for being my tangible link to the Air Force during my long-term full-time training assignment.

Further, this research could not have been conducted without the support of the Controls and Displays Laboratory, directed by Dr. Harry L. Snyder, which supported this work with office space, equipment, and technical assistance. Special thanks to Willard W. Farley who patiently invested time and energy in creating the misconvergence system which was the key to this experiment. As my advisor, I am deeply indebted to Dr. Snyder for his superb professional guidance and personal encouragement which helped make this dissertation a reality. To Dr. Robert Beaton I owe a debt of gratitude for the support and guidance he willingly provided and for the hours he invested in generating the computer code which made the model a reality.

My special thanks go to Dr. Rome Walker and his staff who patiently provided information, guidance, and counsel during the most difficult time. Without his stable support, I would have lost sight of the "big picture" and only focused on obstacles.

Last, but not least, I want to thank my mother, Virginia Domingue Tracy, for giving me a positive attitude and a strong belief system, and my sister, Pat Delahoussaye, for being a strong pillar, on which I lean often, and for reading and editing this dissertation during her vacation. Most of all, I would like to thank my daughters, Terri Michele King and Cindy Rene Glynn, for providing loving support and a stable base to my life.

TABLE OF CONTENTS

LIST OF FIGURES

LIST OF TABLES

INTRODUCTION

Technological advances in the area of electronic information displays have resulted in color displays being widely available and used routinely. Color displays can be found in almost any setting, from the normal office environment to process control systems, color graphic displays for design, medical imaging, command-control-communications systems, and commercial and military airplane cockpits. Additionally, the performance characteristics of color electronic displays may soon rival those of monochrome displays in areas such as cost, addressable resolution, and "crisp" readability, thereby further extending their usage. Distinct advantages are cited for using color in display design, such as: (1) aesthetic benefits of color, supported by the general preference for color over monochrome presentations, (2) potential for increasing information coding capability and flexibility, (3) potential for reducing visual search time on complex displays, and (4) advantages derived from the use of color contrast to increase symbol visibility and reduce display luminance requirements (Silverstein, 1987).

The increased use of color displays also highlights some major disadvantages inherent to color display systems. In a review of the available literature on color displays, Hale and Billmayer (1988) listed the following disadvantages: (1) The improper use of colors can lead to the design of a display screen which contains too many colors or irrelevant colors. Such a display will be detrimental rather than helpful to the user of the system. (2) Aesthetic overindulgence (i.e., when aesthetics are preferred over useful performance data) should be avoided in the design of any system. (3) Detrimental perceptual phenomena (e.g., peripheral color vision, chromatic aberration, color stereoscopy) can interfere with predicted color perception. We may be able to define precisely a color in the physical sense, but the perceptual response to that color depends on the viewing conditions and other visual stimuli in the field of

view (Walraven, 1984, p. 13.8). (4) Misconvergence of the primary colors in a shadow-mask display is one of its disadvantages relative to monochrome displays.

The effective use of color requires a detailed understanding of how both the human user and the electronic display system process color information. While the ramifications of using color systems are not completely understood, the number of color display devices in use today continues to escalate. Thus, the increasing usage of color displays intensifies the need to investigate their advantages and disadvantages.

Color CRTs

Many available display technologies are capable of producing color images. Some technologies use discrete color emitting or reflecting elements to achieve full-color capability, e.g., the liquid crystal display (LCD), the plasma display, and the vacuum fluorescent display. The color cathode ray tube (CRT) technology is an extension of the monochrome CRT, with the color CRT devices typically using three electron guns rather than one. Due to its high reliability and low cost, the color CRT is used far more than the other color display technologies. Therefore, the shadow-mask CRT is the focus of this research.

The design alternatives for color CRT displays can be categorized into four basic configurations (Figure 1). Each uses a specific geometric arrangement (dots, stripes, or layers) for the deposition of red, blue, and green phosphor on the screen. An internal mask structure, which lies behind the phosphor layer, directs the energy from the electron gun to a given color phosphor. The three electron guns for the red, green, and blue primary colors are arranged either in a delta (or triangular) fashion, in-line with each other, or combined as a single in-line unit. The most common arrangement is the delta-gun/delta-mask (or shadow-mask) color CRT. This configuration uses a triangular arrangement for the electron guns with small holes (apertures) in the mask structure in front of a screen with red, green, and blue phosphor dots.

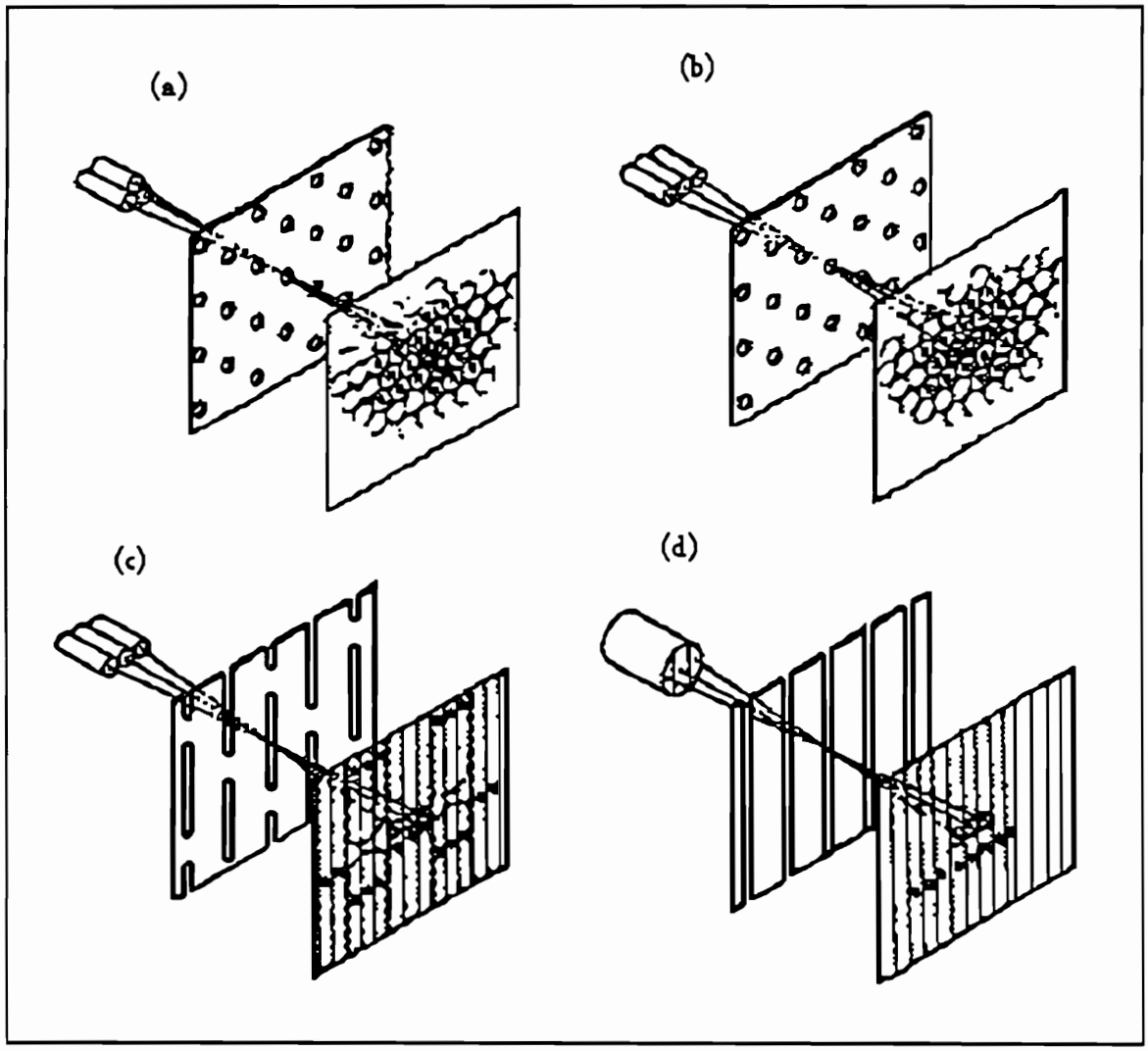

Figure 1. Four basic structures for color cathode ray tubes (CRTs) include (a) delta-gun/delta-mask CRTs, (b) in-line gun/delta-mask CRTs, (c) in-line gun/slotted mask CRTs, and (d) single lens in-line gun/metal strip mask CRTs. (Adapted from Merrifield, 1987, p. 70).

Color generation. The screen of the shadow-mask CRT display contains a regular array of colored phosphor dots or triads corresponding to red, blue, and green primary colors. The apertures in the shadow-mask correspond with the physical arrangement of the phosphor droplets. Hence, the shadow-mask directs energy from the electron guns through its aperture and onto the appropriate phosphor dots (i.e., energy from the red electron gun only falls upon the red phosphor droplets, etc.). Only a certain portion of the available energy is passed through the apertures, while the rest is blocked by the shadow-mask screen. The three independent guns provide color control by proportional activation of the color phosphor dots. The simultaneous trace distributions from the electron beams overlap and combine in an additive manner. Primary colors are created when a single gun activates its associated phosphor color dots on the screen. Non-primary colors are created when at least two electron guns activate phosphor dots in the same region of the screen and are "mixed" by the observer's visual system.

Misconvergence. When all three electron guns are perfectly registered, the centers of the electron beam distributions on the phosphor screen overlap and converge to yield an additive color. If the guns do not converge properly, the trace centers do not overlap and the colors in the resulting image are misconverged. The visual effects of misconvergence vary. For example, a yellow image is created with converged traces from the red and green electron guns. If the registration between the red and green electron guns is incorrect, the resulting image may appear as a yellow trace with a red fringe on one side and a green fringe on the other. If misconvergence is extensive, no yellow image will appear; rather, only separate red and green traces will exist without overlap. Intuitively, extreme levels of misconvergence between the color beams should produce a profound effect upon the perception of the image color and quality of the resulting screen.

Image Quality

The wide-spread and growing use of color displays has intensified the need for a metric of image quality devoted to these color systems. While such a metric would be useful for display evaluation, user performance prediction, and device quality assurance, the development of a color image quality metric is not an easy task. Some studies have investigated the influence of individual color display parameters in terms of subjective quality estimates and simple observer performance tasks (e.g., Benzschawel, 1985; Christ, 1975; Matthews, 1987). However, there has been little effort toward the development of analytical models which incorporate the chrominance and luminance variables inherent within a color display.

Monochrome display systems. Current resolution measurement techniques for color systems have been adapted from the monochromatic CRT evaluation practices. Image quality metrics based on the modulation transfer function (MTF) have been developed for a monochrome display system. The MTF is based upon the theory of linear systems analysis and the mathematics of Fourier transformations. This approach quantifies the ability of the display system to transmit images in the spatial frequency domain. The modulation transfer function area (MTFA) is an image quality metric that takes into account the MTF of the display system as well as the contrast sensitivity of the human visual system. Experimental studies have shown good correlation between MTFA and visual task performance (Beaton, 1984; Snyder, 1988; Task, 1979).

Another approach to an image quality metric, the square root integral (SQRI), has recently been published (Barten, 1987, 1989). As with the MTFA, the SQRI metric employs the MTF of a display as well as the CTF of the human visual system. The SQRI metric has shown high correlation with other measures of image quality.

Color display systems. Some attempts have been made toward the development of appropriate metrics which quantify how well the observer can resolve information presented on a color display. To be useful, an integrated approach accounting for both human operator and color display characteristics must be used in the development and evaluation of effective color display systems. The fundamental structural differences between a monochrome CRT and a color CRT display system center around the inherent sampling process introduced by the presence of the shadow-mask structure and the use of three electron guns rather than one. While some research approaches have included a parameter for the spacing (pitch) of the apertures on the shadow mask, the phase relationship between the electron guns and the shadow mask has not been addressed directly, but is represented with an average value (Kubo, 1982).

Another issue that has yet to be resolved is the appropriate representation of the luminance of a spot profile when the shadow-mask is present. As noted above, the aperture of the shadow-mask allows only part of the energy to pass through and fall on the phosphor dots. Hence, the luminance profile emitted through the shadow mask has a spiked appearance due to the sampling process (Figure 2). This sampling process is further complicated by the phase relationships between the beam profile and the shadow mask structure. These are some of the major differences between the monochrome and color CRT which remain to be adequately addressed in the formation of an image quality metric for a color display system.

Summary

In summary, there are unique engineering aspects of color CRTs which have a direct bearing upon the quality, and hence utility, of these devices. While some industry-accepted guidelines are in use today, adequate information does not exist to verify whether the guidelines are

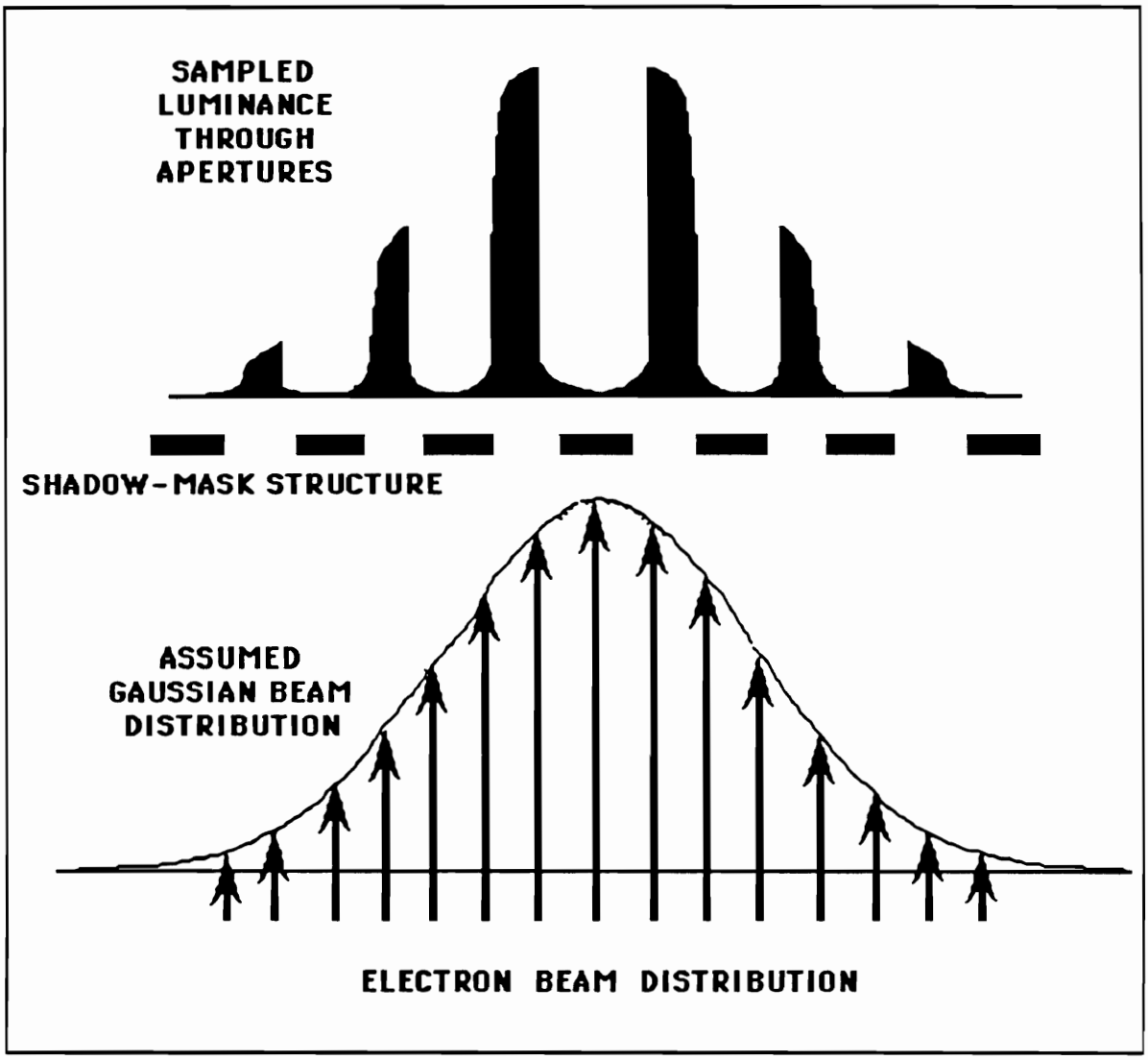

Figure 2. The expected luminance from a color CRT with a Gaussian beam profile which is sampled by the shadow mask structure.

appropriate for a variety of human visual task predictions. An investigation of conditions which quantify the effects of misalignment of the electron guns should contribute to the improvement and enhancement of these standards for color CRT display systems. Additionally, examining the effects of the shadow mask sampling pattern is needed to develop procedures to objectively evaluate the merits of a particular color CRT display design.

Research Objectives

To further understanding of the effects of misconvergence in a shadow-mask CRT display system, the objectives of this research are:

(1) to develop an analytical model to predict the expected luminance distribution through the shadow-mask structure on a color CRT display system,

(2) to determine detection thresholds for various levels of misconvergence of the electron guns on a shadow-mask CRT,

(3) to demonstrate the effect of misconvergence on operator subjective quality estimates and visual task performance with a representative reading task, and

(4) to evaluate the ability of selected unitary metrics of image to predict threshold detection, subjective image quality, and visual task performance at various misconvergences.

LITERATURE REVIEW

Color shadow-mask CRT displays use three electron guns and a mask structure coated with colored phosphor dot triads to produce red, blue, and green primary colors. When the guns are perfectly registered, the trace distributions are overlapped and converged, yielding the perceptually additive color. If the guns are not registered properly, the trace centers do not overlap and the resulting image is misconverged. While misconvergence is often described as the distance between trace centers, the impact of varying misconvergence levels on the performance of human operators is more complex. For example, viewing distance, minimum line width, spacing between characters or symbols, and ambient illumination jointly determine the quality of an image and the potential visual effects of misconvergence. Somewhere between the threshold for detection and total color separation, the observer's ability to perform required tasks becomes impaired. Misconvergence measurement, detection threshold, subjective image quality ratings, and performance data are important related aspects needed to define fully acceptable levels of misconvergence and the potential effects of misconvergence.

Luminance Model

The development of a quantitative model of image quality for color CRT display systems has lagged behind the wide-spread use of these systems. Among the reasons underlying this problem is the absence of an engineering methodology to represent the image output from a color CRT display system. The sampling process introduced by the shadow-mask structure and phosphor dot pattern complicate both the definition and the measurement of line width, convergence, and symbol element luminance. Recent efforts to develop a methodology to

evaluate the influence of various system parameters on the perceptual qualities of a multichromatic CRT primarily have been empirical in nature.

Mathematical formulation. Results from 10 years of research and development at NHK (Japan Broadcasting Corp.) for high definition CRTs and HDTV were presented by Kubo in 1982. Included in his paper is a mathematical formulation for the response characteristics of the shadow-mask structure of the CRT. This formulation has subsequently been used by other researchers (Infante, 1984; O'Callaghan and Veron, 1987; Veron, 1985) in their efforts to characterize shadow-mask CRT displays. Two fundamental expressions for the shadow-mask response are

$$Y_{max}(u) = \cos^2\left[\frac{\Theta}{2}\right] \pi \ell u \tag{1}$$

$$Y_{min}(u) = \cos\left[\frac{\Theta}{2}\right] \pi \ell u \quad \cos\left[\frac{\Theta}{2}\right] \left[2 - |\Theta| \pi \ell u\right] \tag{2}$$

for the shadow-mask response, where u is spatial frequency in cycles per mm, $\Theta = 2\left[\frac{1}{2 \ell u}\right] - \mathrm{INT}\left[\frac{1}{2 \ell u} + 0.5\right]$ where the function INT[x] represents the integer part of x and ℓ is the the horizontal distance of shadow mask apertures (Figure 3). These expressions represent the "best" and "worst" cases of spatial phase relationship between the scanning pattern and the dot structure. Note that the factor (ℓ) is included in these expressions to account for the mask pitch in the horizontal direction, and it is the only parameter specific to the geometric configuration of the shadow-mask CRT.

Resolution metric. As an outgrowth of examining the influence of spot size on the modulation depth of luminance patterns on monochrome CRTs, Barten (1984) proposed a modulation index as a resolution metric. Based on his experimental investigation, he proposed to define resolution as a modulation depth of 50% for the highest spatial frequencies to be displayed. This "rule of thumb" has been useful for display designers as a guideline in designing and specifying CRT display systems (Infante, 1984). While such a metric is useful for

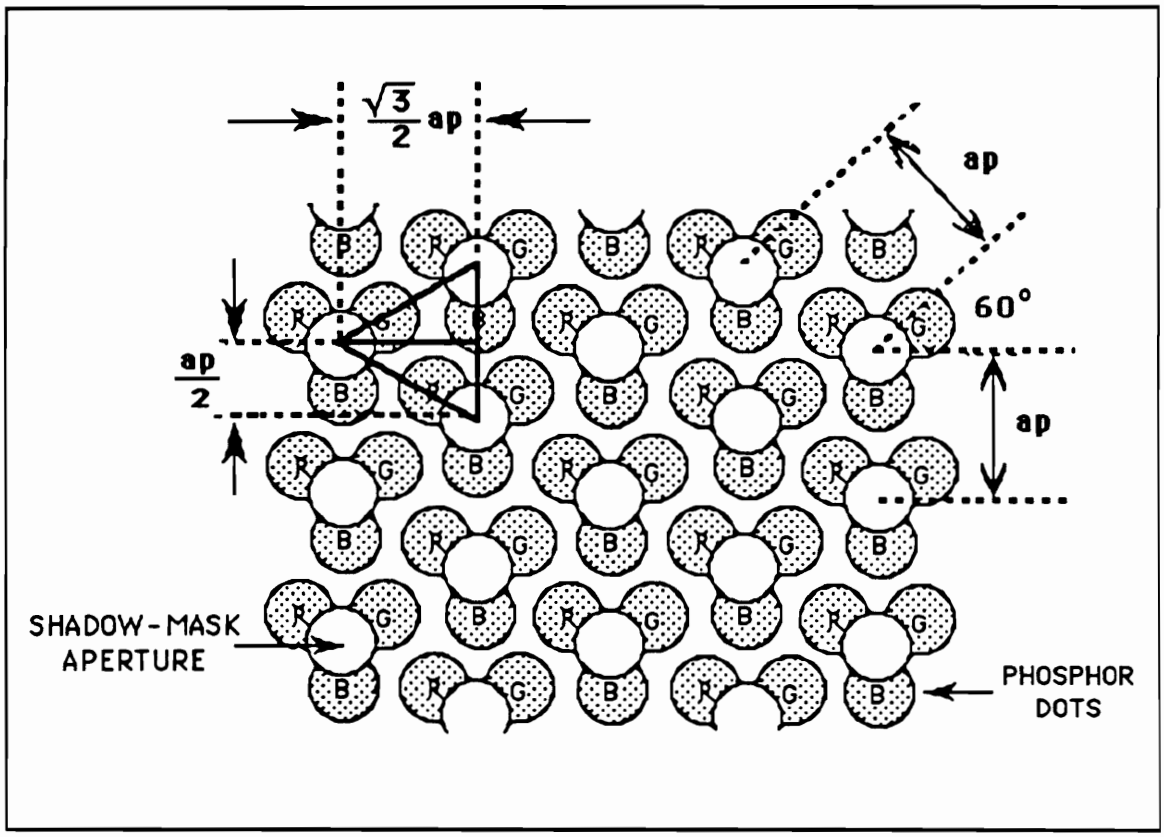

Figure 3. Shadow mask and phosphor dot structure with parameters defined by Kubo, 1982.

monochrome CRTs, the shadow-mask (SM) sampling process obscures its usefulness for SM-CRTs. In discussing some basic considerations concerning the influence of spot size and shadow-mask pitch on the resolution capability of SM-CRTs for data display, Barten stated that for color display tubes, resolution is completely determined by the shadow-mask pitch. Therefore, Barten concluded, when the spot size is adapted to the limitations imposed by the shadow-mask (i.e., spot width at 50% luminance ≤ pitch of the shadow mask) optimal results occurs.

Design tradeoffs. Infante (1984) used the MTF concept as a method to evaluate the influence of various physical display parameters (such as beam size, bandwidth, shadow-mask pitch, and viewing distance) on perceptual qualities. Infante began with a combined MTF for a monochrome high-resolution CRT and its video system:

$$MTF(u) = M_c(u)\ M_v(u) \tag{3}$$

where $M_c(u)$ is a function of the CRT spot size and $M_v(u)$ is a function of the video frequency. Appendix A provides further detail on the development of these transfer functions.

To describe the quality of the monochrome system, a measure of image quality called the modulation transfer function area (MTFA) was defined as:

$$MTFA = \int_0^{u_0} \left[MTF(u) - CTF(u_r) \right] du \tag{4}$$

where $CTF(u_r)$ is the contrast threshold function of the eye as a function of the spatial frequency at the retina, and u_0 is the spatial frequency at which MTF(u) = CTF(u). With such a representation for monochrome CRTs, different display design parameter sets (i.e., spot size, video frequency, viewing distance) can be evaluated and compared.

To extend this expression to color CRTs, Infante (1984) replaced the video system MTF term $M_v(u)$ with an expression for the shadow mask which is the average of Kubo's Y_{max} (u) and Y_{min} (u). Hence, this term represents the average of the "best" and "worst" cases of the spatial phase relationship between the scanning pattern and the dot structure

$$MTF(u) = M_C(u) \frac{\left(Y_{max}(u) + Y_{min}(u)\right)}{2} . \quad (5)$$

Using the same procedure that he used to predict the monochrome CRT system performance, Infante inferred that the perceptual qualities of the color CRT system can be represented with

$$MTFA = \int_0^{u_0} \left[MTF(u) - CTF(u_r)du \right] \quad (6)$$

for representative conditions, such as a 50-cm viewing distance and essentially infinite bandwidth. Hence, this methodology could be used as a predictor of display quality. Infante concluded with the statement that the validity of these conclusions should be verified with independent human factors experiments.

Automated resolution measurements. A technique for the automated measurement of the resolution of SM-CRT displays was presented in a series of papers by Veron and O'Callaghan (O'Callaghan and Veron, 1987; Veron, 1985, 1989; Veron and O'Callaghan, 1987). Their technique utilizes a linear systems approach to relate Barten's monochrome modulation index to an effective shadow-mask modulation index. The input waveform is the monochrome plot of intensity as a function of position, and the governing equations for the linear system are

$$H(S) = F(S)\,G(S) \quad \text{and} \quad h(x) = F^{-1}\left[F(S)\,G(S)\right], \quad (7)$$

where F(S) and H(S) are Fourier spectra of the input and output waveforms, respectively. The MTF of the SM-CRT system, G(S), consists of the MTFs described by Infante for the electron beam, the shadow mask, and the observer's eye. The calculated output waveform h(x,L) represents the "brightness modulation" as perceived by the observer located at a distance L from the display.

Luminance model summary. To date the approach taken in the development of a model to represent the expected luminance distribution from an SM-CRT has included a representation for the mask pitch (imbedded in the average Y_{max} (u) and Y_{min} (u)) and a standard expression for the response of the observer's visual system based on viewing distance. The lack of a

quantitative model of image quality for the color components of CRT display systems is problematic since display device engineers and system integrators often must rely on previous successful experiences while specifying and building color CRT systems, rather than relying upon clearly defined engineering guidelines.

Detection Threshold

One of the first areas to be addressed is a determination of the level at which misconvergence is detectable by the observer. How far out of line does a primary beam have to be before the human eye can detect misconvergence? There is little previous research that delves into acceptable levels of misconvergence for use in electronic displays. Two recent studies investigated thresholds for color separation detection with full color electronic displays.

Merrifield, Haakenstad, Ruggiero, and Lee (1979). In a Boeing document addressing the design of the Electronic Flight Instrument System (EFIS), a color display for airborne use, Merrifield, Haakenstad, Ruggiero, and Lee (1979) reported results from a series of psychophysical tests conducted to determine the threshold for misconvergence detection and the operator's level of objection to misconvergence. The levels of misconvergence were created by altering the position of one primary beam relative to the other primary beam, in 0.10-mm increments. Misconvergence levels were expressed as center-to-center beam separation.

Subjects were presented a "DH" symbol in one of two colors, yellow or magenta, on a 35.6-cm monitor at an 81.3-cm viewing distance. When the yellow symbol was used, the red beam was varied above or below the stationary green beam. When the magenta symbol was used, the blue beam was varied about a stationary red beam. Subjects were instructed to indicate which color was "above" or to say "can't tell." Subject's detection responses were analyzed as correct, incorrect, or uncertain. Results revealed that 50% of the subjects could detect 0.13 mm (0.5

arcmin) of misconvergence, but had little or no objection to such a level. However, misconvergence of 0.33 mm (1.4 arcmin) was detectable by and objectionable to 88% of the subjects. The conclusion from this study was that yellow (i.e., red-green) misconvergence was more detectable and objectionable than magenta (i.e., red-blue) misconvergence. No visual task performance data were obtained.

Silverstein and Lepkowski (1986). Silverstein and Lepkowski investigated how relative differences in primary color element size affected the perception of secondary colored lines. The test stimulus was a single horizontal line presented on a Sperry high-resolution shadow-mask avionics display. The line stimulus was controlled by over-writing six stroke lines, i.e., three lines of each of two primary colors. The spot size of the variable beam was altered by stepping two of its three primary lines by 0.0254-mm steps. Results were expressed as the mean line width at half of its maximum value. Subjects were seated 81.3 cm from the display and observed a secondary color line stimulus, in either yellow, magenta, or cyan. The subject continuously varied the relative spot size of one primary until a change in the line was detected. Trials were conducted under both high and low ambient conditions. High ambient condition consisted of high ambient illumination (8600 lx) and high display background luminance (42.5 cd/m^2) while low ambient condition consisted of low ambient illumination (2.15 lx) and low display background luminance (0.005 cd/m^2). Results indicate subjects are more sensitive to spot width changes when either the red or the green primary was varied than they are when the blue primary was varied. Threshold for detecting a change in the line stimulus when the green primary was varied, in either the yellow or cyan line, was approximately 0.70 mm (3.0 arcmin) in both the high and low ambient conditions. Detection threshold when the red primary was varied under either ambient condition was approximately 0.80 mm (3.4 arcmin) when a yellow line was used, but approximately 0.60 mm (2.5 arcmin) when a magenta line was used. When the blue primary was varied in either the magenta or the cyan line, the

threshold line width was approximately 1.07 mm (4.5 arcmin) under high ambient conditions and 1.40 mm (5.9 arcmin) under low ambient conditions. No visual task performance data were obtained.

Detection threshold summary. The same trend is apparent in both studies: observers are more sensitive to changes in a yellow stimulus when the red primary is varied than they are to changes in a magenta symbol when the blue primary is varied. Although the Silverstein and Lepkowski (1986) study investigated threshold detection of changes in line width with changes in the spot size of a primary beam, their results suggest misconvergence detection, when all three primary beams are involved, may be influenced more by the primary beam that is misconverged than by the overall color itself.

Subjective Reactions

The visual effects of misconvergence can be distracting or annoying to the observer. The subjective acceptability of misconvergence may be critical in wide-spread use of a full color display. Two studies investigated subjective reactions to various levels of misconvergence, and similar results were found.

Merrifield, Haakenstad, Ruggiero, and Lee (1979). In the Merrifield et al. study, a six-point scale was used to assess subjective reactions, ranging from "no objection" to "highly objectionable." As discussed above, at an 81.3-cm viewing distance, 50% of the subjects could correctly identify 0.13 mm of misconvergence on a display with a 0.34-mm spot size, but had little or no objection to that level of misconvergence. Eighty-eight percent of their subjects correctly identified 0.33 mm of misconvergence and found it objectionable.

Robertson and Jones (1984). Robertson and Jones explored subjective reactions to both small-area and large-area misconvergence on a color display with a 355-mm diagonal tube and seven

colors. Both graphics and text were used with the color of each chosen randomly. Subjects were allowed to view the display at an "uncontrolled distance from the screen" (Robertson and Jones, 1984, p. 166) with normal office lighting. Thus, the visual angle subtended was not constant for all subjects. Since misconvergence was determined visually with a hand microscope as the distance between the brightness centers, the results are also expressed as center-to-center beam separation.

Subjects viewed a display screen and rated it based on how they would feel if they had to use the display regularly every day. A seven-point scale (excellent to very bad) was used to record subjective reactions to the various degrees of misconvergence on the display. A level of misconvergence was considered acceptable if 90% or more of the subjects rated that level as adequate or better. They summarized their results by stating "to obtain a subjectively acceptable picture quality, misconvergence should be no more than about 0.30 mm and should be better than 0.2 mm over the majority of the screen" (Robertson and Jones, 1984, p. 165). Since the display used had a 0.8-mm spot size (measured at 5% peak luminance), these values are also reported as 38% and 25% of the spot size, respectively.

Subjective reaction summary. When the results of these two studies are compared, there is agreement upon the general level at which observers find misconvergence objectionable. Merrifield et al. (1979) found the objectionable level of misconvergence at 0.33 mm center-to-center separation, or about 100% of the spot width at half maximum luminance. Robertson and Jones (1984) concluded that misconvergence of more than 0.30 mm was unacceptable to subjects. Since the reported spot width for their display was 0.80 mm at 5% luminance, the spot width at 50% luminance (assuming a spot with a Gaussian distribution) is 0.38 mm. Hence, a level approximately equal to 100% of the spot width at half maximum luminance also constituted their result.

Performance Data

An important consideration in understanding the impact of misconvergence is the ability of an operator to perform a given task under various levels of misconvergence. Only one study has collected any type of performance data with respect to given levels of misconvergence.

Snadowsky, Rizy, and Elias (1966). Snadowsky, Rizy, and Elias investigated the impact of primary color misregistration on the performance of a symbol identification task. A multiple observer environment was simulated by using a three-channel projector system and by having subjects read symbols from a projection screen display. Misconvergence was created by shifting the registration of one of the primary channels to the right of the normal channel-projector axis registration. Misregistration (i.e., misconvergence) was calculated at the screen as a percentage of the original spot width with the formula [(M-S)/S] X 100, where M is stroke width of the misregistered symbol, and S is the stroke width of the registered symbol.

Matrices of alphanumeric symbols which subtended a 27-arcmin vertical visual angle were displayed on a screen located 5.6-m in front of the subjects. Each matrix contained symbols in each of seven colors and was presented at seven levels of misconvergence (0%, 33%, 67%, 100%, 133%, 167%, and 200% of stroke width). On each trial subjects were instructed to read symbols of a specified color and ignore all other symbols. Results indicated that the time to correctly identify color-coded symbols was significantly impacted by an interaction among the amount of misregistration, the color of the symbol, and the primary color that was misregistered. The number of symbols correctly identified per second decreased as misregistration of a primary color increased. Overall, 33% and 67% misregistration were not significantly different from 0% misregistration, while greater misregistration (100%, 133%, 167%, and 200%) differed significantly. The interaction between the percent of misregistration and the primary color being misaligned revealed that in the lower misregistration levels (i.e., 33% and 67%)

performance was not affected as much by misalignment of the blue channel as it was by misalignment of the red or green channel.

Performance summary. Although this study used a three-channel projection system with subjects seated 5.6 m from the center of the screen, the results have been used as a starting point for dealing with electron displays that are typically viewed at 81 cm. This study is referenced frequently as the basis for stating that misconvergence of 100% of the stroke width is needed to produce significant changes in performance with different spot widths (see, for example, Farrell and Booth, 1986; Robertson and Jones, 1984). It is further noted that there was less of a performance decrement when the blue primary channel was misaligned than there was when either the red or the green channel was misaligned.

Misconvergence Measurement

Different methods have been used to define, measure, and report misconvergence. Reporting misconvergence levels only in terms of center-to-center separation of the misconverged traces without reference to the spot size or the viewing distance can lead to unclear results, as illustrated in Figure 4.

Hand-held microscope. Robertson and Jones (1984) used a low-power microscope to estimate visually the "brightness" centers of primary colored lines used to display a compound color. Misconvergence was defined as the distance, to the nearest quarter of a dot pitch, between the "brightness" centers. This value was converted to millimeters based on the known dot pitch of the display. A typical spot size for the display used in this study was reported to be about 0.8-mm at 5% of the peak luminance.

Spatial scan. Merrifield et al. (1979) verified their programmed levels of misconvergence by scanning each primary beam separately with a spatial scanning system using

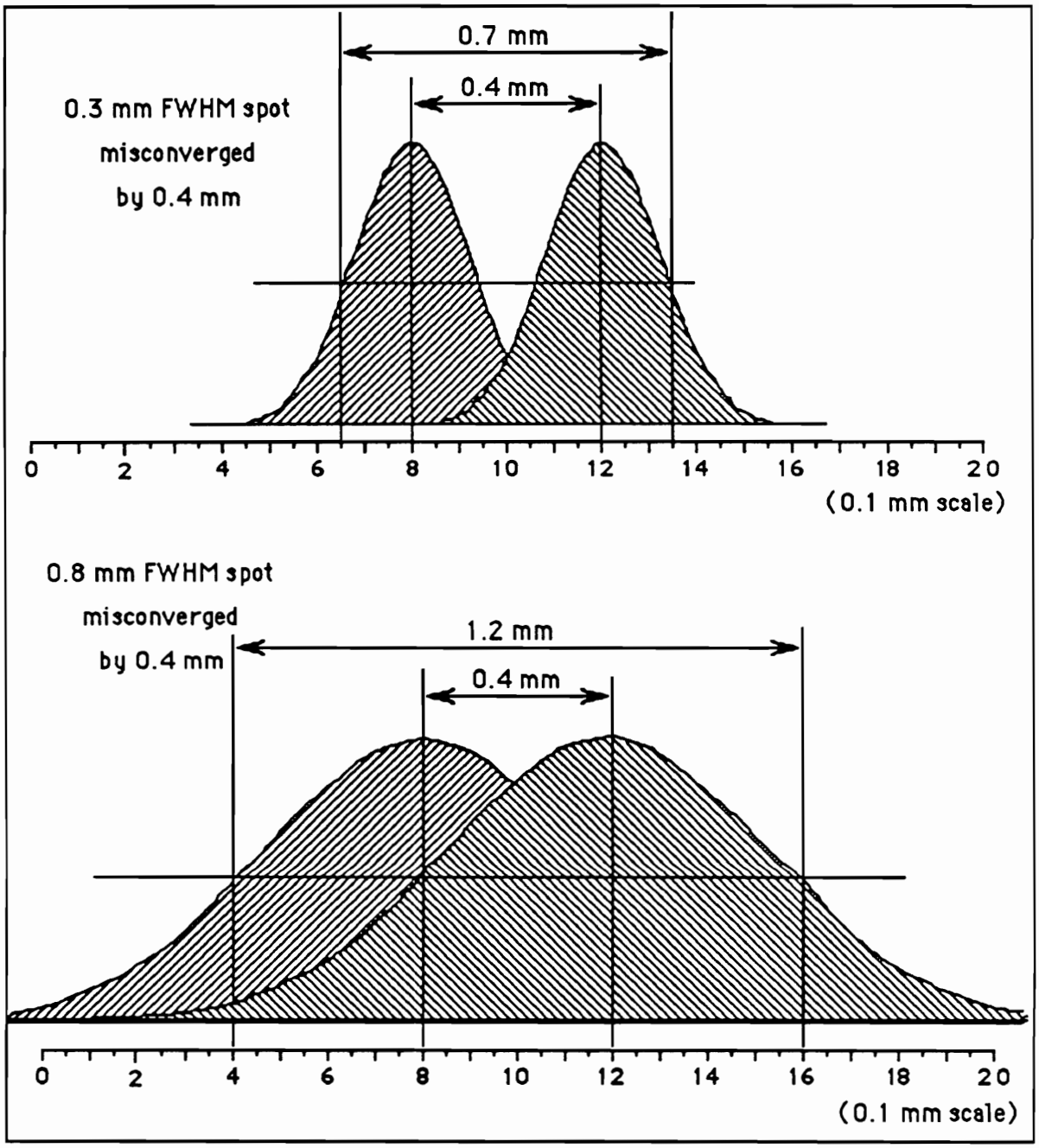

Figure 4. Spot width illustrations. When two spots of different spot widths are misconverged by the same amount, the resulting distributions overlap by varying amounts. Hence the perceived amount of misconvergence should be different.

a 0.2 X 7.6 mm parallel photometer slit. The scans for each primary combination were superimposed on the same graph and misconvergence was measured from the graph as center-to-center beam separation. Beam center was defined as the mid-point of the full spot width at 50% peak luminance.

Summary. While research into the required level of convergence on a color CRT to preserve color information has not been extensive, some industry-accepted standards and guidelines has been developed. For example, the Society of Automotive Engineering misconvergence requirement for airborne electronic displays states: "misconvergence to be no greater than the minimum half-amplitude line width of the display" (Merrifield, 1987, p. 77). Stated in this manner, the guideline does not address all of the necessary parameters, such as the distance from which the display will be viewed. In discussing the parametric considerations for color CRTs used in aircraft cockpits, Silverstein and Merrifield (1985, p. 175) stated: "A good rule of thumb for misconvergence specifications is no more than a half-amplitude line width or 0.35 mrad (1.2 arcmin) from the design eye position, whichever is less." They added to this statement: "In light of the difficulty of finely converging shadow-mask CRTs at their edges and the paucity of performance data on the effects of misconvergence, a greater misconvergence tolerance should be accepted over the outer 20% of the usable display area." (Silverstein and Merrifield, 1985, p. 175). It is clear that a research effort that addresses the detectability threshold for misconvergence as well as the impact of misconvergence on performance is needed. Such data would provide information about whether the accepted rule of thumb is appropriate, too stringent, or too lenient.

Image Quality Metrics

Most of the research in the area of image quality has been concerned with images in the spatial domain (i.e., two-dimensional space) and most metrics have been derived from the MTF

concept. As has been noted, the MTF is fundamentally the ratio of the output to the input signal of a display system.

MTF Area. The MTF concept quantifies the extent to which any system can transmit a signal. In the transmission process, some of the signal's amplitude is often lost due to the limitations of the transmission system. A Fourier analysis of the displayed information can be used to quantify the response of the system. At any given spatial frequency (ω), the modulation transfer factor is the ratio of the modulation which is output from a system to the modulation which was input into the system. This factor can be expressed as

$$T(\omega) = \frac{M_o(\omega)}{M_i(\omega)} \tag{8}$$

where $T(\omega)$ is the modulation transfer factor at a specific spatial frequency (ω), and $M_o(\omega)$ and $M_i(\omega)$ are the respective output and input modulations. When viewed across all spatial frequencies (upper curve in Figure 5) the system MTF curve characterizes the ability of the display to transmit any signal. The broader the MTF curve, the larger the area under the MTF curve, and the greater the ability of that system to transmit high frequency information. Because of this relationship, the MTF area has been used to develop several image quality metrics. Studies have shown MTF-based image quality metrics correlate significantly with visual task performance (Decker, et al., 1987).

MTFA. The modulation transfer function area (MTFA) was developed as a method to combine the imaging system MTF with the spatial capabilities of the human visual system. The rationale underlying the MTFA is the measurement of excess signal (MTF) over the threshold requirement of the visual system (Snyder, 1988). The MTFA concept is illustrated in Figure 5. The upper curve indicates the MTF of the system, that is, the amount of input signal at each spatial frequency which is transmitted through the system and becomes the output signal. The lower curve indicates the detection threshold for the human visual system. The area above this lower curve indicates modulations at each spatial frequency which can be

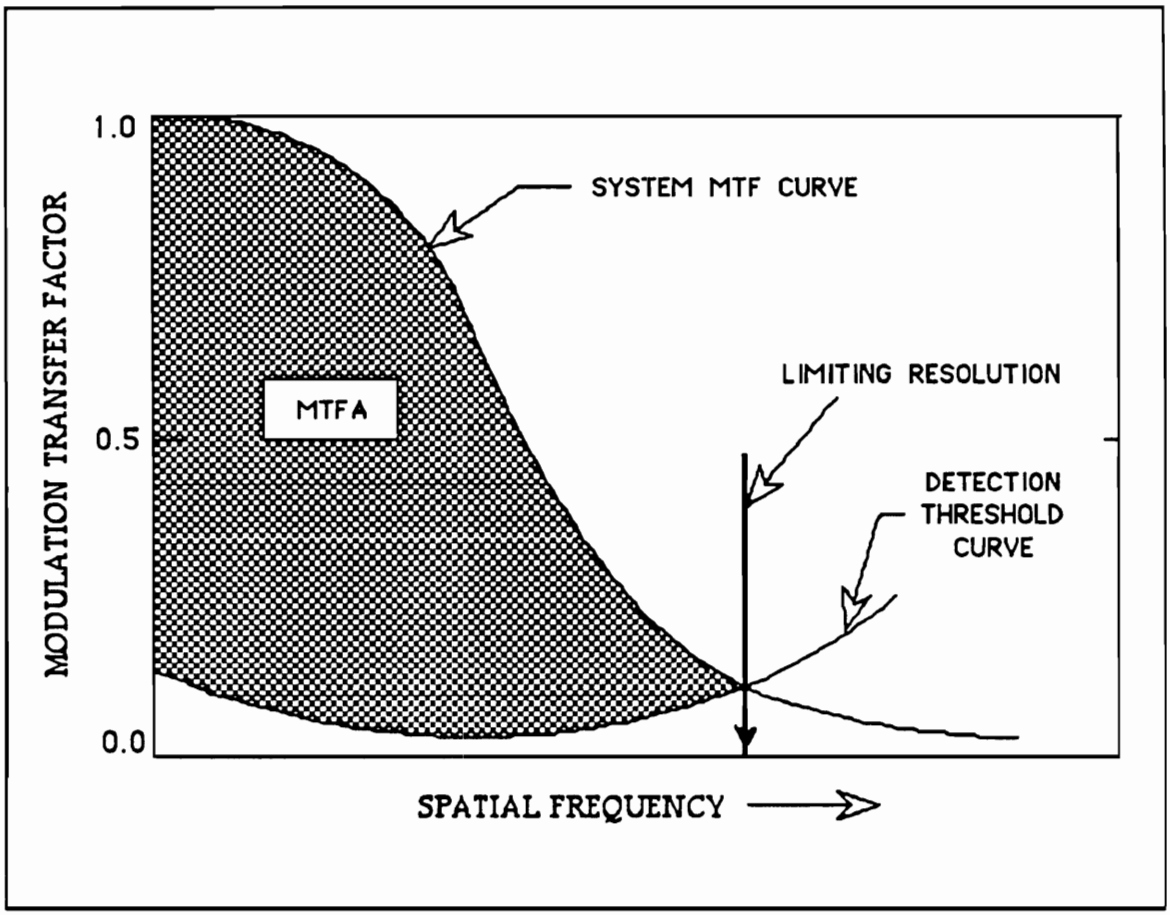

Figure 5. The MTFA concept. (Source: Snyder, 1988, p. 26).

detected by the visual system, while the area below this curve indicates modulations which will not be detected. The area between these two curves (the shaded area in Figure 5) is computed and termed the modulation transfer function area (MTFA). Very high correlations ranging from 0.717 to 0.912 were obtained between this MTFA metric and visual task performance (Beaton, 1984; Task, 1979).

SQRI. A new method for the evaluation of visible resolution, the square root integral (SQRI), has been proposed by Barten (1987, 1989) to take into account a nonlinear visual process within the visual system as well as various display parameters. This metric is expressed as

$$J = \frac{1}{\ln 2} \int_0^{u_{max}} \sqrt{\frac{M(u)}{M_t(u)}} \, \frac{du}{u} \tag{9}$$

where u is the spatial frequency in cycles per degree, u_{max} is the maximum angular spatial frequency displayed, and M (u) is the MTF of the display system. The modulation threshold function of the eye M_t (u) is expressed in terms of L, the display luminance in cd/m^2 as follows

$$\frac{1}{M_t(u)} = a\,u \exp(-b\,u) \sqrt{1 + c \exp(b\,u)}\,, \tag{10}$$

with $a = 440\left(1 + \frac{0.7}{L}\right)^{-0.2}$, $b = 00.30\left(1 + \frac{100}{L}\right)^{0.15}$, and $c = 0.06$.

COLOR CRT MTF MODEL

The development of a quantitative model of image quality for color CRT display systems has lagged behind the widespread use of these systems. The approach taken in this research to develop a model of the image quality of the color CRT display stems from an analytical description of the modulation transfer function (MTF). The MTF is a well-known transfer function concept in imaging science and is the foundation for many image quality metrics for a monochrome CRT. The utility of the MTF in describing the imaging capacity of discrete-sampled display systems has only recently been investigated (Beaton, 1988).

The Color CRT MTF model incorporates three major elements which either are overlooked or not needed in the MTF model of continuous-element display systems. The three elements include a flexible electron beam profile to accommodate deflection and defocusing phenomena, a discrete sampling filter to introduce the sampling characteristics of the shadow-mask and phosphor-dot structures, and the ability to specify desired phase relationships among the three electron beams as well as between the beam bundle and the shadow-mask/phosphor-dot structure. Figure 6 illustrates the major components of the model. This color CRT MTF model provides a complete empirical algorithm for display engineers to assess the impacts of and trade-offs between these physical elements of the system.

Electron Beam Profile

The shape and width of electron beam profiles have been taken to represent the impulse response characteristics of electronic display systems. Consequently, the beam profile has played an important role in specifying the spatial frequency transmission properties of these systems. As was noted in the work of Infante, the shape of the electron beam profile

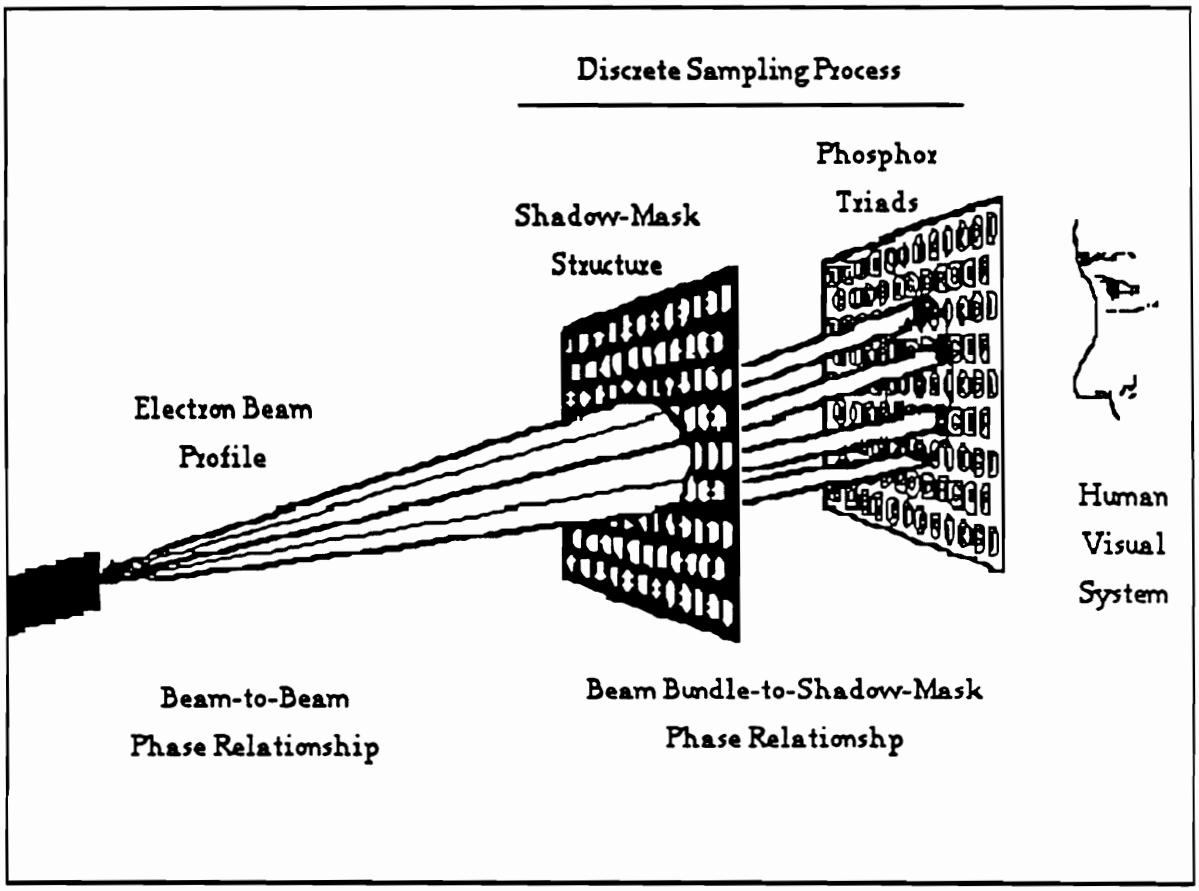

Figure 6. The major components of the Color CRT MTF model.

traditionally is represented by a Gaussian distribution in luminance. While the Gaussian representation is convenient, it does not represent various aberrations which may occur in the beam profile.

Gaussian beam profile. The method by which the Gaussian (or normal) distribution has been used represent the beam profile was used as a starting point in the development of a flexible beam profile capable of representing the wide variety of profiles which might occur in a display system. The equation for the Gaussian distribution centered about zero and normalized to be one at its maximum value is

$$f(x) = \exp\left(\frac{-x^2}{2\sigma^2}\right) \tag{11}$$

where x is the distance from the center value. There are two ways in which a spot profile is commonly specified (Figure 7). The first, S, is defined as the full-width, half maximum (FWHM) spot size. Therefore, to obtain an expression in terms of the standard deviation of the Gaussian, one finds the ordinate value (x) for which f(x) in equation 10 is equal to 50% or $\frac{1}{2}$. Since S is the distance between $\pm x$,

$$S = 2\sigma\left[\sqrt{2 \ln 2}\right]. \tag{12}$$

It should be noted that Equation 12 differs from the equation used in Infante's work by the inclusion of a 2 in the radical in the denominator of Equation 12. This resulted from the omission of the 2 in the denominator of Equation 11 (see Appendix A for further details).

The second measure is D, the width at which the density has decreased to 5% of the maximum value. Therefore, an expression in terms of the standard deviation of the Gaussian is obtained when one finds the ordinate value (x) for which f(x) in equation 10 is equal to 5% or $\frac{1}{20}$. Since D is the distance between $\pm x$,

$$D = 2\sigma\left[\sqrt{2 \ln 20}\right]. \tag{13}$$

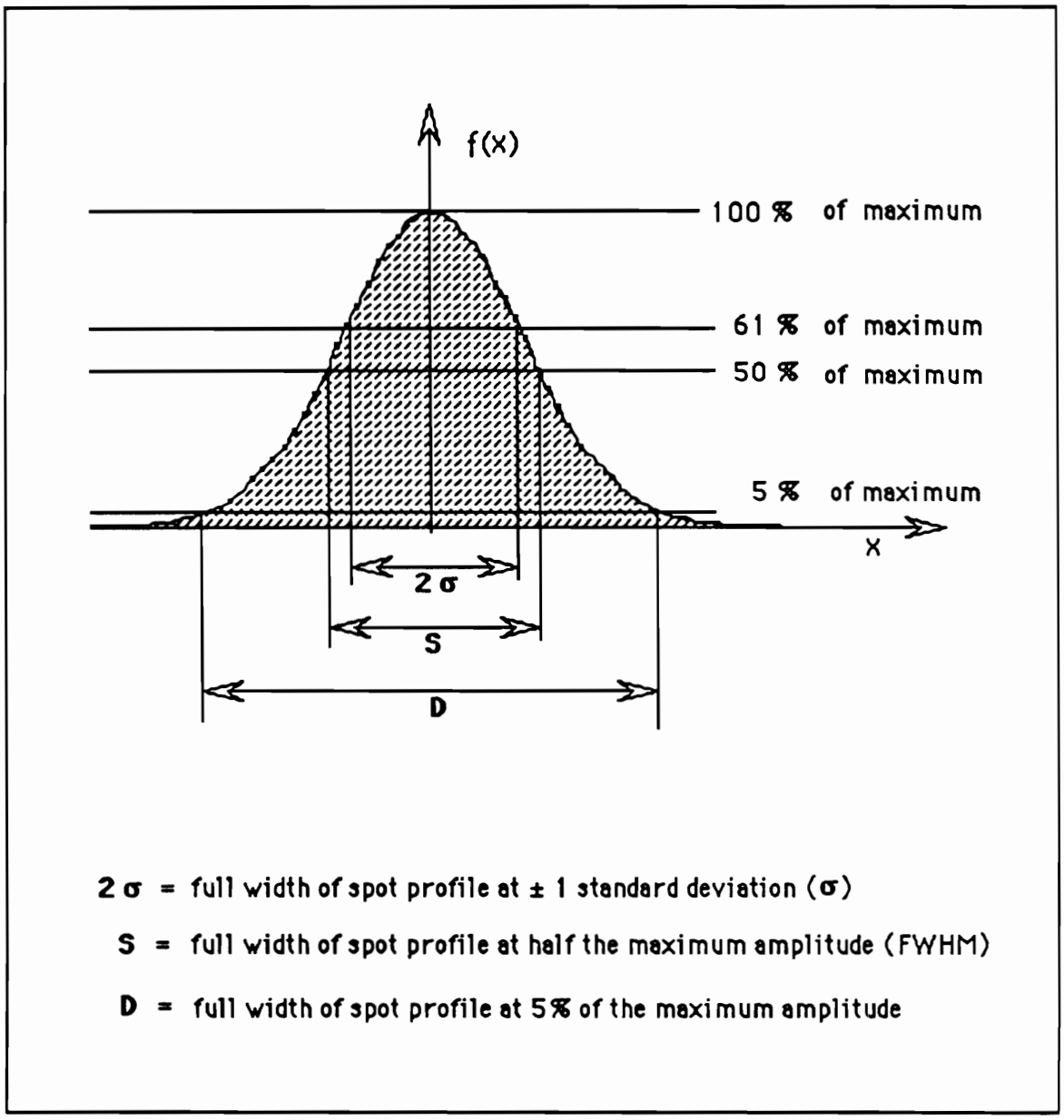

Figure 7. Beam profile represented with a Gaussian distribution.

This measure is used in Barten's expressions. After evaluating this approach to describing a beam profile, a natural extension to find a flexible expression to represent the beam profile was to investigate families of statistical distributions to find an appropriate candidate.

In general, there two major ways in which an electron beam profile deviates from the Gaussian distribution. The first is by flattening and broadening the center of the distribution (i.e., decreasing the kurtosis of the distribution). The other major deviation from the normal distribution would be an increase in one tail (i.e., skewness) of the distribution as the beam deviates from the center of the screen. In the current research effort, the model will focus on changes in the kurtosis of a symmetrical profile. Hence, the skewness will be zero.

Johnson system of distributions. The Johnson system of distributions uses the method of translation to transform any variate into a normal variate. Johnson (1949) used monotonic functions f (x), each specified with four parameters (γ, δ , ζ, and λ), to translate a non-normal variate (x) into a standard normal variate (z) by

$$z = \gamma + \delta f\left[\left(x - \zeta\right) / \lambda\right]. \tag{14}$$

The parameters γ and δ determine the shape of the distribution, while λ provides a scale factor and ζ provides a location factor. Since the parameters λ and ζ affect the distribution in a straightforward manner, attention is concentrated on the relationship between γ and δ and the distribution of x. Equation 13 can also be expressed as

$$z = \gamma + \delta f\left(y\right) \tag{15}$$

where $y = \left(x - \zeta\right) / \lambda$. By utilizing the properties of the standard normal distribution, density functions p(y) for the non-normal variates can be expressed. Further details of the development of these equations in provided as Appendix B. The basic density functions for the three forms of the Johnson translation system are as follows:

Bounded System

$$p(y) = \left(\frac{1}{\sqrt{2\pi}}\right)\left(\frac{\delta}{[y(1-y)]}\right)\exp\left[-\frac{1}{2}\left\{\gamma + \delta \ln\left(\frac{y}{(1-y)}\right)\right\}^2\right], \quad \text{for } 0 < y < 1 \tag{16}$$

Lognormal System

$$p(y) = \left(\frac{1}{\sqrt{2\pi}}\right)\left(\frac{\delta}{y}\right)\exp\left[-\frac{1}{2}\left\{\gamma + \delta \ln(y)\right\}^2\right], \quad \text{for } 0 < y < 1 \tag{17}$$

Unbounded System

$$p(y) = \left(\frac{1}{\sqrt{2\pi}}\right)\left(\frac{\delta}{\sqrt{y^2+1}}\right)\exp\left[-\frac{1}{2}\left\{\gamma + \delta \ln\left(y + \sqrt{y^2+1}\right)\right\}^2\right], \quad \text{for } -\infty \le y \le \infty. \tag{18}$$

To simplify the use of the Color CRT MTF model, the user will provide information about the desired beam profile, such as the amount of kurtosis and an estimate of the variability in the profile, that is the desired FWHM width. The model estimates the necessary parameters and computes the appropriate Johnson function. To illustrate some of the possible beam profiles, Figure 8 provides three profiles, each of which has an FWHM of 0.60-mm. The top profile is a Gaussian distribution with 76% of the density within the bounds of the 0.60 mm FWHM. The other two profiles demonstrate the effect of reducing the kurtosis, that is, becoming more platykurtic. Comparisons are included to indicate the amount of the energy within the FWHM on these profiles.

Shadow-Mask/Phosphor-Dot Filter

The second major component of the model is the discrete sampling which occurs as a result of the combined shadow-mask and phosphor-dot structure. In this research, only the horizontal dimension of a color CRT screen is simulated. Therefore, discussion is limited here to a one-dimensional filter which represents the shadow-mask and phosphor-dot sampling. A more

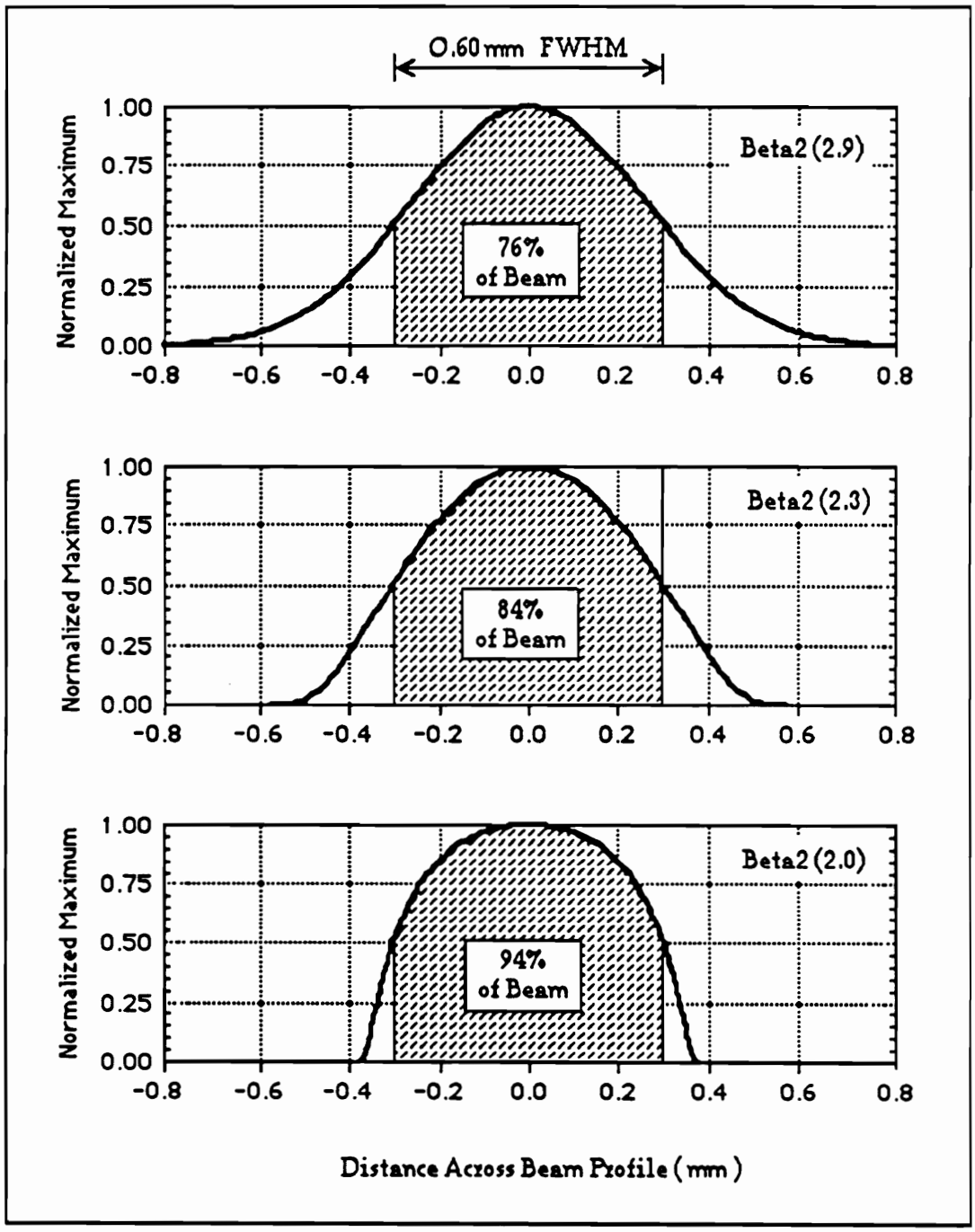

Figure 8. Basic shapes of beam profiles which can be represented with this model.

complete discussion of the development of this filter, as well as the two-dimensional filter, is presented as Appendix C.

The basic arrangement of the phosphor dots is a triad, depicted in Figure 9a. The triads are arranged together to form a hexagon pattern for phosphor dots of one color (see Figure 9b). Finally the shadow-mask structure is aligned with the phosphor layer to selectively allow the beam to pass through apertures and land on the phosphor dots, Figure 9c. This combined phosphor-dot and shadow-mask structure is incorporated into the model as a binary (0,1) filter. In other words, where the beam strikes an aperture on the shadow mask. it is allowed to pass through and strike the phosphor layer. Hence, the luminance in that area is multiplied by one. In the areas where the beam strikes the solid mask between the apertures, it is prevented from proceeding on the phosphor layer. Hence, the luminance in that area is multiplied by zero.

The Color CRT MTF model simulates a single horizontal scan of a color CRT. Therefore, an infinitesimal aperture would progress across the screen and sample only a single row of phosphor dots (see Figure 9d). The mathematical expression for the filter is

$$f(x,y) = \begin{cases} 1 \text{ for } \begin{cases} -r < y < r \text{ and} \\ -\sqrt{r^2 - y^2} < \left[x + 2n P_H + h\right] < \sqrt{r^2 - y^2} \end{cases} \\ 0 \text{ otherwise} \end{cases} \tag{19}$$

where $n = 0, \pm 1, \pm 2$, etc, and $h = 0$ for the green beam, $+\frac{2}{3} P_H$ for the red beam and $-\frac{2}{3} P_H$ for the blue beam. The simulated scan occurs at one value for y, the vertical distance. It should be noted that the model can simulate a scan along the center of the phosphor dots (i.e., $y = 0$), or can be shifted to the desired phase by selecting a different y value.

It should be noted that a single horizontal scan across the display is inherently a two-dimensional process, since a single aperture in the shadow-mask structure impacts two adjacent

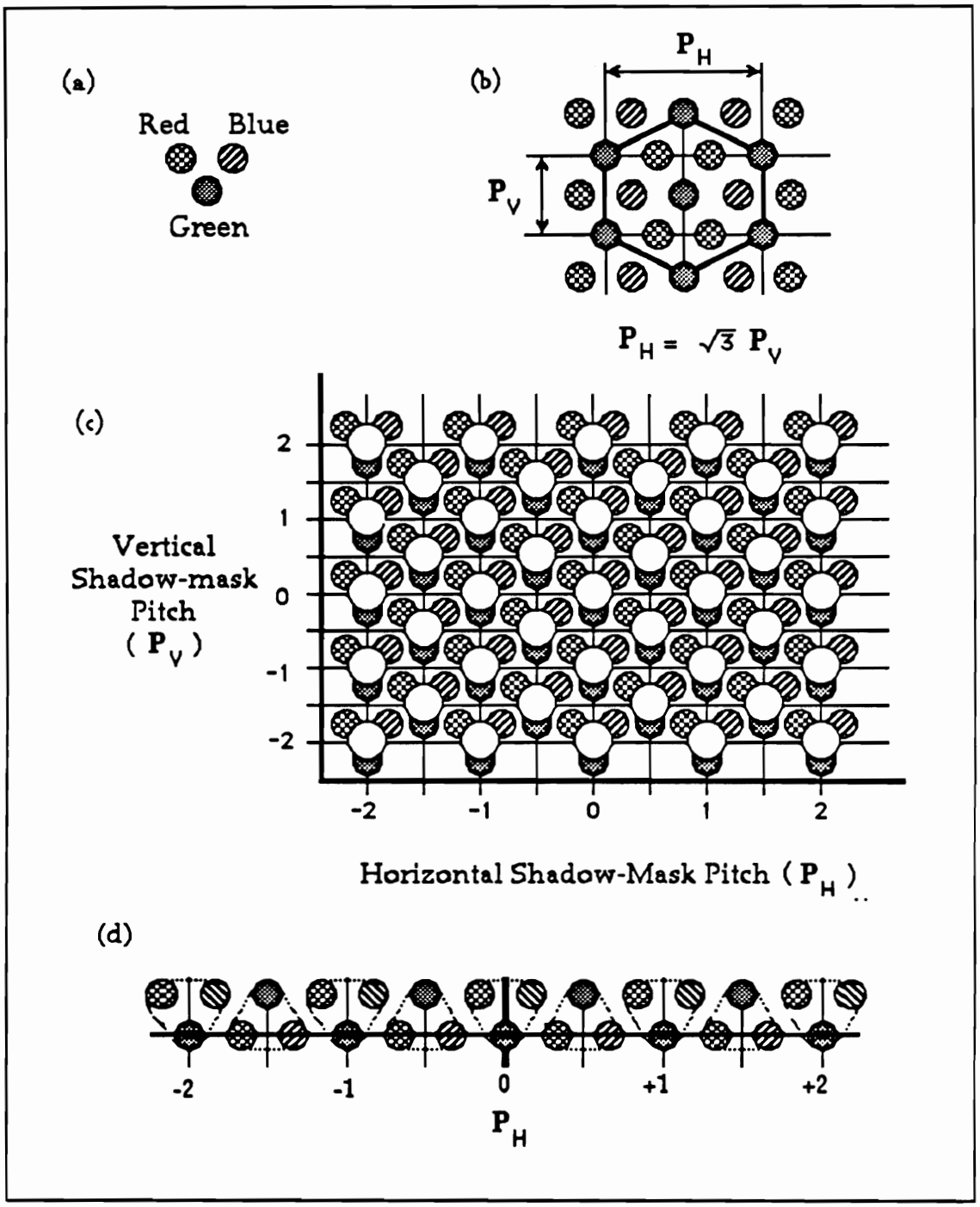

Figure 9. Phosphor dot and shadow-mask structure.

phosphor dot rows. Hence, any one-dimensional model will undersample the luminance by excluding the second row of phosphor dots.

Phase Relationships

The third major component of this model addresses the issue of the phase relationships inherent in the display system. When the phosphor-row filter samples the beam profile, the result is a jagged luminance profile. Figure 10 illustrates this process with a normalized Gaussian beam profile (top) being sampled, that is multiplied, by the binary filter (center) and resulting in the spiked profile (bottom).

The first phase relationship is between the beam bundle (all three primary beams considered together) and the shadow-mask structure. Figure 10 assumes the center of the beam profile is aligned with the center of a shadow-mask aperture. Hence, the major peak is located in the center position. If, however, the beam bundle is out of phase with the center of the shadow-mask structure, a different profile will result (see Figure 11). In this model, the user has the ability to specify the phase relationship between the beam bundle and the shadow-mask structure.

The second phase relationship addressed in this model is the relationship between the three beams themselves. To handle this relationship, the model defines the absolute center as the center of a green phosphor dot. The location of the red and blue beams is then specified by the user. A converged beam is one in which the centers of the red and blue beams correspond with the center of the green beam. A horizontally misconverged beam is specified by setting the centers of the red and blue beams a specified distance from the green center. Therefore, the user of this model is allowed to specify the desired horizontal relationship between the three beams to investigate the impact of misconvergence.

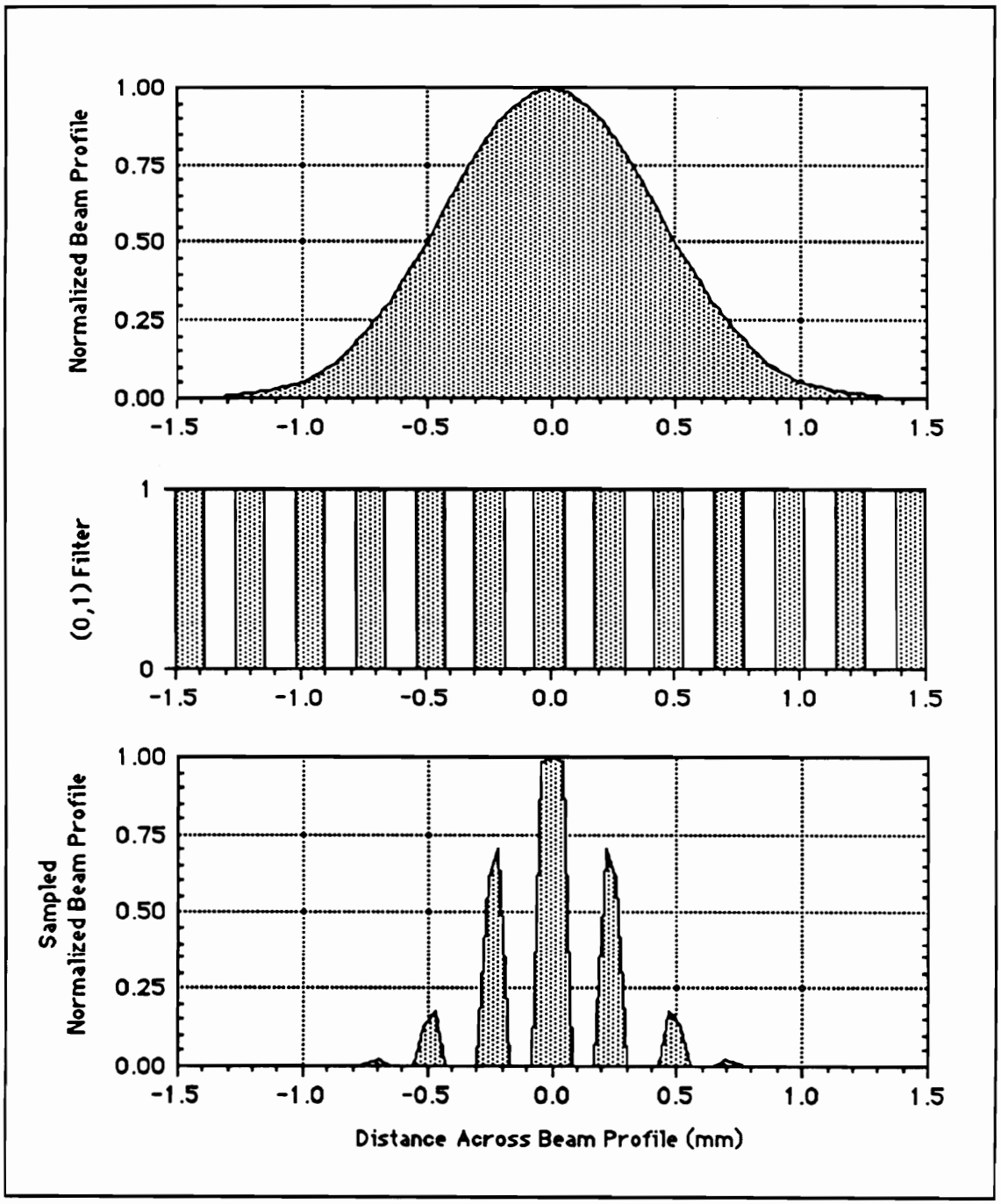

Figure 10. The sampling effect of the shadow-mask filter upon a beam profile.

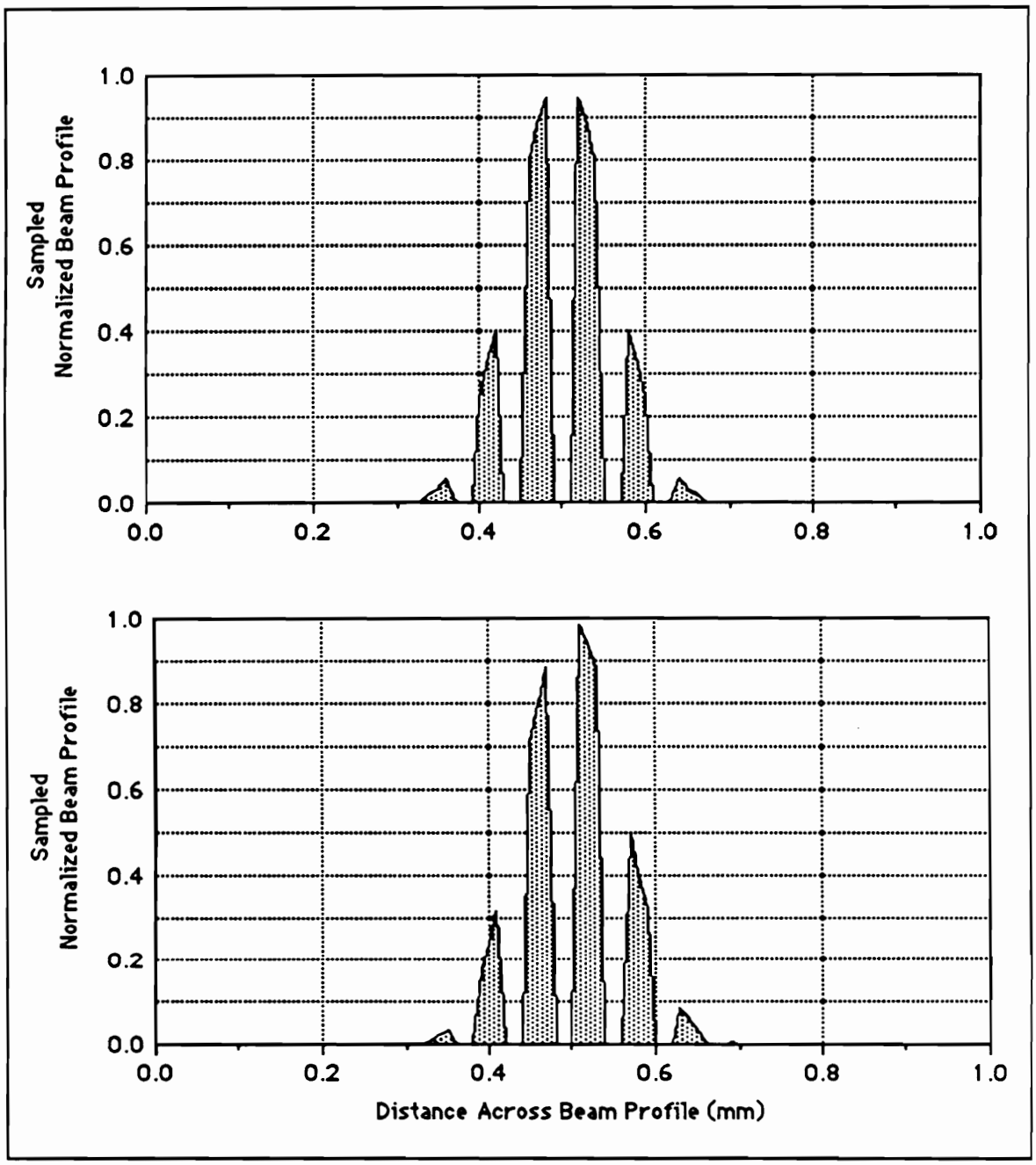

Figure 11. Effect of an out-of-phase relationship between the beam bundle and shadow-mask filter.

Model

These components are combined in a program written for a Macintosh IIcx computer in Lightspeed C to produce the Color CRT MTF Model. Figure 12 provides a sample listing of the parameter settings and output for an example model. With the "Scan Parameters" the user can specify the total distance (in mm) over which a simulated scan will be performed, as well as the number of points to be taken in that scan. From this information the model determines the sampling rate and the first, center, and last points of the scan. The "Mask Parameters" provide the user with the ability to enter the specifics of the display to be simulated, that is, information about the vertical and horizontal pitches and a description of the phosphor dots. Included in this group of parameters is the specification of the phase relationship (misconvergence) between the beam bundle and the shadow-mask structure. The "Observer Parameters" specify the conditions in which the display is to be viewed and the distance from which it will be viewed.

The "Beam Parameters" allow individual specification of each electron beam. The full width, half maximum dimension of each beam is used to describe the width of each beam profile. The total display luminance (in this example 105 cd/m^2) is proportioned out between the beams according to the user-specified percentage of the total luminance. Within this group of parameters is the specification of the phase relationship (misconvergence) between the three beams. From this value and the structure of the phosphor dots, the center of each beam profile is computed centered about the green profile. The factors for the skewness and kurtosis of the beam profile are used to describe the shape of the profile. A Gaussian distribution, as used in this example, has skewness = 0 and kurtosis = 3. A symmetrical platykurtic distribution (flatter topped) varies from this by having a kurtosis < 3, while leptokurtic distributions (more peaked centers) have kurtosis > 3. The amount of skewness specifies the degree by which the

SCAN PARAMETERS		MASK PARAMETERS		OBSERVER PARAMETERS	
Total Points	512	Misconvergence	0.000	View Distance (mm)	600.0
Total Distance (mm)	5.000	Triad V Pitch (mm)	0.280	Adaptation Lum. (cd/m^2)	10.0
Sampling Rate	0.010	Triad H Pitch	0.485	Glare Luminance	0.0
First Point	0.000	Dot V Pitch	0.140		
Last Point	5.010	Dot H Pitch	0.162		
Center Point	2.505	Dot Diameter	0.108		

BEAM PARAMETERS	GREEN	BLUE	RED
50% Width (mm)	0.254	0.254	0.254
Luminance (cd/m^2)	72.500	8.500	24.000
Skewness	0.000	0.000	0.000
Kurtosis	3.000	3.000	3.000
Misconvergence (mm)	0.000	0.120	0.000
Mean Position	2.505	2.787	2.343
Johnson Delta	3.937	3.937	3.937
Johnson Gamma	-9.862	-10.971	-9.225
Johnson Lambda	1.000	1.000	1.000
Johnson Xi	0.000	0.000	0.000

METRICS:

MTF Area = 12.138805 MTFA = 7.413228 SQRI = 159.572032

Figure 12. Input parameters and output metrics from the Color CRT MTF model.

distribution shifts from an ideal, symmetrical distribution. This information is combined within the computer to estimate the necessary parameters for the Johnson system (i.e., delta, gamma, xi, and lambda).

After the user has specified all of the above parameters, the model computes the beam profiles for each beam, combines them into a beam bundle, then samples the resulting beam profile with the shadow-mask/phosphor-dot filter. The Fourier transform of the resulting waveform is then taken to produce the modulation transfer function (MTF) for the display being simulated. The area under the MTF curve is then taken, and two image quality metrics are computed, that is, MTFA and SQRI.

Model Validation

To verify the results of this model, an experiment was conducted with a representative display. This experiment focused upon changing the horizontal misconvergence among the three primary beams; it also obtained three user visual performance measures. The display and misconvergence conditions were simulated to obtain the MTF area, MTFA, and SQRI metrics for each misconvergence condition. These measures were then correlated with the results from the human performance study to determine how well the Color CRT MTF model predicts performance.

METHOD

An experiment was conducted in this research effort to provide a comprehensive data set with perceptual and performance measures of the effects of various levels of misconvergence of the primary guns on a shadow-mask CRT display. Three tasks were performed in this experiment to determine the detection threshold for misconvergence, the effect of misconvergence on performance, and a subjective evaluation of the color image quality as a function of misconvergence.

Setting

All aspects of this experiment were conducted under the same ambient conditions with no attempt to simulate the full range of operational conditions under which color CRTs are regularly used. A "normal" office working environment was provided with indirect ambient illumination in the range of 100 lux, measured at the display. All subjects were seated at a fixed 60-cm viewing distance in front of the display which was 0.5 arc minutes below their line of sight. This viewing distance was held constant with the use of a head rest in which the subject's forehead was rested during each task.

Subjects. Twelve subjects (six males and six females) ranging in age from 21 to 26 years of age were recruited from the college population to participate in this experiment. Subjects were tested for normar, or corrected to normal, vision using a Bausch and Lomb Orthorater. Only subjects with 20/25 performance or better for binocular, left, and right near visual acuity were acceptable. The lateral and vertical phoria of each subject was measured, accepting those whose responses were within the 67% and 88% population limits, respectively. The pseudo-isochromatic plates were used to test subjects for color deficiencies, accepting those who responded correctly to the left and right plates.

Equipment. An IBM XT personal computer was used as the overall controller of the experiment and data were collected through a software interface. The various screen images required by the tasks were created by an OPIX Imager video generator. These screen images were sent to the special misconvergence generator (detailed below). The image was then displayed on a Zenith Data Systems ZCM-1490 high resolution 14-inch color monitor. This monitor has a 0.28-mm vertical pitch and a 0.48-mm horizontal pitch. The horizontal active video time is 25420 nanoseconds with a horizontal display area of 256 mm. Hence, the horizontal raster sweep rate is 10 micrometers per nanosecond. The measured luminance of the red, green, and blue electron guns was 24, 72.5, and 8.5 candelas per meter squared, respectively.

Misconvergence generator. This experiment focused on misconvergence in the horizontal dimension only, which is expressed as the linear separation between the centers of the primary beams. Misconvergence was created on the display with the introduction of a discrete signal delay (in nanosecond increments) to any of the electron beams. The misconvergence generator provided four channels to which one or more of the primary beams could be assigned at any give time. These channels were capable of providing the following delay ranges:

Channel 0 -- no delay in the signal

Channel 1 -- 0 to 63 nanoseconds of delay in the signal

Channel 2 -- 0 to 126 nanoseconds of delay in the signal

Channel 3 -- turned off signal from beams assigned to this channel.

For each trial, the amounts of signal delay assigned to Channels 1 and 2 were defined to produce the desired misconvergence. Following this delay definition, the red, green, and blue beams were assigned to the appropriate channels. Therefore, the misconvergence generator allowed complete control over which gun was to be displayed or turned off, as well as the amount of delay that was assigned to a particular gun to produce the desired misconvergence.

Experimental Design

Tasks. Three tasks were used in this experiment. The first task was designed to quantify the probability that a user of the display system will be able to detect misconvergence. For this threshold detection task, subjects were presented a vertical line segment at the center of the display screen. The subjects were instructed to respond to the question "Do you see any misconvergence" with either "yes" or "no". This binary response was entered into the IBM PC by the experimenter. Each subject received six replications of each of the possible conditions.

The second task was a representative performance task, that is, reading a block of text, to quantify the effect of various misconvergence levels on the ability of the user to perform a given visual task. The reading task used was the Tinker Speed of Reading Test originally developed by M. A. Tinker in 1947 to investigate the effects of typographical and illumination variations on reading speed (Feldt, 1959) and modified by Carver (Feldmann, 1972). This test provides 500 short passages to measure the reading time of the reader and has been successfully used in other video display studies. Each passage contains one target word which is clearly "wrong" when used in the context of that passage. The subjects were instructed to read the passage and identify the target word as quickly and as accurately as possible. As an example, the target word that is used out of context in the following passage is "car":

> Marge was on the lake when the lightning
> started flashing, and she rowed back home
> as fast as she could because she was
> frightened that the car would hit her.

Each paragraph was randomly selected and presented to the subject in the center of the display. The text was presented in a 5 X 7 mixed upper and lower case font which is standard for the OPIX image generator.

The third task was a subjective rating of the overall image quality of text presented on the screen. For this task a standard block of text containing eight lines of text with approximately ten words per line was used. The standard block was constant for all trials and presented in the center of the screen. The subjects were instructed to describe the screen with one of the following nine adjectives:

Best Imaginable
Excellent
Good
OK
Passable
Marginal
Poor
Awful
Worst Imaginable

Dependent variables. For the detection threshold task as described above, each condition was randomly presented to the subject six times. The probability of detection was computed as the number of times the subject responded "yes" (i.e., the subject perceived misconvergence on the screen) divided by six, the total number of times the subject was presented that condition. Therefore, the dependent variable for this task was the probability of detection, ranging from 0.0 to 1.0.

In the performance task, when a random Tinker passage had been selected and processed for the subject, the IBM PC issued a "BEEP" to signal the subject that the task was ready to begin. To begin the task, the subject depressed and held down a mouse button. When the target word was identified, the subject released the button, then told the experimenter the target word. The reading time was automatically captured by the controller as the time between the initial presentation of the passage (i.e., the subject pressed the button) and the subject's identification of the target word (i.e., the subject released the button). Following the subject's response, the

experimenter entered a "Y" into the computer if the response was correct, or a "N" otherwise. Therefore, the dependent variable for this task was the reading time of the subject and was recorded in hundredths of a second.

For the subjective image quality task the subject was provided the adjective list without any numbers associated to the levels. For data analysis, a numerical ranking of 1 to 9 was assigned to the adjective list, ranging from 1 = "worst imaginable" to 9 = "best imaginable." The experimenter entered the corresponding numeral into the computer when the subject rated each screen. Therefore, the dependent variable for this task was the numerical value of the subject's response and ranged from 1 to 9.

Independent variables. The experimental design of this experiment was a mixed design with three independent variables. The blocking variable was the Order in which the subjects received the three tasks. Two subjects (one male and one female) were assigned to each of the six possible Orders. The other two independent variables were the Position (P) of the three primary beams and the level of Misconvergence (M) in the display screen. Data were collected over a three-day period with the Positions presented to the subject on each day counterbalanced among subjects.

Primary beam positions are used to define the color of the display as well as to define the relative arrangement of each of the guns. Figure 13 illustrates the definition employed to specify the Position variable. All positions are defined with reference to the position of the Green gun, which is defined as Level 0. The varying gun (either the Blue or the Red gun) was varied with the nine different misconvergence levels. Finally, the position of the third gun (either the Red or the Blue gun) was specified and could take on one of the five levels or be in the off position when gun-pairs are used. The one exception to this procedure occurs when the Red-Blue pair is displayed, where the Green is in the OFF position, the Red gun is defined as the reference position and the Blue gun is in the Varying position.

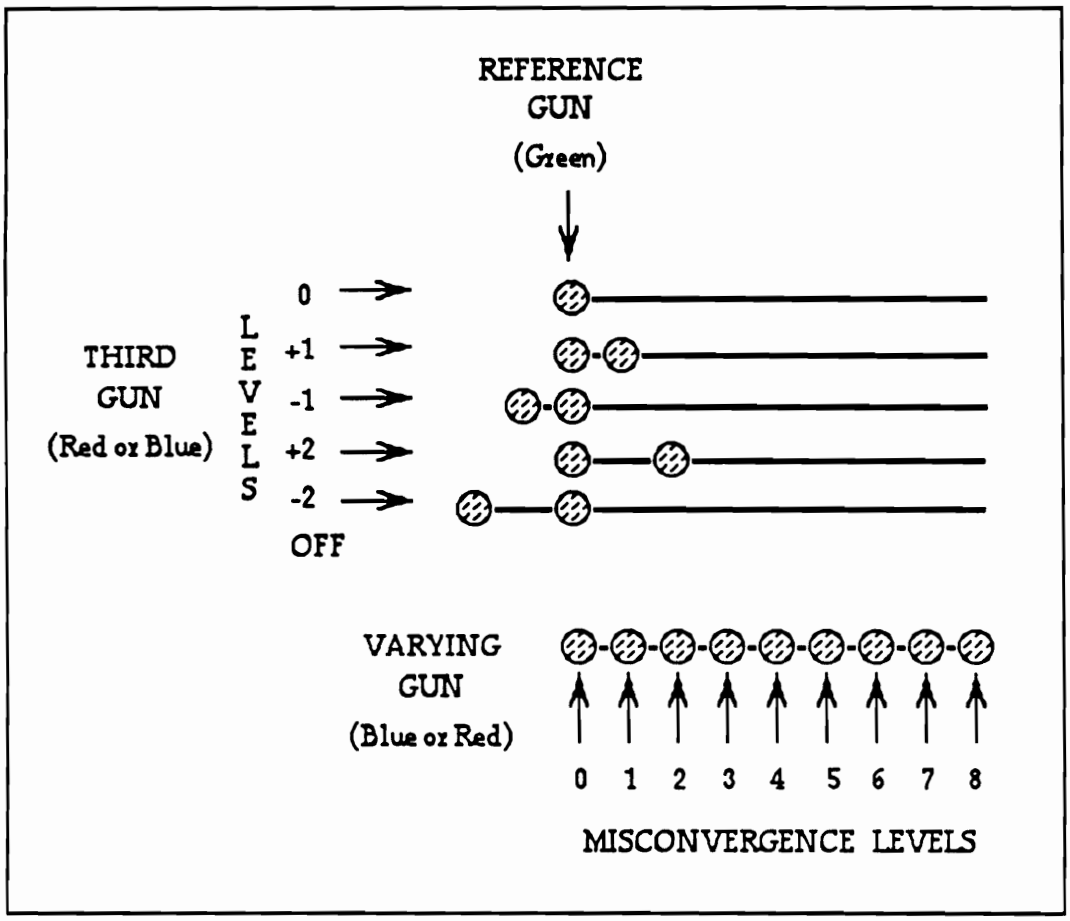

Figure 13. Fundamental relationships between the three primary beams which form the basis for the definition of the 13 distinct gun Positions.

A special notation was incorporated to specify the Position variable. This notation identifies each of the beams with the letters R, G, and B to represent the red, green, and blue beams, respectively. Omission of a letter indicates that the beam is in the OFF position. The symbol "-" is used to indicate which beam is in the varying position. The symbol "." indicates the third gun is at level +1 or -1. Finally, the the symbol ".." indicates the third gun is at level +2 or -2. This notation is used to describe the 13 unique beam Positions (see Figure 14) used in this experiment. The first three Positions involve beam pairs which produce secondary colors, that is, cyan (created with green and blue primaries), magenta (created with red and blue), andyellow (created with the red and green). The other 10 Positions involve all three guns, thereby creating a white. Half of the whites are defined with the blue gun in the misconverging position, while the other half involve misconvergence in the red gun.

Misconvergence levels were systematically varied during each of the tasks. Levels of misconvergence were assigned as increments of the horizontal distance (P_H) between the same color phosphor droplets in adjacent phosphor triads. Note that this measure is one-half of the traditional horizontal pitch of a display, which is defined as the horizontal distance between consecutive same-color phosphor droplets on the same row of phosphor dots. Because of the relationship of the phosphor triads, this measure is between every other phosphor triad. Refer to the illustrations included in Appendix C, which describes the construction of the shadow-mask/phosphor dot filter.

In this experiment P_H is equal to 240 micrometers. Since the beam on this display travels at 10 micrometers per nanosecond, a 24-nanosecond delay in a beam is equivalent to a delay of one P_H. At a fixed viewing distance of 60 cm, beam separation of one P_H is equivalent of 1.35 arcminutes. As noted earlier, previous research demonstrated that the detection threshold level for misconvergence is approximately 1-2 visual arcminutes. The nine misconvergence levels used in the detection threshold task were set between 0 and 2 P_H (i.e., 0, 6, 12, 18, 24, 30,

NUM	POSITION		GUN PLACEMENT		
	CODE	ILLUSTRATION	GREEN GUN	RED GUN	BLUE GUN
1	G-B	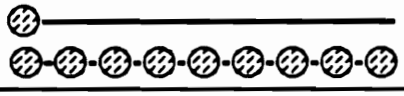	Reference (0)	OFF	Varying
2	R-B	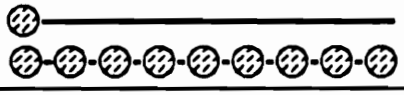	OFF	Reference (0)	Varying
3	G-R	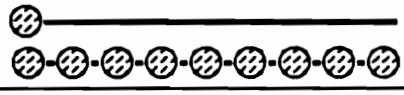	Reference (0)	Varying	OFF
4	R..G-B	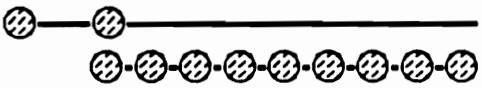	Reference (0)	Third Gun (-2)	Varying
5	R.G-B	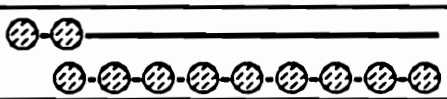	Reference (0)	Third Gun (-1)	Varying
6	GR-B	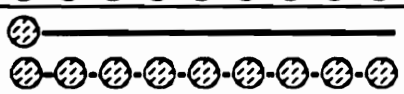	Reference (0)	Third Gun (0)	Varying
7	G.R-B	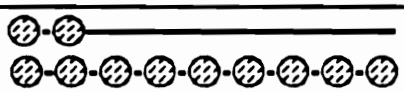	Reference (0)	Third Gun (+1)	Varying
8	G..R-B	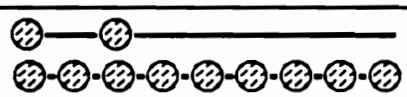	Reference (0)	Third Gun (+2)	Varying
9	B..G-R	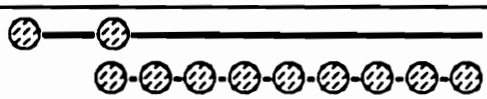	Reference (0)	Varying	Third Gun (-2)
10	B.G-R	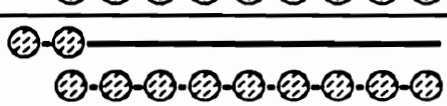	Reference (0)	Varying	Third Gun (-1)
11	GB-R		Reference (0)	Varying	Third Gun (0)
12	G.B-R	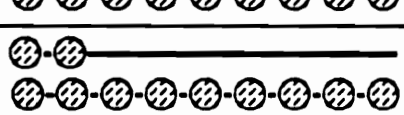	Reference (0)	Varying	Third Gun (+1)
13	G..B-R	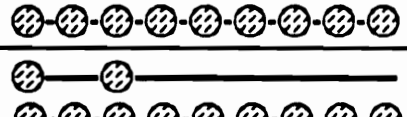	Reference (0)	Varying	Third Gun (+2)

Figure 14. Notation used to identify the positions of the primary beams for the levels of misconvergence used in the three tasks.

36, 42, and 48 nanoseconds of delay). The nine misconvergence levels used for the reading task and the subjective rating tasks were set between 0 and 4 P_H (i.e., 0, 12, 24, 36, 48, 60, 72, 84, and 96 nanoseconds of delay) to extend the distortion well beyond detection threshold and into levels which would strongly impact performance.

The experimental design for the threshold detection task is presented as Figure 15. The design for the reading and subjective ratings tasks varies from this only in the definition of the misconvergence levels.

Procedure. Data were collected over a three-day period with all three tasks being performed each day with one set of beam Positions. The beam Positions were broken into three blocks which were defined as follows. On the first and third days, all tasks were performed with either all white Positions blue varying (i.e., Positions 4 to 8), or all white Positions with red varying (i.e., Positions 9 to 13). On the second day, the subjects performed all tasks with a random presentation of the three beam-pair positions. The presentation of the white with blue varying and the white with red varying on the first day was counterbalanced across all subjects and all Orders of presentation.

Analysis. The three independent variables were analyzed with a three-factor between-subjects analysis of variance (ANOVA), blocked by the Order in which the three tasks were performed during each session. A correlation analysis was also performed between pairs of the three independent measures.

BEAM POSITION		MISCONVERGENCE (mm)								
Number	Code	0.00	0.06	0.12	0.18	0.24	0.30	0.36	0.42	0.48
1	B-G									
2	B-R									
3	R-G									
4	R..G-G									
5	R.G-B									
6	GR-B									
7	G.R-B									
8	G..R-B									
9	B..G-R									
10	B.G-R									
11	GB-R									
12	G.B-R									
13	G..B-R									

Figure 15. Experimental design for threshold detection task. Definitions for beam positions are described in the previous figure.

RESULTS

Threshold Detection Task

The dependent measure for the threshold detection task was the probability of detection. The ANOVA results for this task are presented in Table 1. As expected, the effect of Misconvergence is significant ($p < 0.001$). The effect of Position of the primary beam guns and the interaction between Misconvergence and Position are also significant ($p < 0.001$ for both). The effect of the Order in which the tasks were performed, as well as the two- and three-way interactions involving Order, are not significant.

Post hoc tests were performed on the significant Misconvergence x Position interaction. The results of the simple-effects F-tests are presented as Table 2 and reveal that there is a significant difference between the Position means at all levels of Misconvergence ($p < 0.005$). The results of the Neuman-Keuls comparison of the Position means at each Misconvergence level are presented in Figures 16, 17 and 18. The axis indicates the probability of detection, and the horizontal lines over the axis indicate no significant differences ($p > 0.05$) between or among the means covered by the line.

Examination of the non-significant mean groupings in the Newman-Keuls comparisons provides further information with regard to overall trends. Figure 19 presents the means for the [R-B] and [G-R] combinations, which were significantly different from all other lines. Note that a second horizontal axis has been added to present the visual angle (in arc minutes) for each level of misconvergence at the viewing distance used in this experiment. Figures 20 presents the means for the [G-B], [GR-B], [G.R-B], and [G..R-B] Positions in the top graph, with *all* means at each Misconvergence level *not* significantly different from one another. The means for the [R.G-B] and [R..G-B] combinations are presented in the bottom graph and these

TABLE 1

Analysis of Variance Summary Table for Threshold Detection Task

Source of Variance	df	MS	F	p
Between Subjects				
Order (O)	5	0.9721	0.34	0.871
Subjects /Order S(O)	6	2.8466		
Within Subjects				
Misconvergence (M)	8	10.7752	174.92	< 0.001
M x O	40	0.0580	0.94	0.575
M x S(O)	48	0.0616		
Position (P)	12	2.1029	21.90	< 0.001
P x O	60	0.0960	1.00	0.498
P x S(O)	72	0.0960		
P x M	96	0.2013	5.61	< 0.001
P x M x O	480	0.0344	0.96	0.686
P x M x S(O)	576	0.0359		
	1403			

TABLE 2

Simple-Effects F-Tests for the 13 Beam Positions at Nine Misconvergence Levels for the Threshold Detection Task

Position	df	MS	F	p
P x M x S(O)	576	0.0359		
0.00 mm Misconvergence	12	0.3125	8.70	< 0.001
0.06 mm Misconvergence	12	0.2606	7.26	< 0.001
0.12 mm Misconvergence	12	0.5005	13.94	< 0.001
0.18 mm Misconvergence	12	0.4276	11.91	< 0.001
0.24 mm Misconvergence	12	0.7317	20.38	< 0.001
0.30 mm Misconvergence	12	0.7058	19.66	< 0.001
0.36 mm Misconvergence	12	0.3796	10.57	< 0.001
0.42 mm Misconvergence	12	0.3080	8.58	< 0.001
0.48 mm Misconvergence	12	0.0870	2.42	0.005

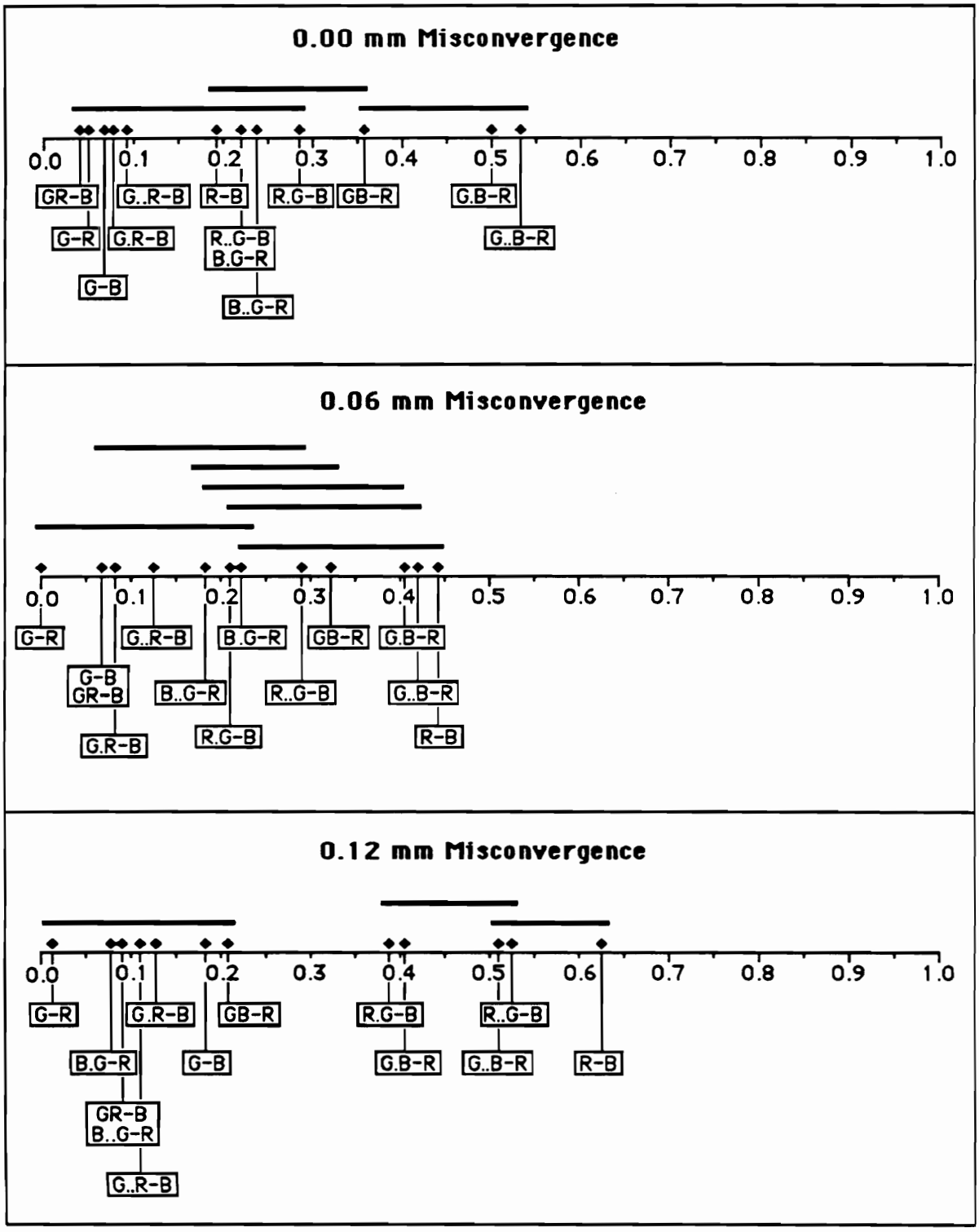

Figure 16. Newman-Keuls comparisons of the probability of detection means for all Positions at 0.00, 0.06, and 0.12 mm levels of Misconvergence.

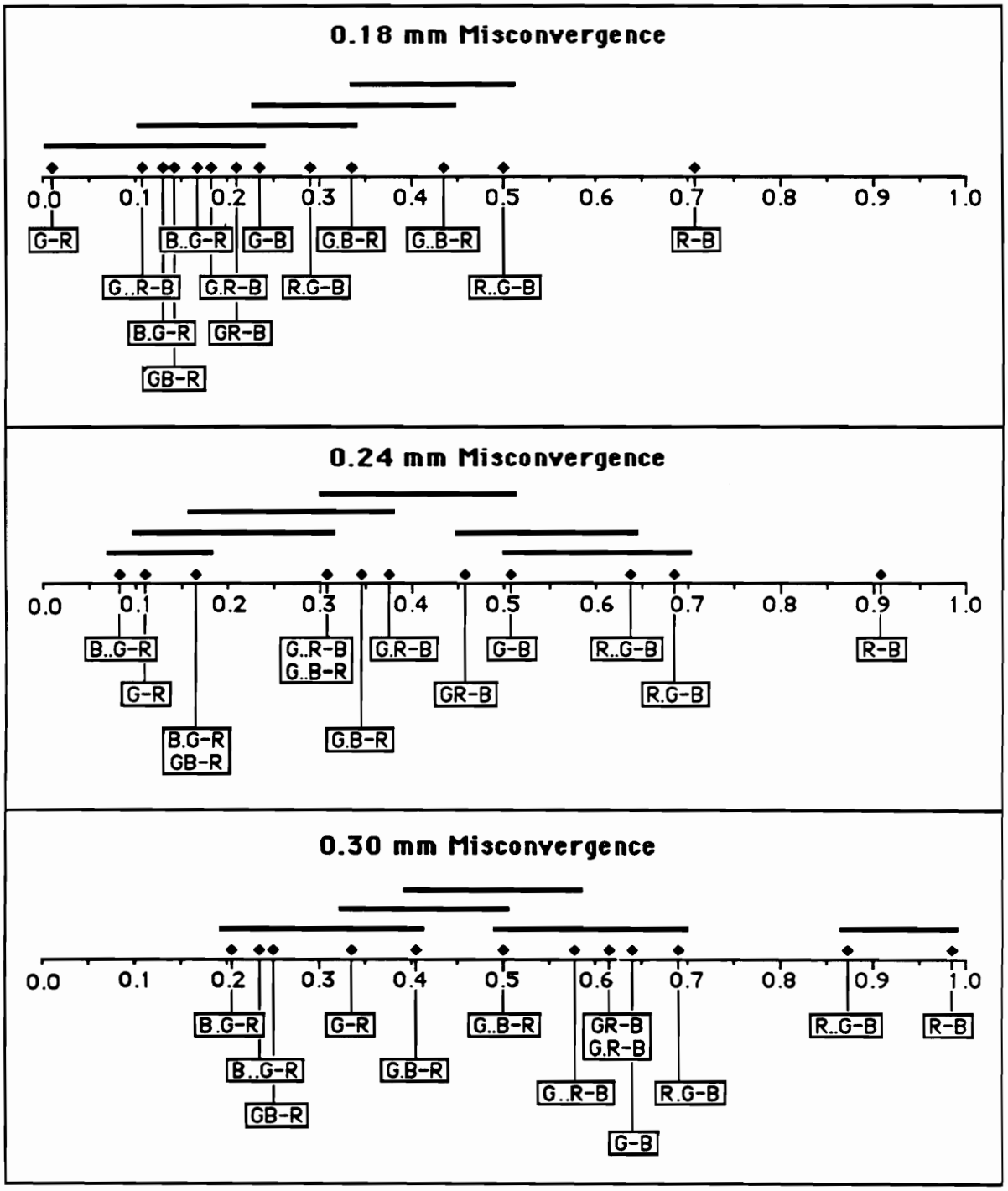

Figure 17. Newman-Keuls comparisons of the probability of detection means for all Positions at 0.18, 0.24, and 0.30 mm levels of Misconvergence.

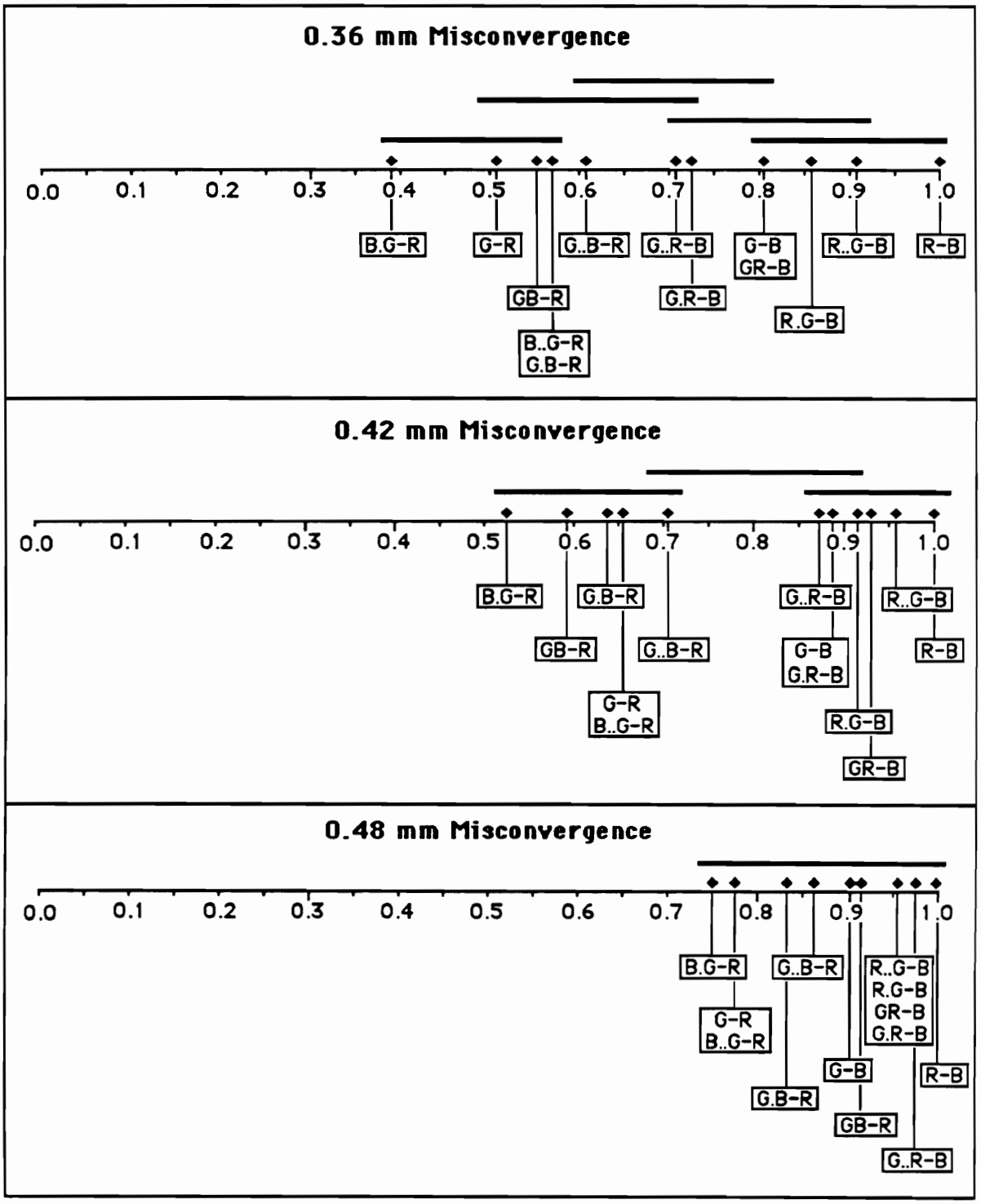

Figure 18. Newman-Keuls comparisons of the probability of detection means for all Positions at 0.36, 0.42, and 0.48 mm levels of Misconvergence.

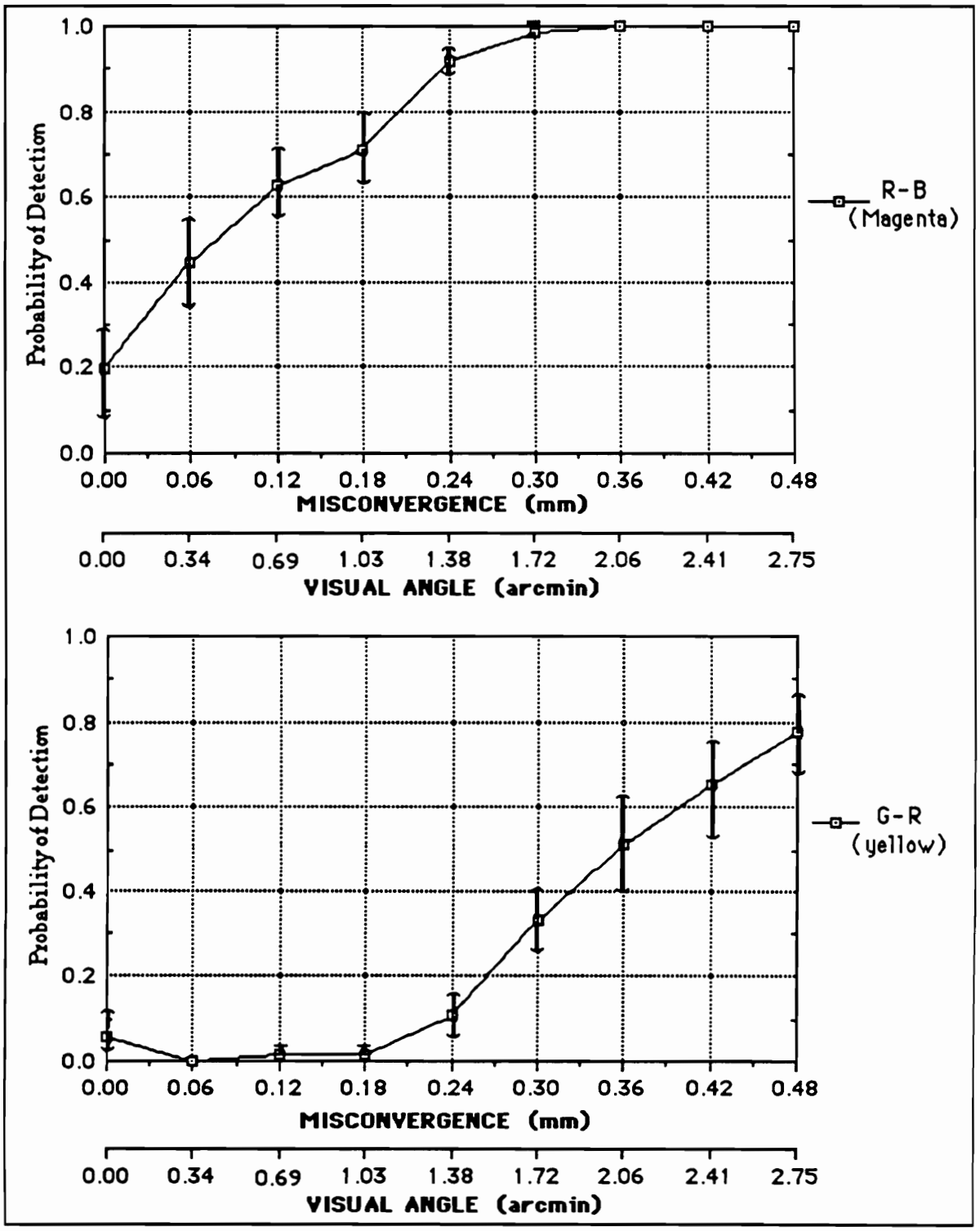

Figure 19. Probability of detection for stimulus presented in magenta or yellow color combinations with bars to represent ±1 standard error of the means.

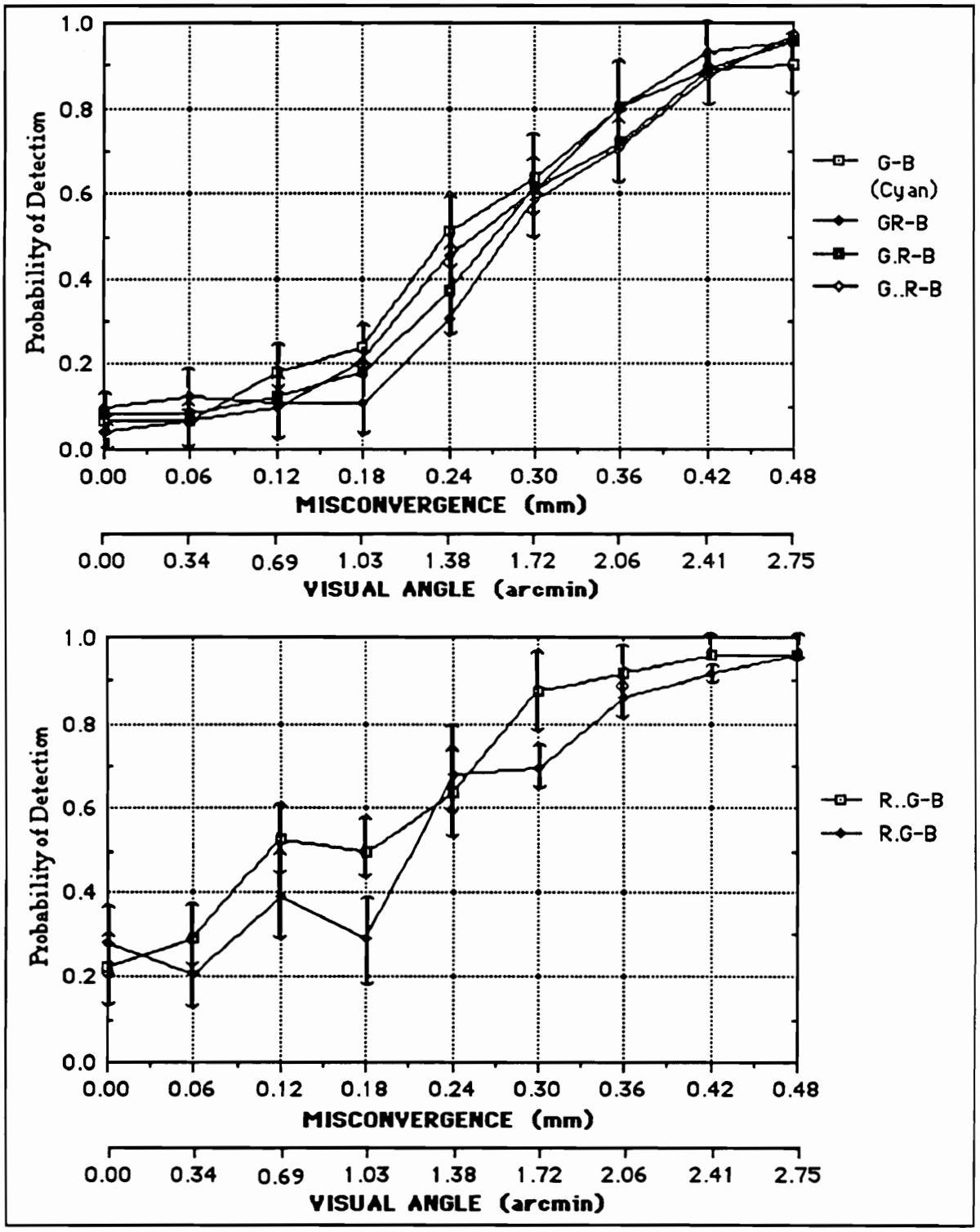

Figure 20. Probability of detection for stimulus presented in cyan or white with blue varying color combinations with bars to represent ±1 standard error of the means.

means are *not* significantly different, except at the 0.18 and 0.30 Misconvergence levels. Note that all Positions used in this figure represent combinations where the blue gun was in the varying position. Figure 21 presents the means from the [G.B-R] and [G..B-R] Positions in the top graph and the means from the [GB-R], B.G-R], and [B..G-R] Positions in the bottom graph. All means in each grouping are *not* significantly different from one another across all levels of Misconvergence. Thus, a patterning of threshold detection means clearly exists for different beam orderings used to create misconvergence.

Reading Task

The ANOVA summary for the reading task is presented as Table 3 and reveals no significant differences for any of the independent variables. Therefore, no further analysis is required on these data. The overall average reading speed was 6.55 s and Figure 22 presents the average reading speed across all levels of misconvergence.

Subjective Rating Task

The dependent measure for the subjective rating task was the rank order of the subjective adjectives provided to the subject. The ANOVA results for this task are presented in Table 4. As expected, the effect of Misconvergence was significant ($p < 0.001$). A parametric statistical test (ANOVA) was used instead of a nonparametric test after an verifying that subjects tended to use the full scale, hence there was comparability in the variances. It has been shown that parametric tests for differences in the means of ordinal data perform very well when sampling comes from populations with homogeneous variances (Gregoire and Driver, 1987). The effect of the Position of the primary beam guns and the interaction between Misconvergence and Position

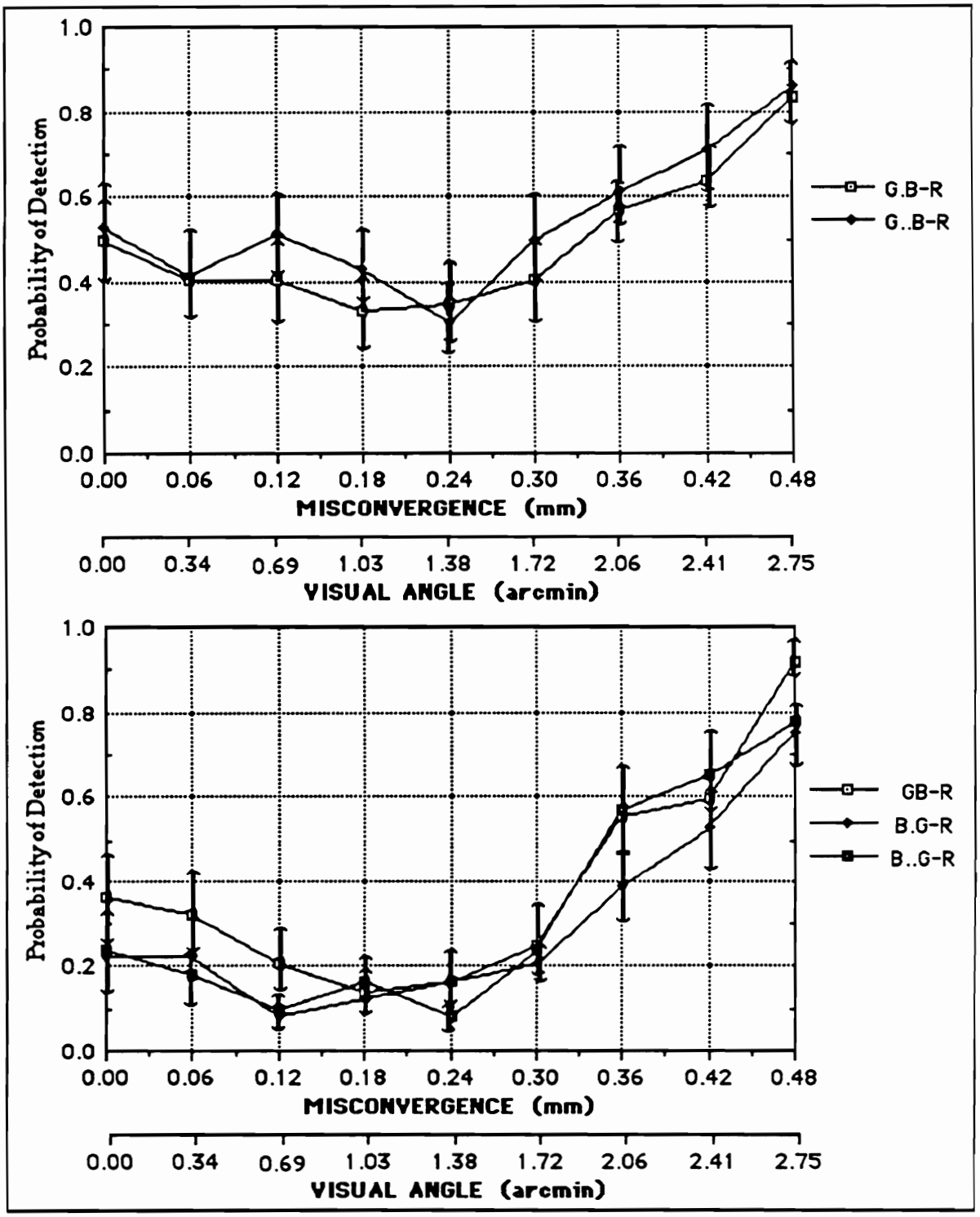

Figure 21. Probability of detection for stimulus presented in cyan or white with red varying color combinations with bars to represent ±1 standard error of the means.

TABLE 3

Analysis of Variance Summary Table for Reading Times

Source of Variance	df	MS	F	p
Between Subjects				
Order (O)	5	655.6584	1.92	0.224
Subjects /Order S(O)	6	340.8713		
Within Subjects				
Misconvergence (M)	8	2.1914	0.84	0.576
M x O	40	3.1848	1.22	0.258
M x S(O)	48	2.6209		
Position (P)	12	3.3497	0.64	0.804
P x O	60	2.5504	0.49	0.998
P x S(O)	72	5.2567		
P x M	96	2.2274	0.88	0.787
P x M x O	480	2.7225	1.07	0.215
P x M x S(O)	575 *	2.5415		
	1402 *			

* One degree of freedom lost due to missing data

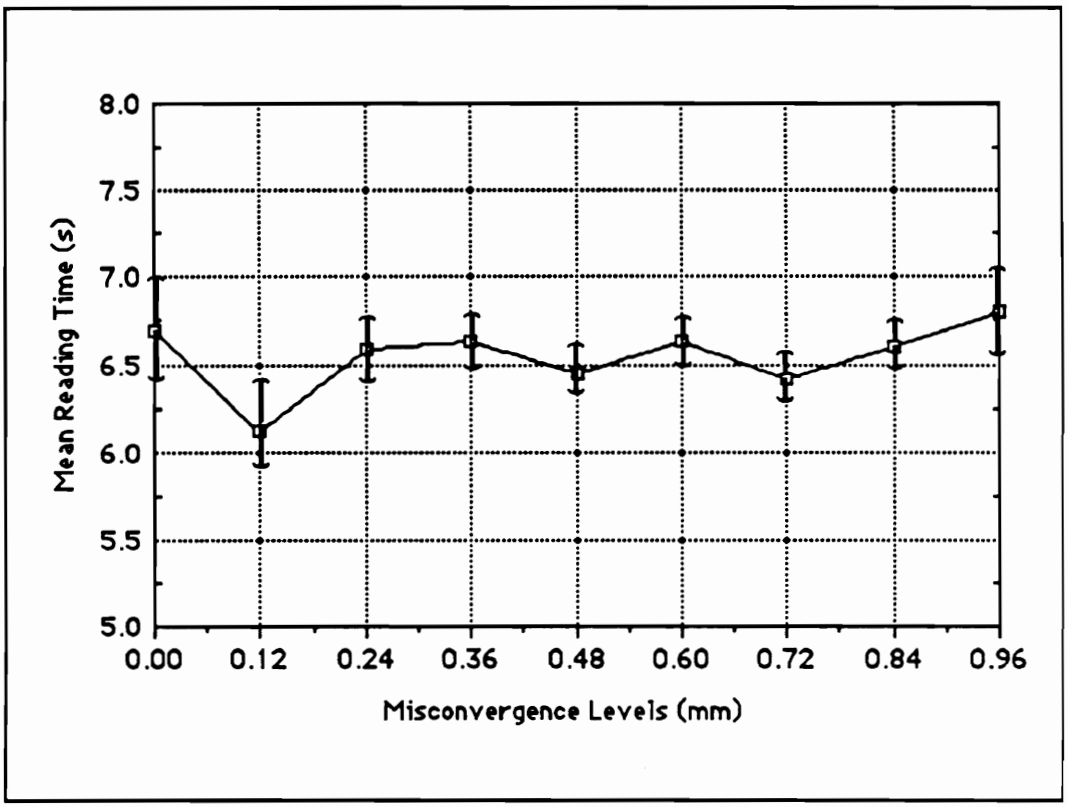

Figure 22. Mean reading times for all levels of misconvergence with bars to represent ±1 standard error of the means.

TABLE 4

Analysis of Variance Summary Table for Subjective Rating Task

Source of Variance	df	MS	F	p
Between Subjects				
Order (O)	5	58.3823	0.98	0.500
Subjects /Order S(O)	6	59.7908		
Within Subjects				
Misconvergence (M)	8	567.1610	119.03	< 0.001
M x O	40	4.6628	0.98	0.525
M x S(O)	48	4.7648		
Position (P)	12	21.6624	6.25	< 0.001
P x O	60	1.9132	0.55	0.991
P x S(O)	72	3.4672		
P x M	96	1.9032	4.04	< 0.001
P x M x O	480	0.4227	0.90	0.891
P x M x S(O)	576	0.4709		
	1403			

are also significant ($p < 0.001$ for both). The effect of the Order in which the tasks were performed, as well as the two- and three-way interactions involving Order, are *not* significant.

Post-hoc tests were performed on the significant Misconvergence X Position interaction. The results of the simple-effects F-tests are presented as Table 5 and reveal that there is a significant difference among the Position means at all levels of Misconvergence ($p < 0.001$). The results of the Newman-Keuls comparisons of the Position means at each Misconvergence level are presented in Figures 23, 24, and 25. The axis indicates the subjective rating. The adjectives associated with each rating are omitted from these figure but are indicated on the associated graphs of the data. The horizontal lines over the axes indicate no significant differences ($p > 0.05$) between or among the means covered by the line.

Based on the Newman-Keuls results, the subjective ratings are plotted against the misconvergence levels. In Figure 26, the means of each of the two-gun pairs are plotted individually across Misconvergence levels. With the exception of the first two misconvergence levels, all of these means are significantly different. Figure 27 presents the means for Positions [GR-B], [G.R-B], and [G..R-B] at the top of the page. These means are significantly different only at the 0.72-mm Misconvergence level. The graph at the bottom presents the means for Positions [R.G-B] and [R..G-B]. These means are *not* significantly different except at the 0.24 mm Misconvergence level. Figure 28 illustrates the means for the remaining five Positions, [B..G-R], [B.G-R], [GB-R], [G.B-R], and [G..B-R]. All of the means within this grouping are *not* significantly different from each other across all levels of Misconvergence.

Correlation Between Dependent Measures

The Pearson product-moment correlations among the three dependent measures are presented in Table 6. Because the threshold detection task used Misconvergence levels that

TABLE 5

Simple-Effects F-Tests for the 13 Beam Positions at Nine Misconvergence Levels for the Subjective Rating Task

Position	df	MS	F	p
P x M x S(O)	576	0.4709		
0.00 mm Misconvergence	12	1.0558	2.24	0.009
0.12 mm Misconvergence	12	1.1521	2.45	0.004
0.24 mm Misconvergence	12	4.4932	9.54	< 0.001
0.36 mm Misconvergence	12	4.3408	9.22	< 0.001
0.48 mm Misconvergence	12	2.8744	6.10	< 0.001
0.60 mm Misconvergence	12	5.0611	10.75	< 0.001
0.72 mm Misconvergence	12	5.9453	12.63	< 0.001
0.84 mm Misconvergence	12	6.5025	13.81	< 0.001
0.96 mm Misconvergence	12	5.4632	11.60	< 0.001

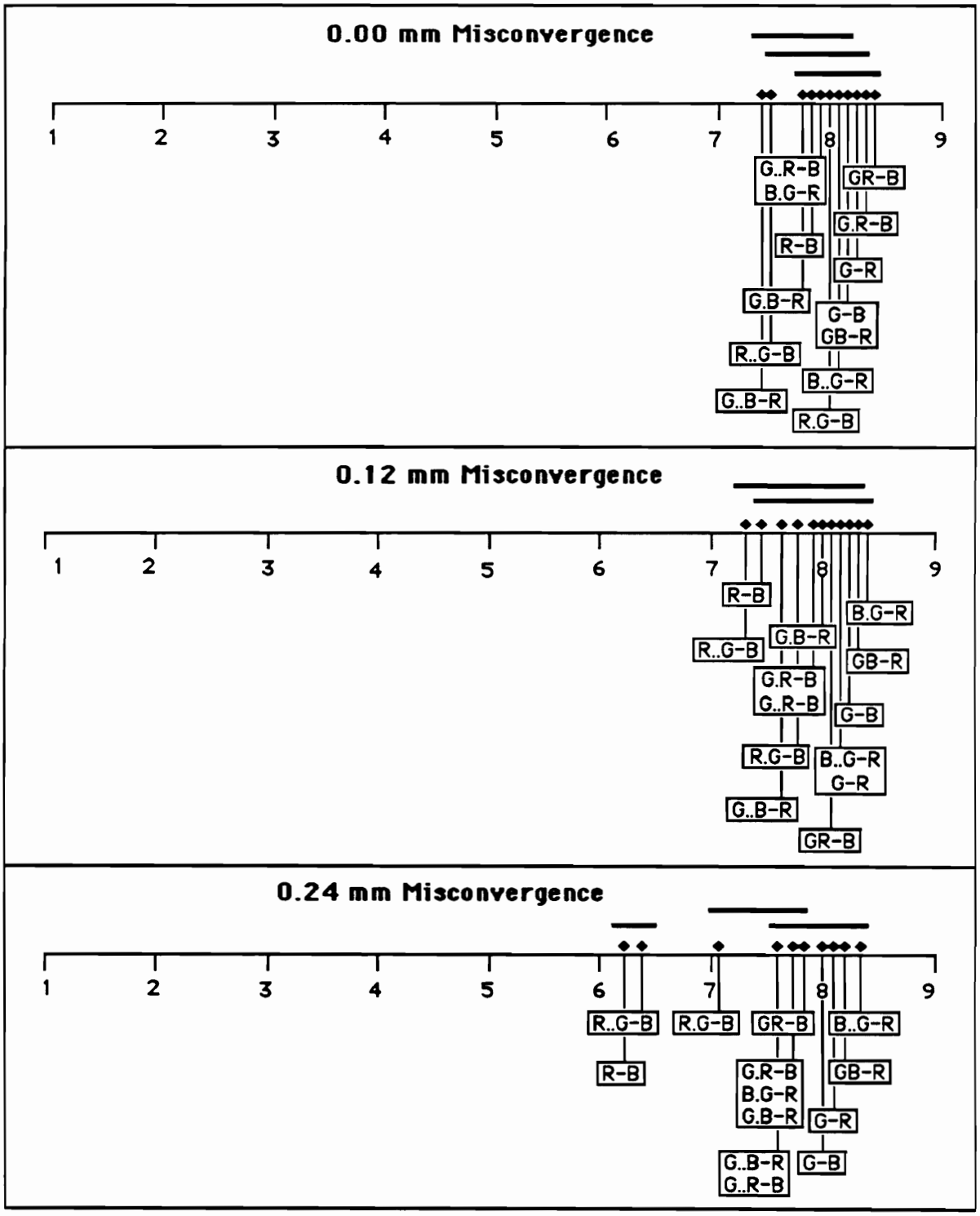

Figure 23. Newman-Keuls comparisons of the subjective rating means of all Positions at 0.00, 0.12, and 0.24 mm levels of Misconvergence.

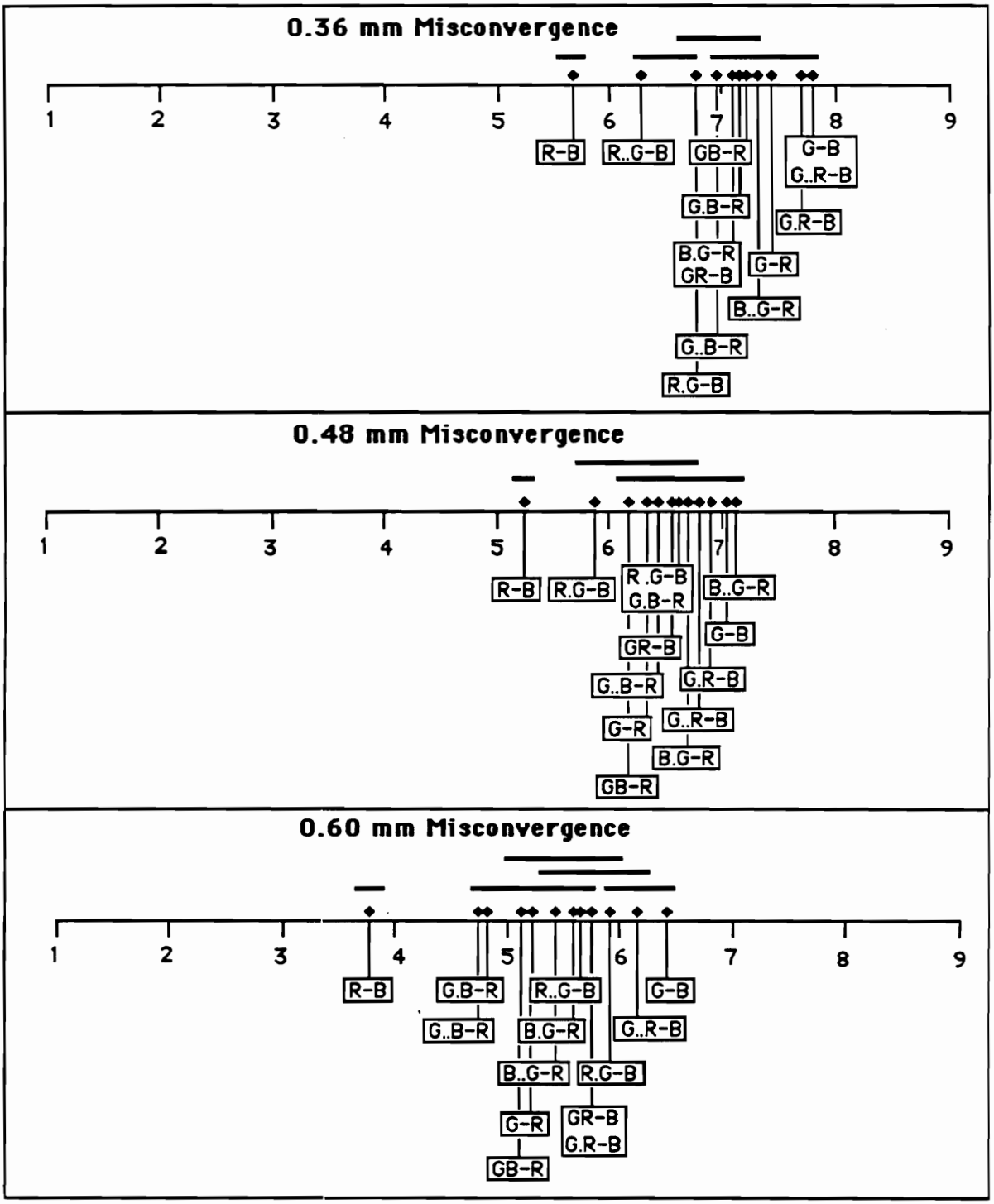

Figure 24. Newman-Keuls comparisons of the subjective rating means of all Positions at 0.36, 0.48, and 0.60 mm levels of Misconvergence.

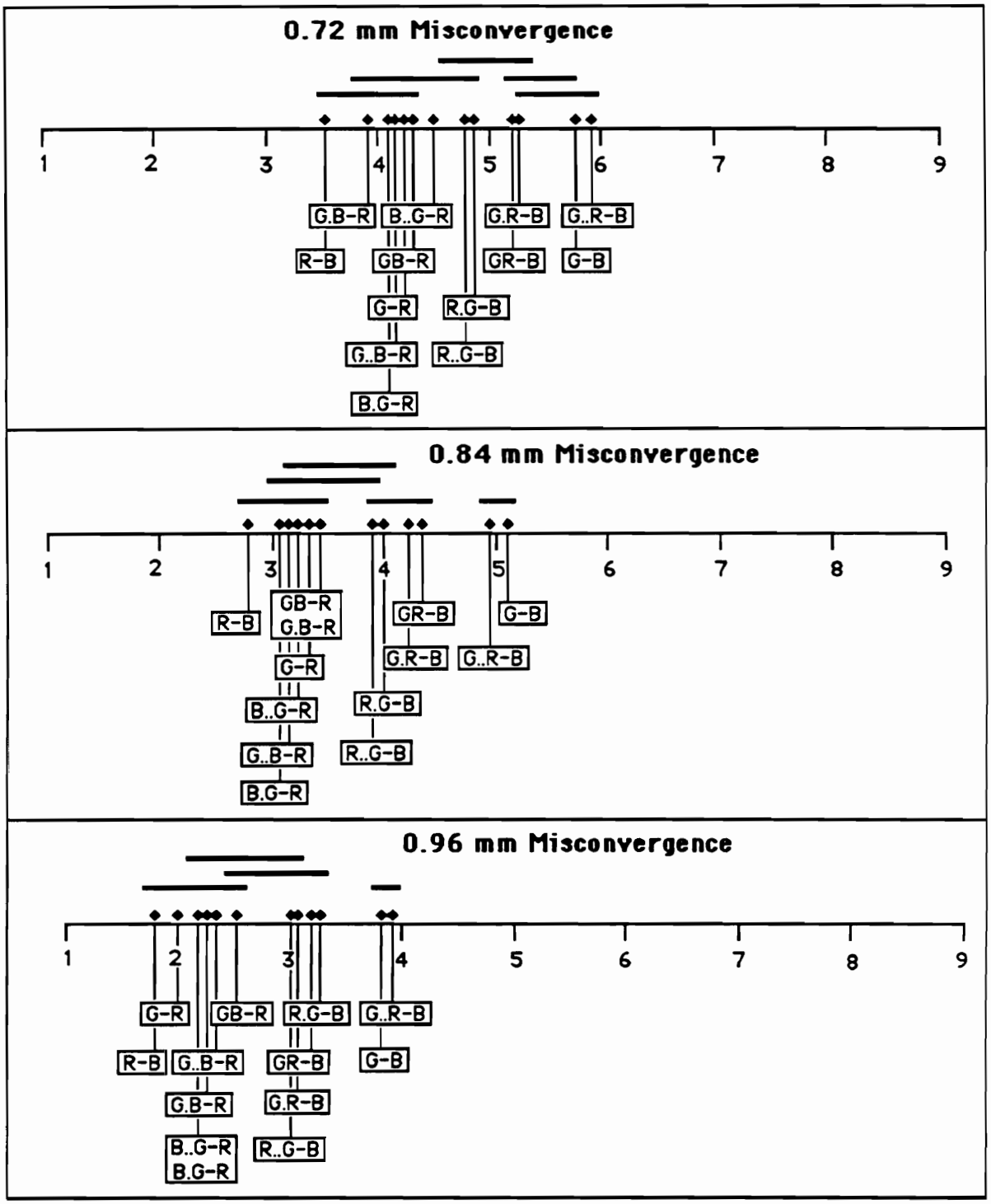

Figure 25. Newman-Keuls comparisons of the subjective rating means of all Positions at 0.72, 0.84, and 0.96 mm levels of Misconvergence.

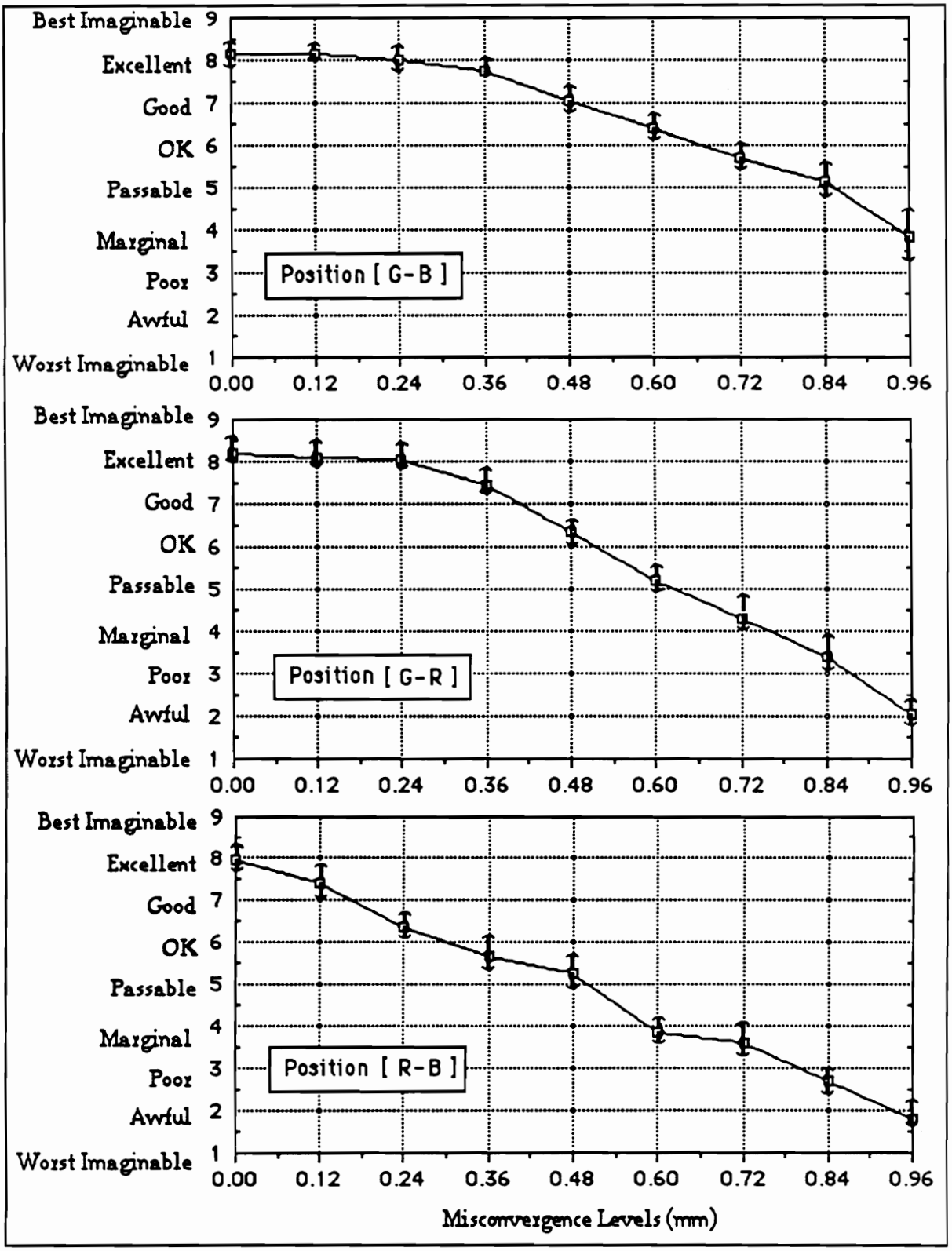

Figure 26. Subjective ratings means for two-beam color combinations with standard error bars.

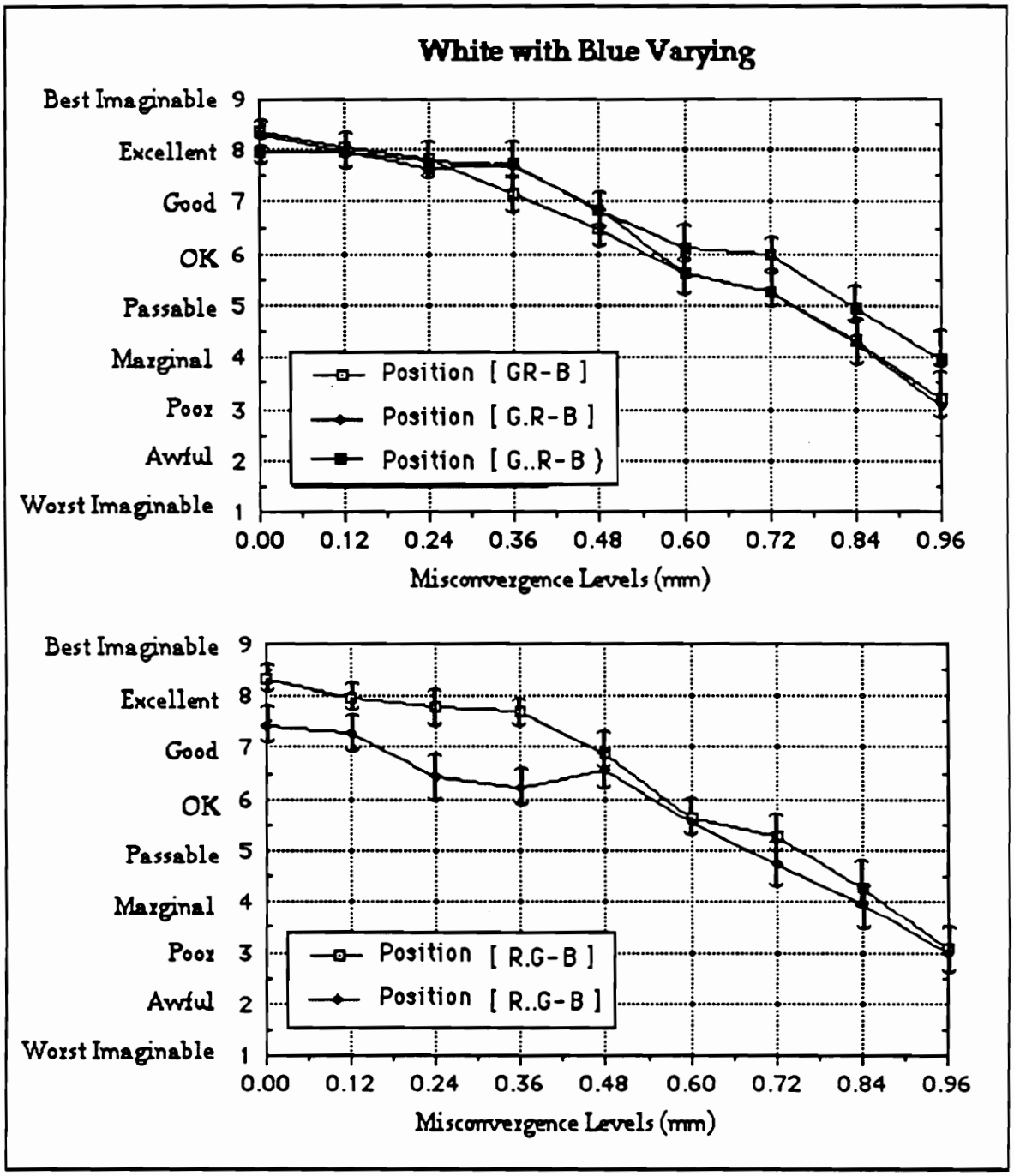

Figure 27. Subjective rating means for white with blue varying color Combinations with standard error bars.

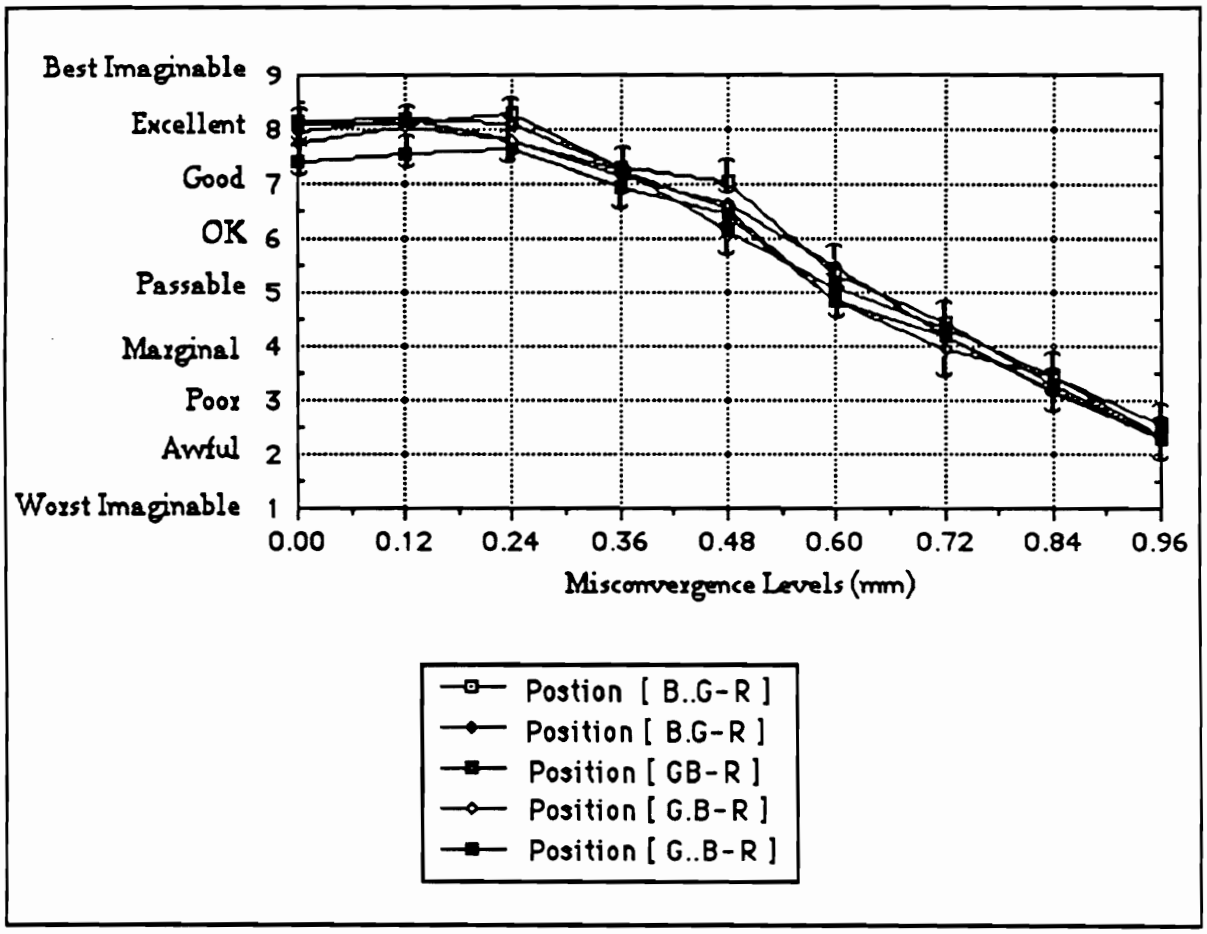

Figure 28. Subjective rating means for white with red varying color combinations with standard error bars.

TABLE 6

Pearson Product-Moment Correlations among Reading Time, Detection Probability, and Subjective Image Quality Ratings

	r	df	p
Reading Time and Detection Probability	- 0.090	65	0.479
Reading Time and Subjective Ratings	- 0.098	117	0.293
Detection Probability and Subjective Ratings	- 0.656	65	< 0.001

contained half the range of misconvergence that was used in the other two tasks, there are only five levels of misconvergence (0.00, 0.12, 0.24, 0.36, and 0.48) in common across the tasks. This constraint accounts for the different number of observations which were used in the correlation.

Reading time is *not* significantly correlated with either detection probability or subjective ratings. However, detection probability and subjective ratings are correlated ($r = -0.6560$, $p < 0.001$). As can be seen in Figure 29, the subjective ratings decrease with increased detection.

Flexible Beam Profile

One of the major components of the Color CRT MTF Model is the ability to represent each electron beam profile with an appropriate profile. The Johnson translation system was used to generate the beam profiles from the user specified kurtosis and skewness values. Figure 30 provides examples of three composite beam profiles which follow Gaussian, platykurtic, and leptokurtic distributions. Notice that these profiles were generated with a very wide (10 mm) FWHM spot size to demonstrate the profiles. The profiles used to simulated the display in this experiment were narrower.

Sampled Spot Profiles

The first step in the completed Color CRT MTF model is to generate the proper spot profile and to sample it with an appropriate shadow-mask phosphor-dot filter. Figure 31 shows the individually sampled beam profiles which combine for a converged white spot profile. This profile simulates Positions 6 [GR-B] and 11 [GB-R] at the 0.00 Misconvergence level. Note that the spot profile is in phase with the sampling filter, which means that the center of the green gun profile is aligned with the center of the shadow-mask aperture. The differences in

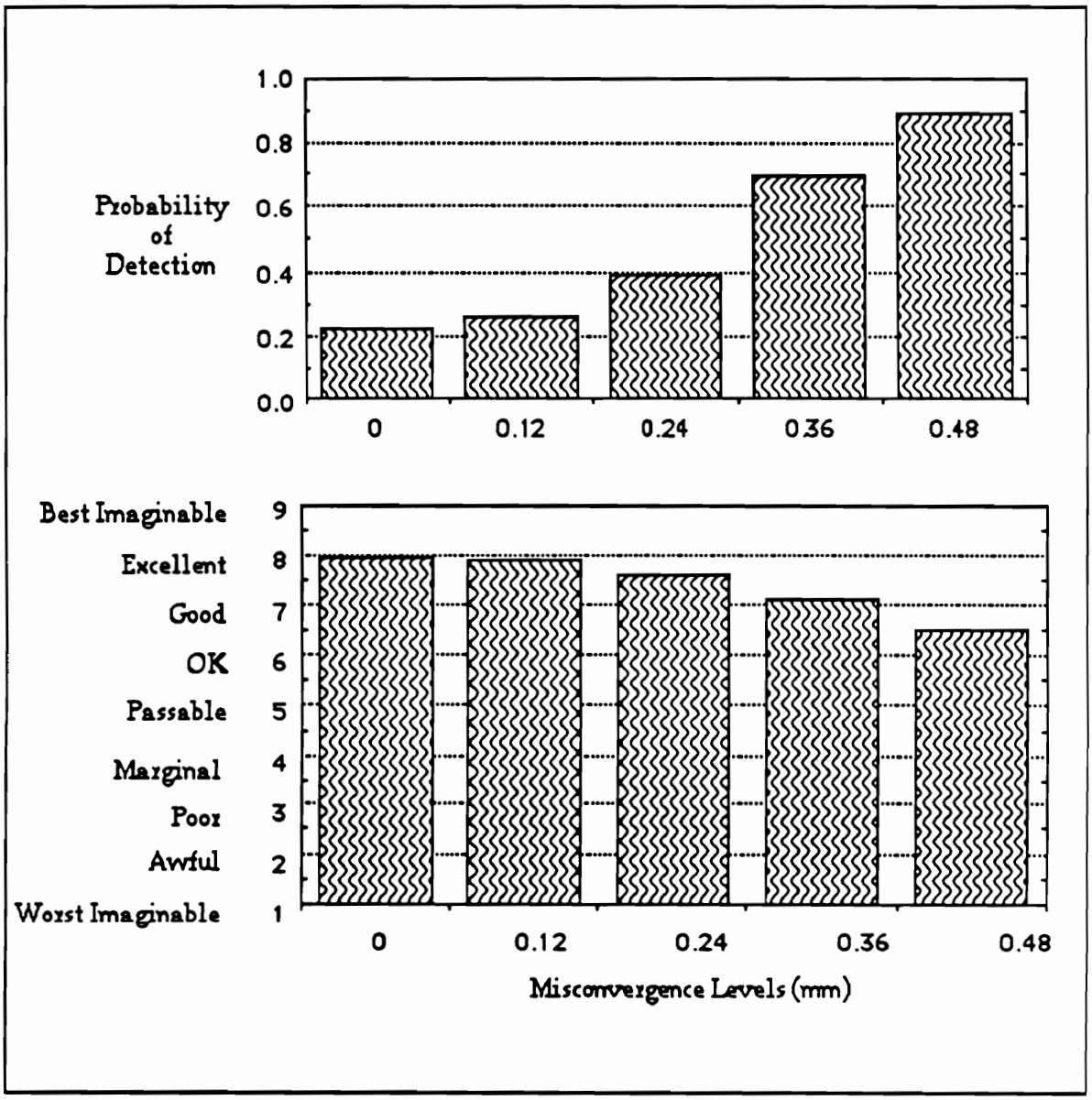

Figure 29. Probability of detection and subjective ratings for all levels of misconvergence.

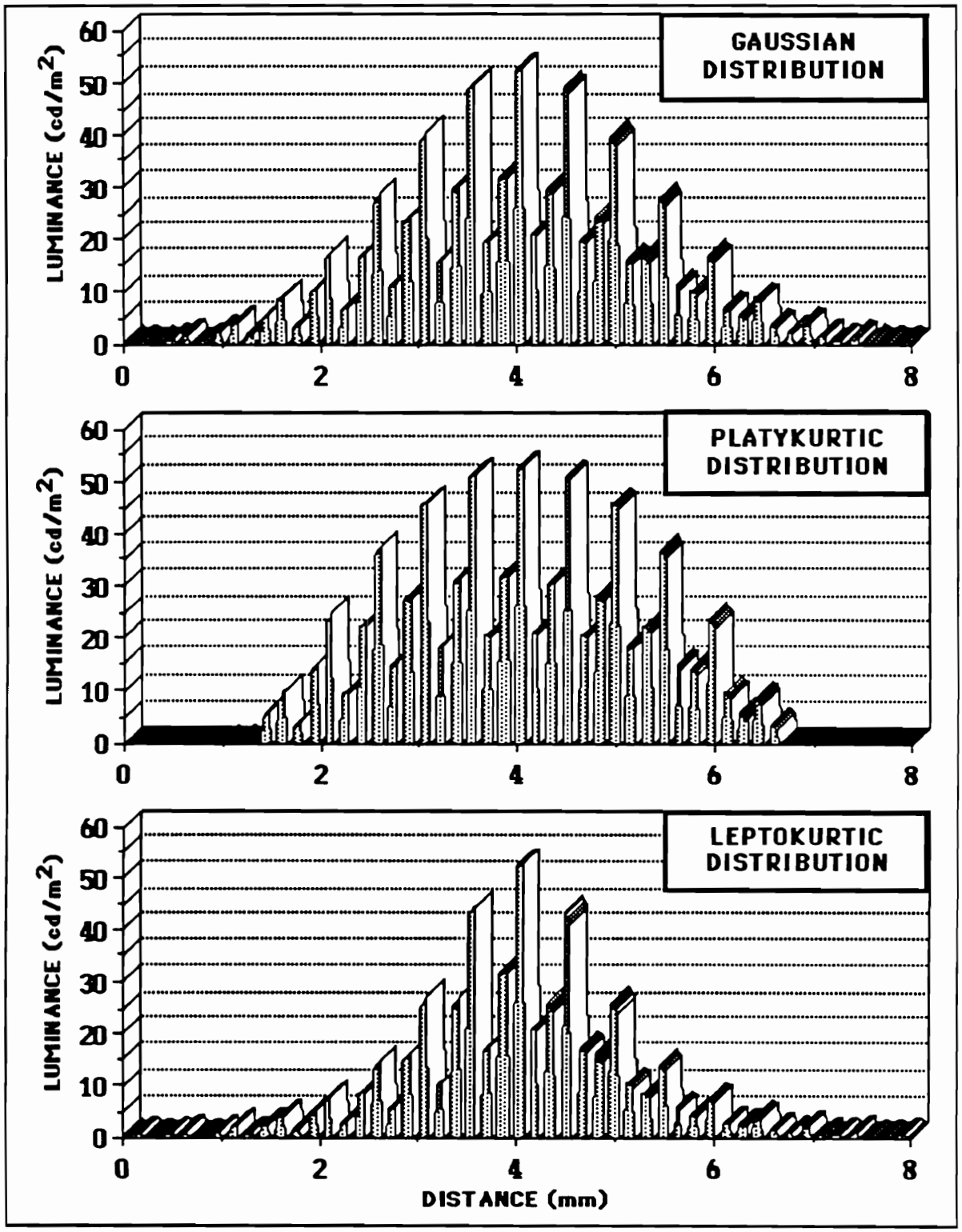

Figure 30. Flexible beam profiles generated by the Color CRT MTF Model.

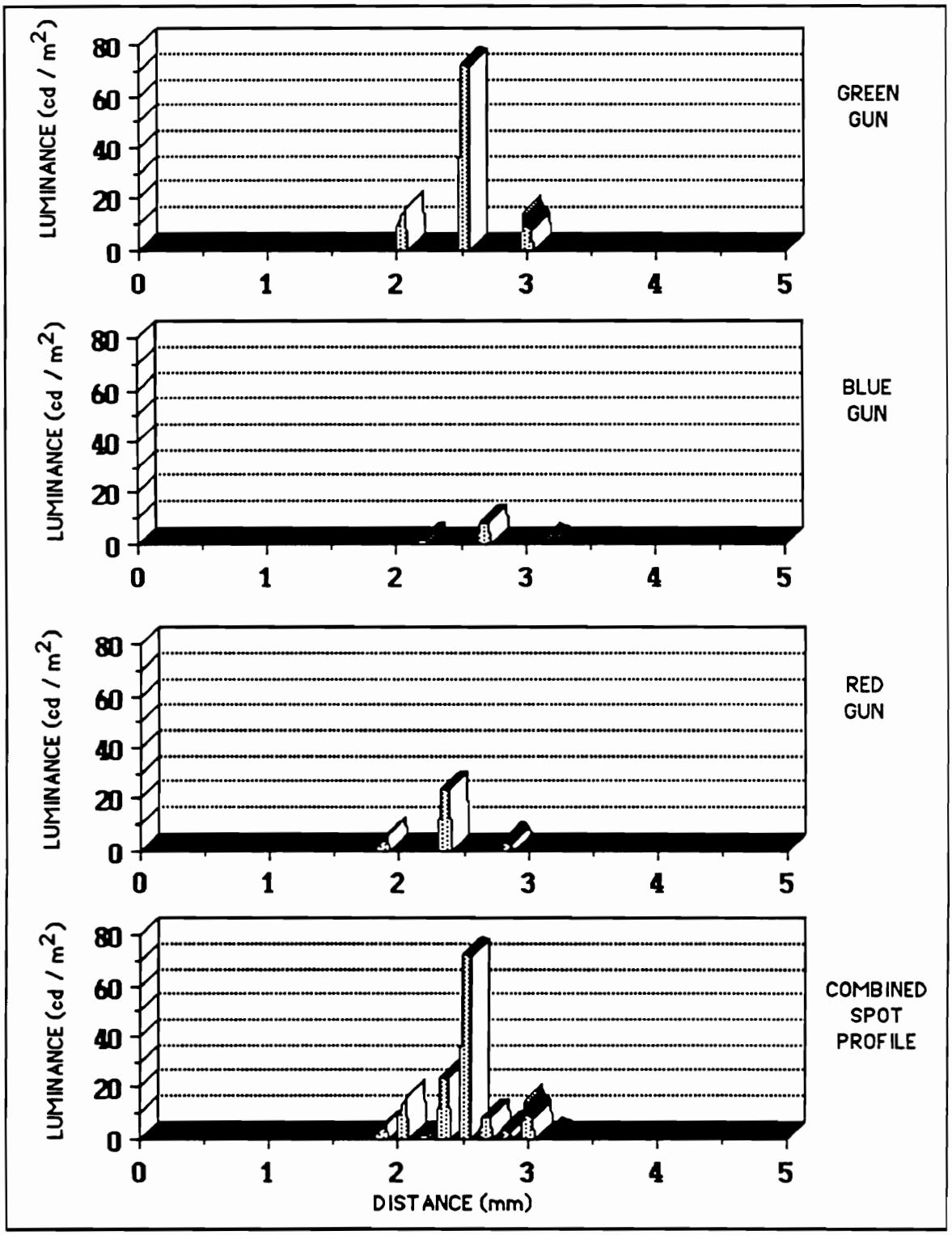

Figure 31. Beam profiles from converged green, blue, and red guns combined into a spot profile (i.e., Position 6 [GR-B] and Position 11 [GR-B] at the 0.00 Misconvergence level).

luminance (cd/m^2) from each of the individual guns are seen in the heights of each of the profiles. This figure also demonstrates the inherent shift in the centers of the green, blue, and red guns which results from the physical spacing of the phosphor dots.

Figure 32 presents the same information, except that the desired spot profile is misconverged. This profile simulates the Position 4 [R..G-B] at the largest amount of Misconvergence that was was used in the performance experiment. At this Position and Misconvergence level, the blue gun is misconverged to the right by 0.96 mm while the red gun is misconverged to the left by -0.12 mm from the green gun. Figure 33 presents the same information for the other maximally misconverged white spot profile (i.e., Position 9 [B..G-R] at the 0.96 Misconvergence level). A comparison between Figures 32 and 33 reveals a difference between these two misconvergence white spot profiles. This difference is a result of the physical placement of the phosphor dots, that is, the red phosphor dot to the left of the green while the blue is to the right.

Color CRT MTF

The combined spot profiles for each of the converged white profile and the two misconverged white profiles (discussed above) are presented as Figures 34, 35, and 36 with their associated MTFs. Notice that these functions terminate at the Nyquist limit (6.2 cycles per mm), which is the inverse of the horizontal phosphor dot pitch (0.162 mm). This results from the sampling theory which states that "any band-limited function can be specified exactly by its sampled values, taken at regular intervals, provided that these intervals do not exceed some critical sampling interval" (Gaskill, 1978, pp. 267). At the bottom of each of these figures are the associated image quality metrics computed for each of these conditions. These graphs represent the final output of the Color CRT MTF model for any given set of conditions. The user

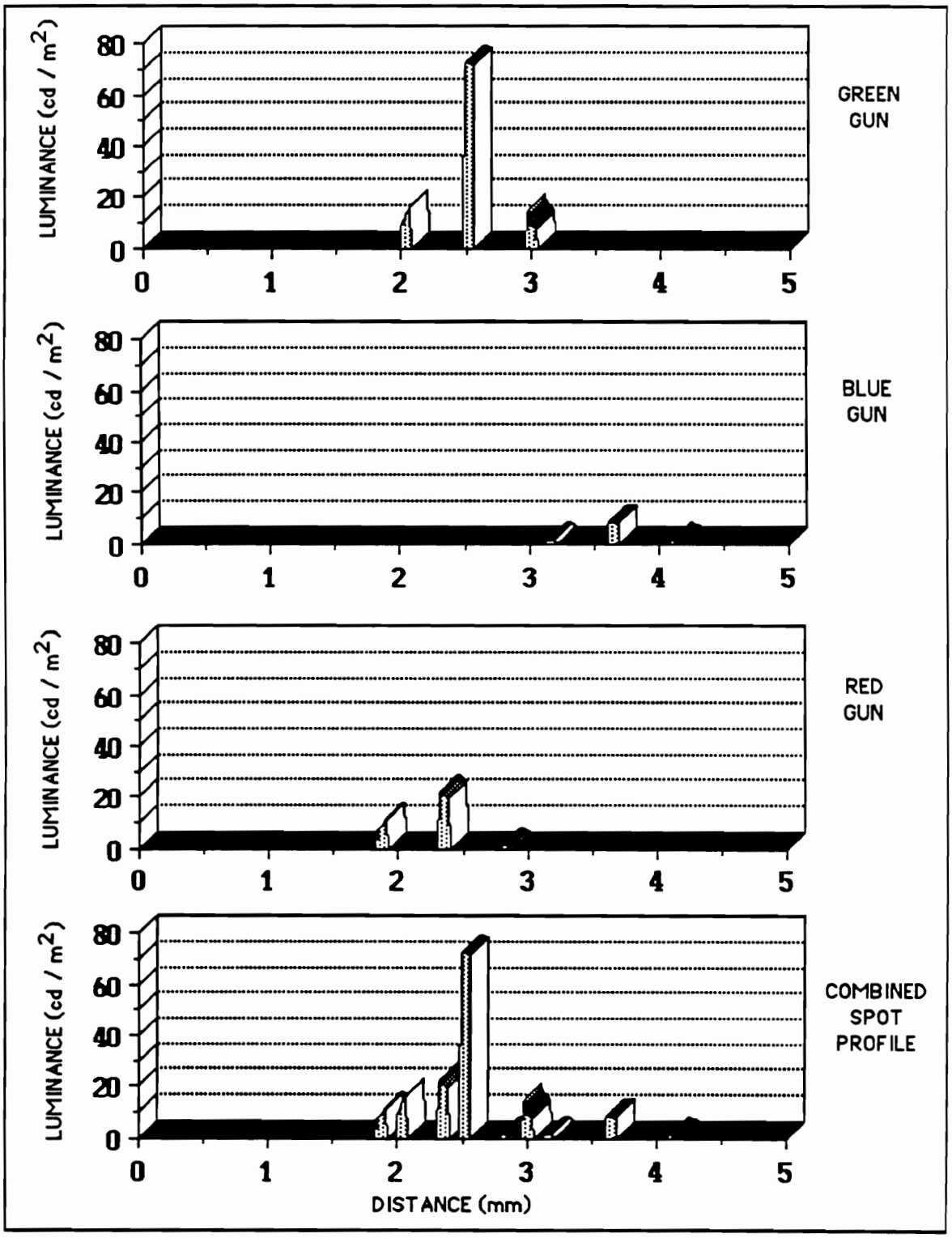

Figure 32. Beam profiles from misconverged green, blue, and red guns combined into a spot profile (i.e., Position 4 [R..G-B] at the 0.96 Misconvergence level).

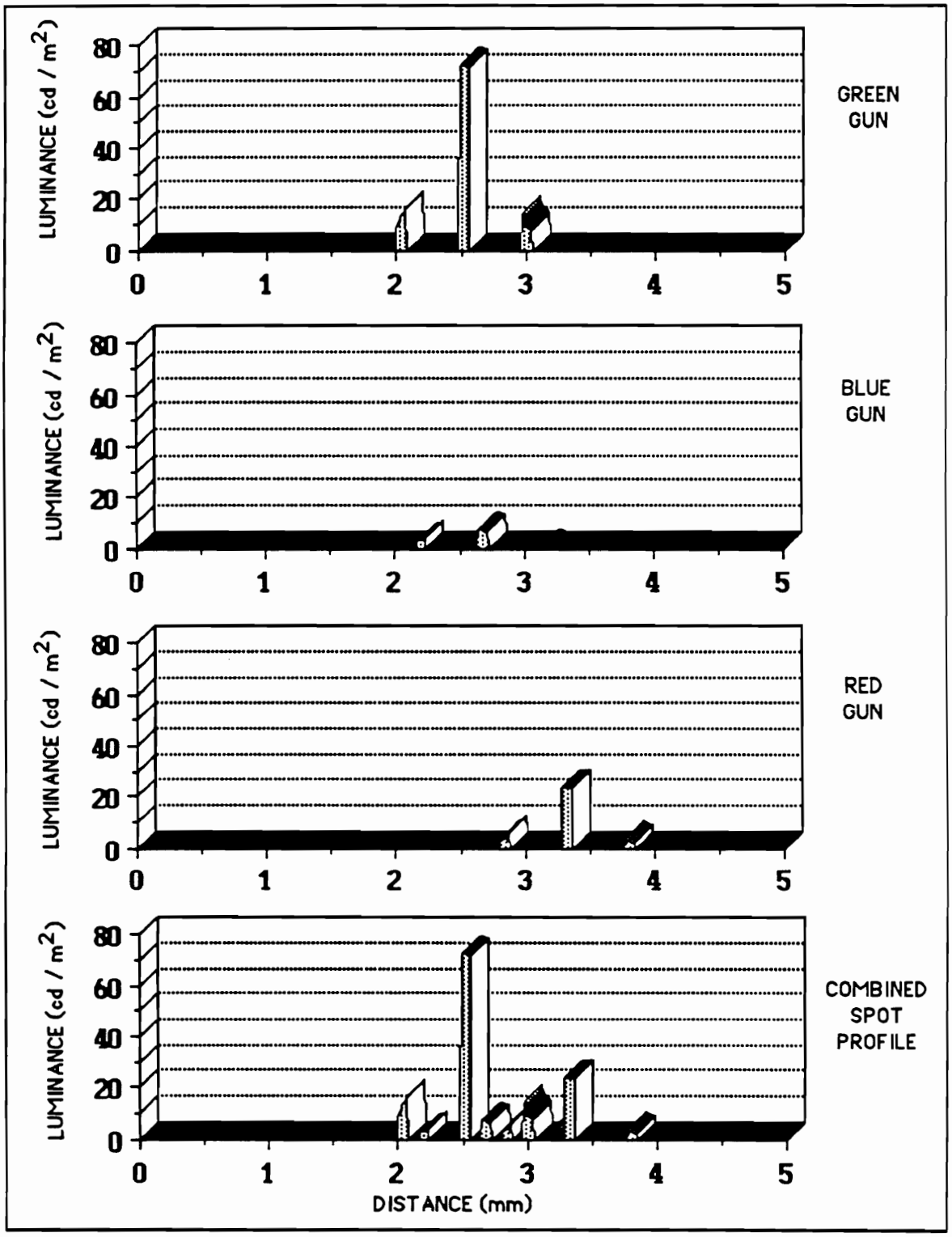

Figure 33. Beam profiles from misconverged green, blue, and red guns combined into a spot profile (Position 9 [B..G-R] at the 0.96 Misconvergence level).

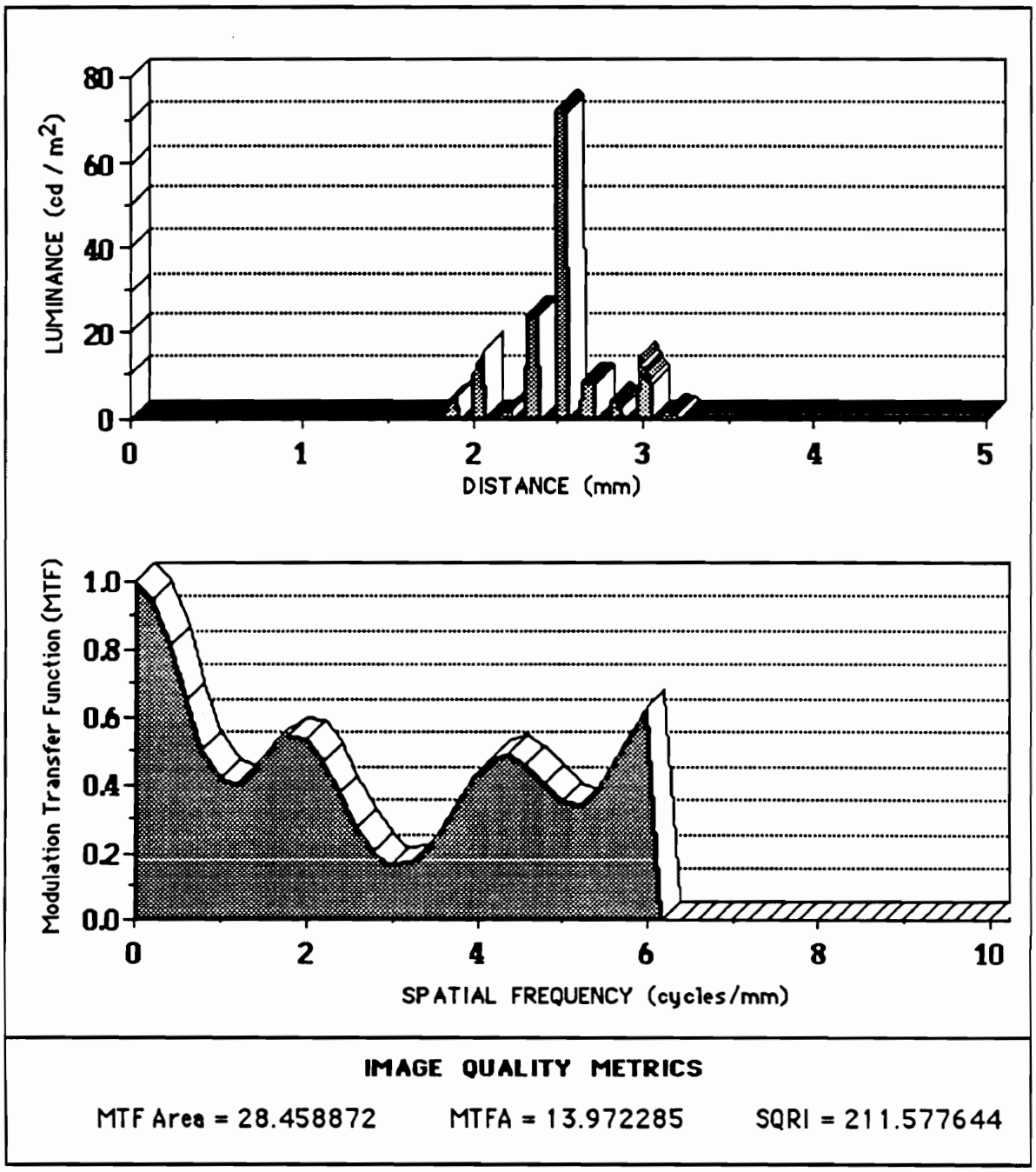

Figure 34. Results from the Color CRT MTF model for Positions 6 [GR-B] and 11 [GB-R] at the 0.00 Misconvergence level.

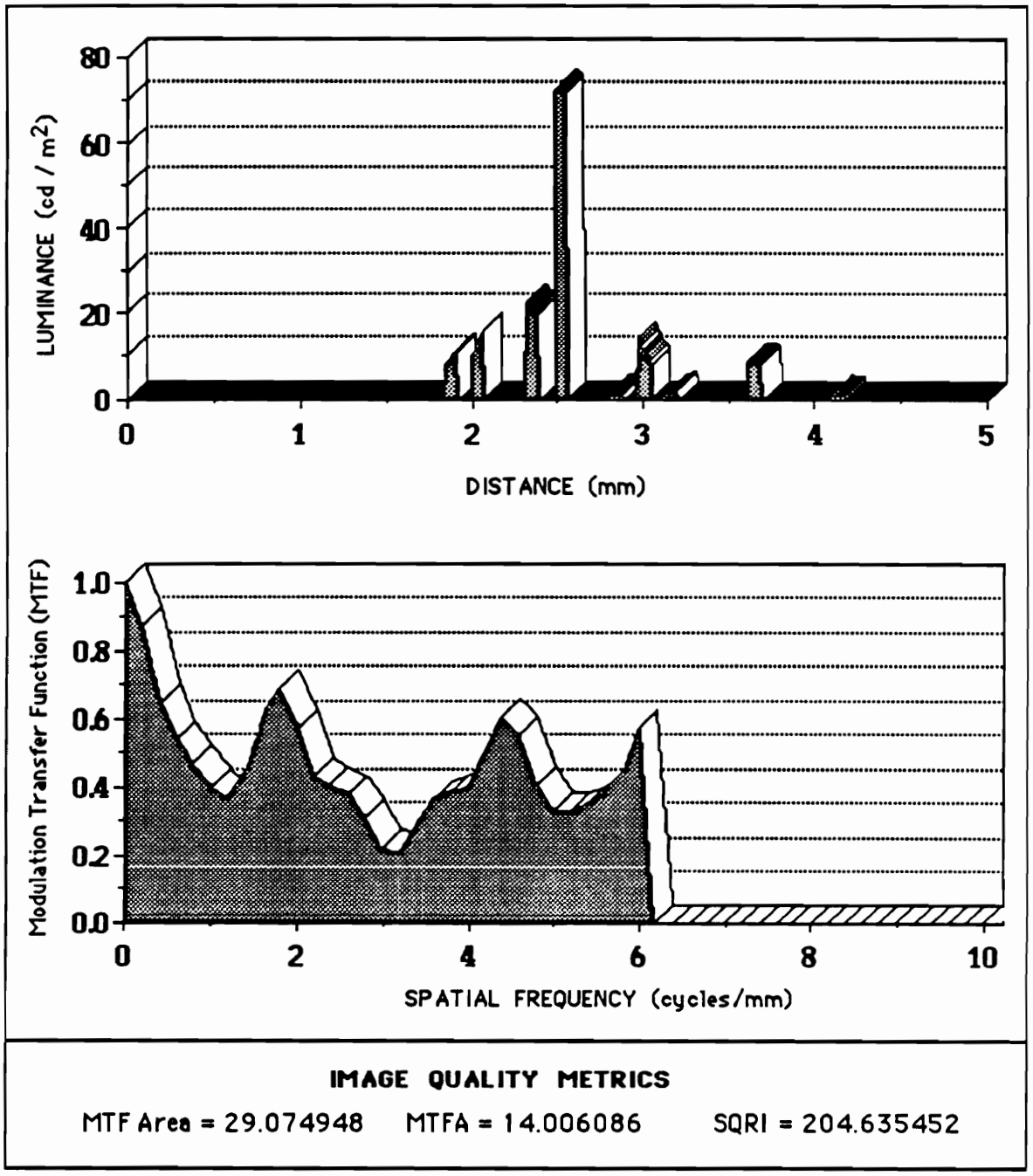

Figure 35. Results from the Color CRT MTF model for Position 4 [R..G-B] at the 0.96 Misconvergence level.

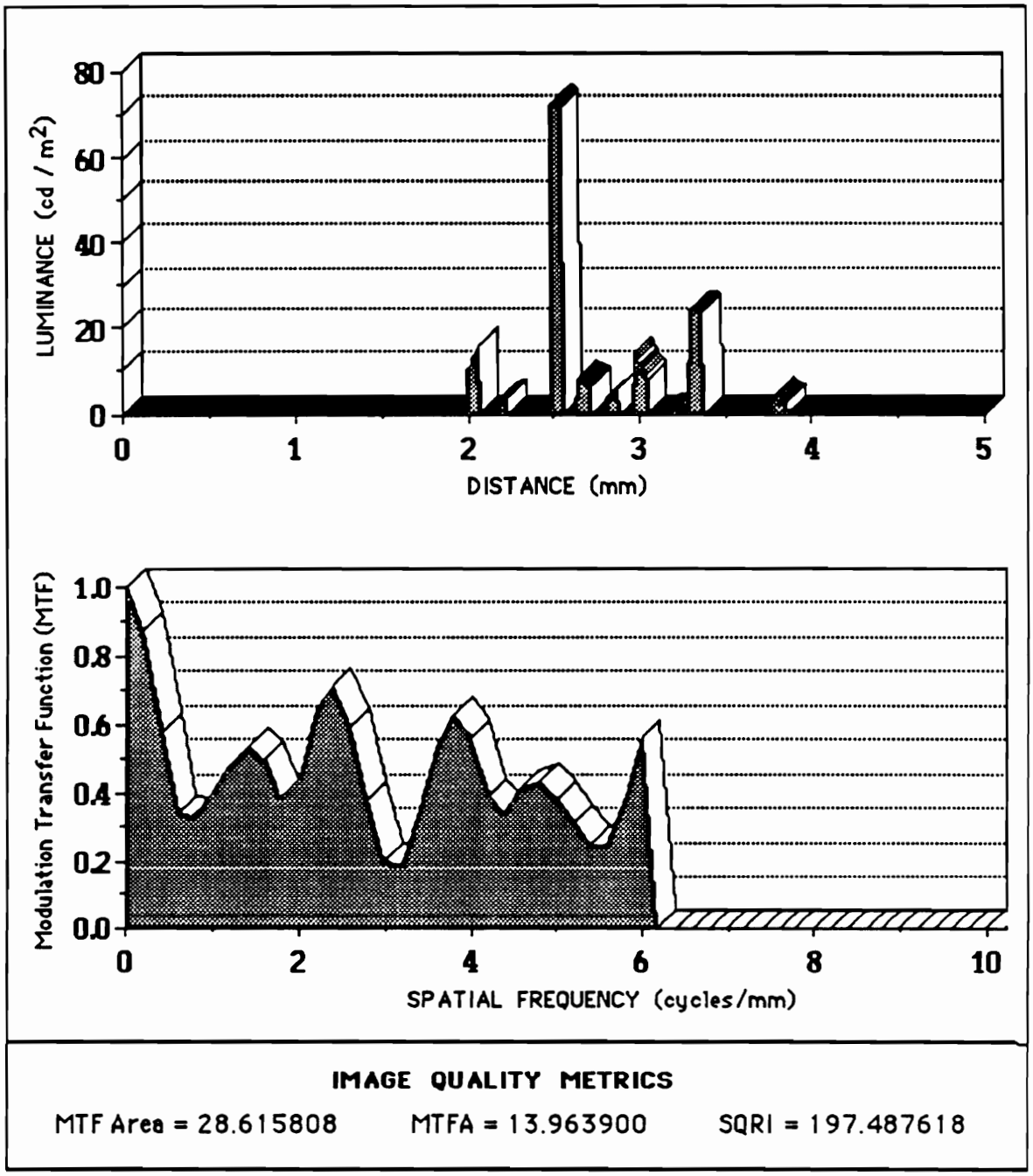

Figure 36. Results from the Color CRT MTF model for Position 9 [B..G-R] at the 0.96 Misconvergence level.

may then vary the conditions, for example, the FWHM or the level of misconvergence, and recompute the model.

Correlations Between Image Quality Metrics and Performance

As previously indicated, three image quality metrics are calculated by the Color CRT MTF model (i.e., MTF Area, MTFA, and SQRI). As Misconvergence increases, image quality metrics are expected to indicate image degradation by decreasing in value. Therefore, it is expected that image quality metrics will be negatively correlated with performance measures (i.e., the probability of detection) which increase with the levels of Misconvergence and positively correlated with measures (i.e., subjective ratings) which decrease with greater Misconvergence.

Probability of Detection. Table 7 presents the correlations between the computed image quality metrics at each level of Misconvergence for each Position with the probability of detection results. The correlations between the three image quality metrics and probability of detection are generally significant ($p < 0.01$), with the exception of the MTFA metric for Position 4 [R..G-B]. As can be seen in Figure 37, the MTFA metric for Position 4 [R..G-B] takes a slight dip in the middle before a slight increase. Hence, a lesser correlation ($r = 0.488$) exists than the other Positions. For all other positions, increases in the probability of detection are correlated with increases in the MTFA metric and decreases in the SQRI metric. That is, greater misconvergence (as indicated generally by greater probability of detection of misconvergence) is accompanied with an *increase* in predicted image quality from MTFA and a *decrease* in predicted image quality from SQRI. These relationships are illustrated with the results for Position 6 [GR-B] (Figure 38).

Two Positions deviate from the overall pattern. For Position 2 [B-R] the MTFA metric is negatively correlated with the probability of detection, and for Position 3 [G-R] the MTF Area

Table 7. Correlations between Image Quality Metrics and Probability of Detection.

Position Number	MTF Area	MTFA	SQRI
1 [B-G]	0.988 **	0.986 **	-0.980 **
2 [B-R]	0.806 **	- 0.934 **	-0.918 **
3 [G-R]	- 0.908 **	0.959 **	-0.983 **
4 [R..G-B]	0.964 **	0.488	-0.965 **
5 [R.G-B]	0.957 **	0.916 **	-0.955 **
6 [GR-B]	0.993 **	0.984 **	-0.992 **
7 [G.R-B]	0.986 **	0.993 **	-0.991 **
8 [G..R-B]	0.963 **	0.969 **	-0.916 **
9 [B..G-R]	0.940 **	0.845 **	-0.891 **
10 [B.G-R]	0.972 **	0.896 **	-0.857 **
11 [GB-R]	0.905 **	0.948 **	-0.820 **
12 [G.B-R]	0.882 **	0.950 **	-0.823 **
13 [G..B-R]	0.861 **	0.947 **	-0.800**

** $p < 0.01$

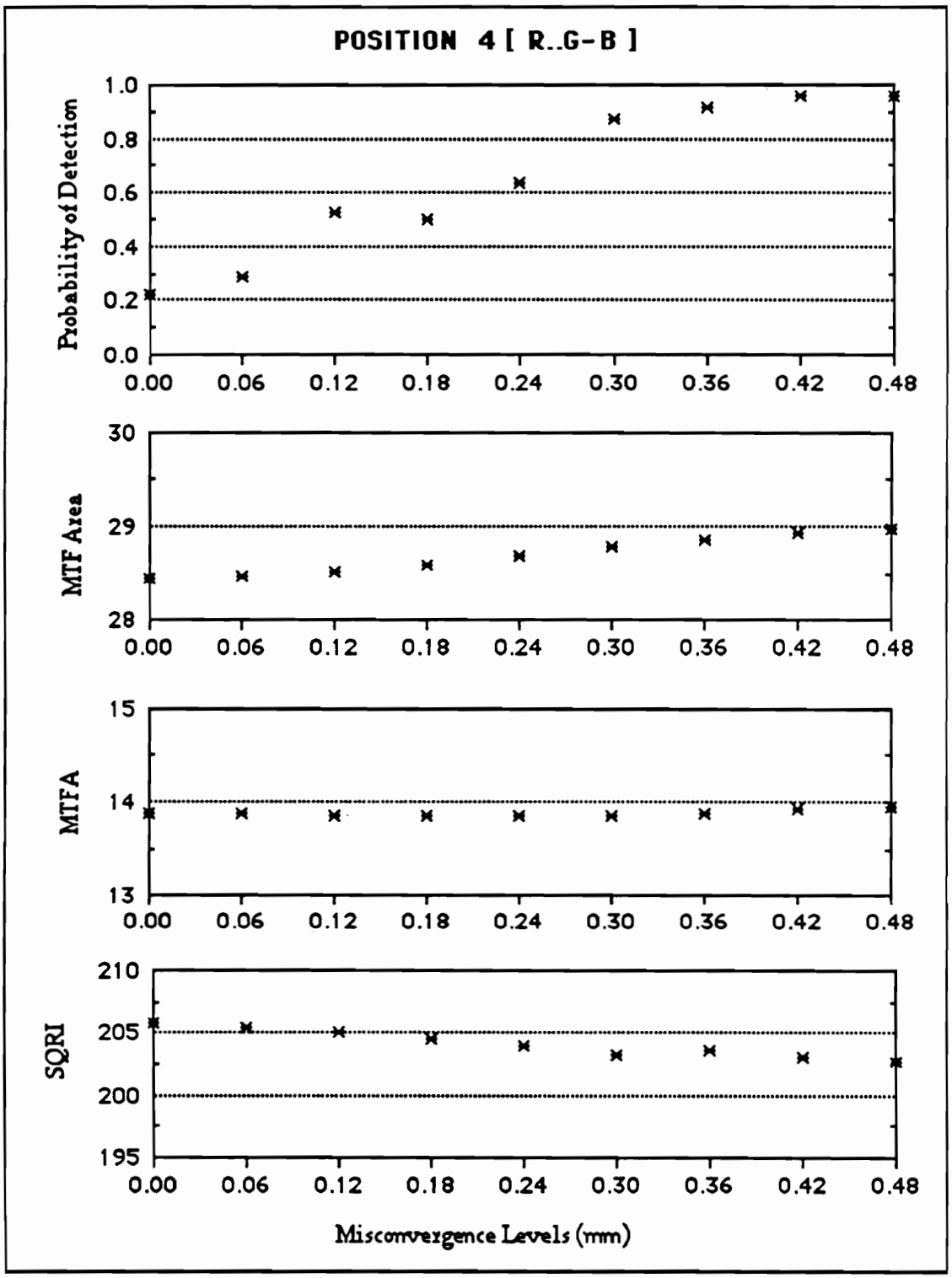

Figure 37. Probability of detection and the computed metrics for Position 4 [R..G-B] at all levels of Misconvergence.

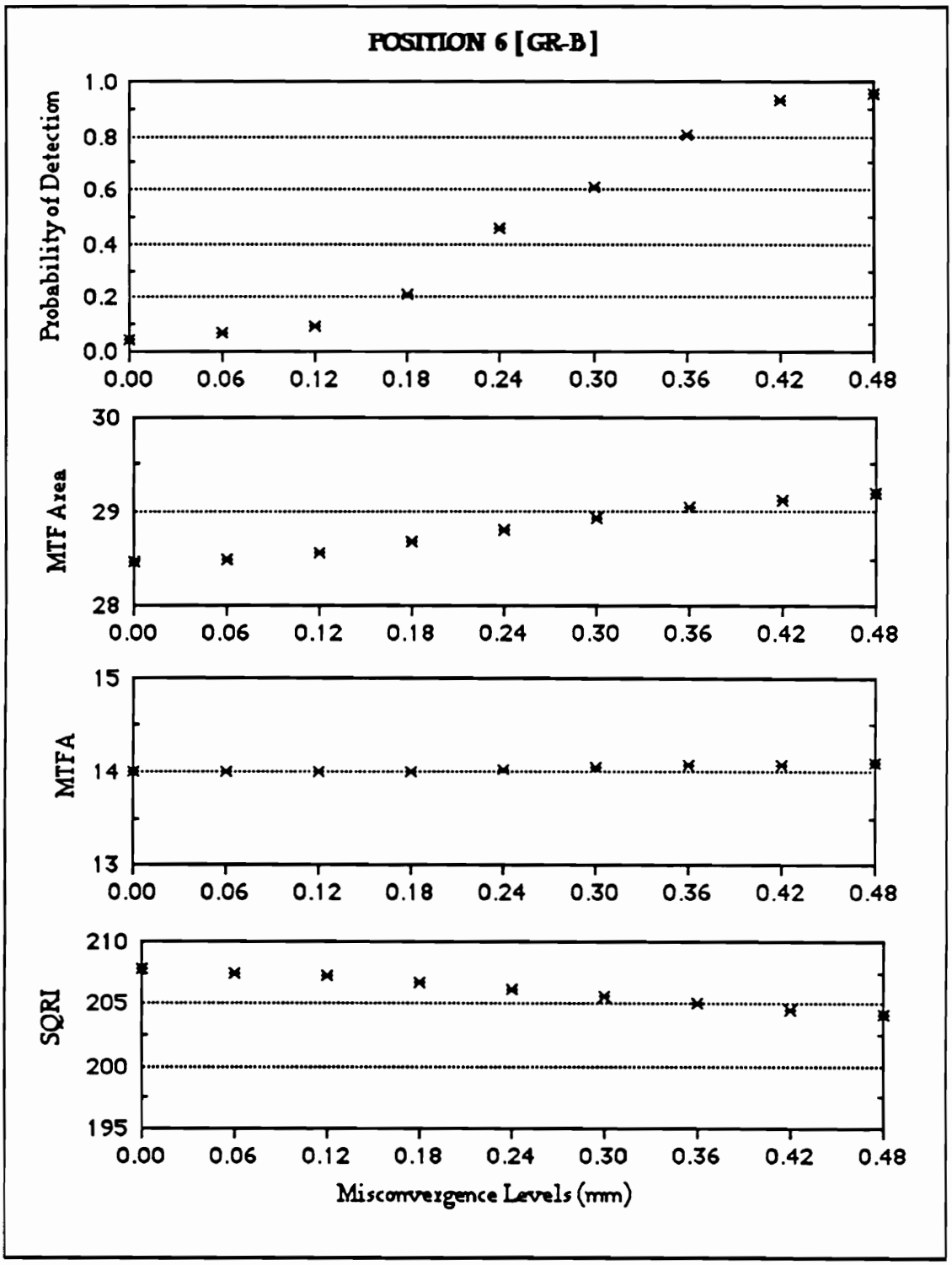

Figure 38. Probability of detection and the computed metrics for Position 6 [GR-B] at all levels of Misconvergence.

negatively correlates with the probability of detection. An examination of the data for these Positions (see Figures 39 and 40) shows the subtle changes in direction, which are responsible for the changes in sign. Even though the trend is slight, it is sufficient to affect the overall correlations.

It should be noted, however, that the probabilities of detection range from nearly zero to nearly unity, that is, over the full range. However, the range of MTF Area (or MTFA or SQRI) is very small, less than 2% of its mean value (see Figures 37 to 40). Thus, while the correlations may be high and statistically significant, the predicted change in image quality, even though in the different directions, is very small and lacking practical significance.

Reading Time. Table 8 presents the correlations between the reading times and the computed image quality metrics for each level of Misconvergence at each Position. As expected, none of the correlations is significantly different from zero.

Subjective Rating. The correlations between the subjective ratings and the computed metrics are presented as Table 9. Since the subjective ratings have been shown to be negatively correlated with the probability of detection, it is anticipated that these correlations will be in the opposite direction as the correlations just discussed. Recall that the range of misconvergence used in the subjective task is twice as wide as the range of convergence used in the detection task. Therefore, the data presented for the previous correlations (Figures 37-40) cover one-half the data range that will be presented for the correlations between subjective ratings and the metrics (Figures 41-43).

The correlations in Table 9 are not as consistent as those for the probability of detection. The first three positions represent the two-gun combinations, with only Position 3 [G-R] (Figure 41) exhibiting significant correlation between the subjective ratings and all three metrics. A comparison between the detection data for Position 3 (Figure 40) and the subjective data (Figure

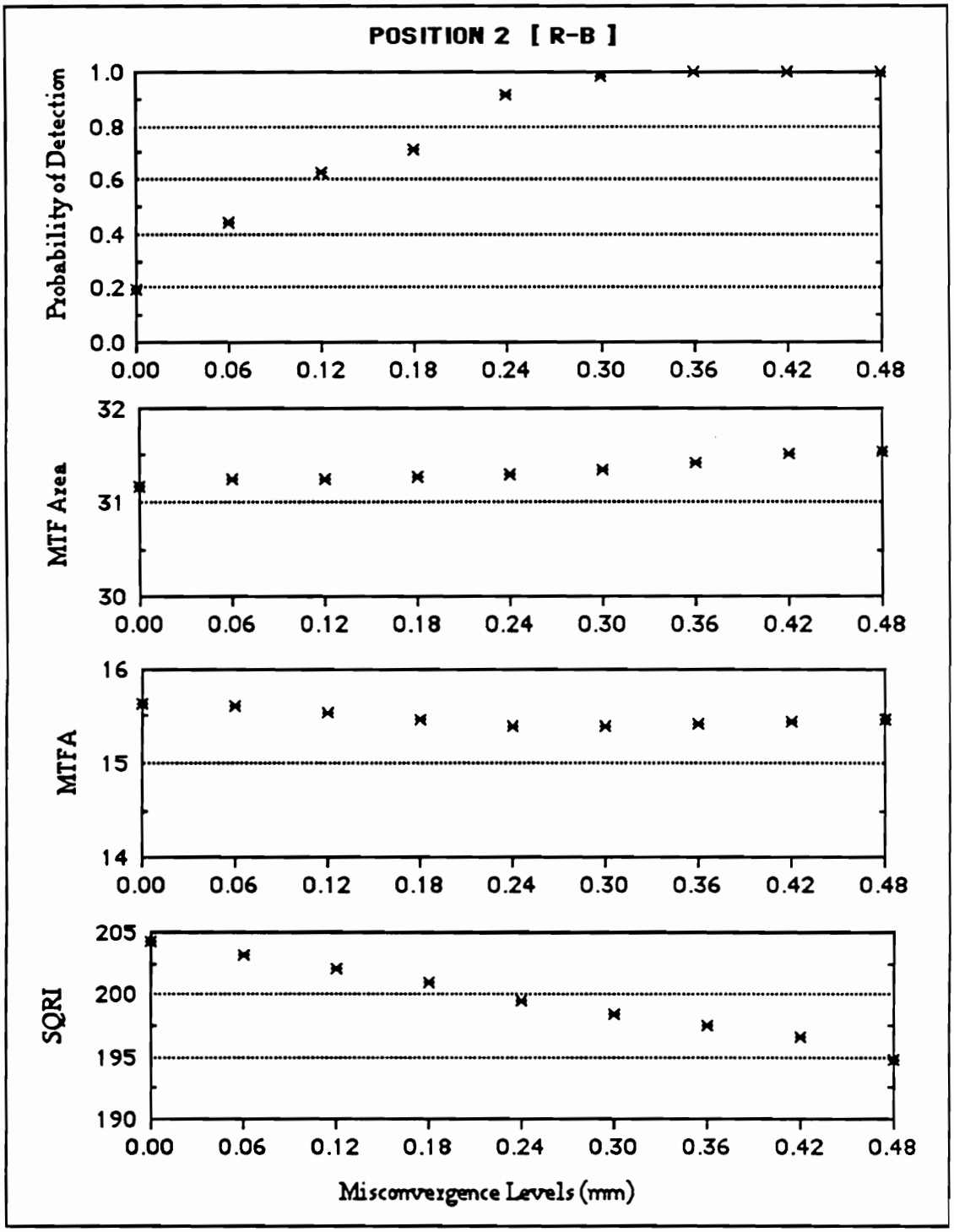

Figure 39. Probability of detection and the computed metrics for Position 2 [R-B] at all levels of Misconvergence.

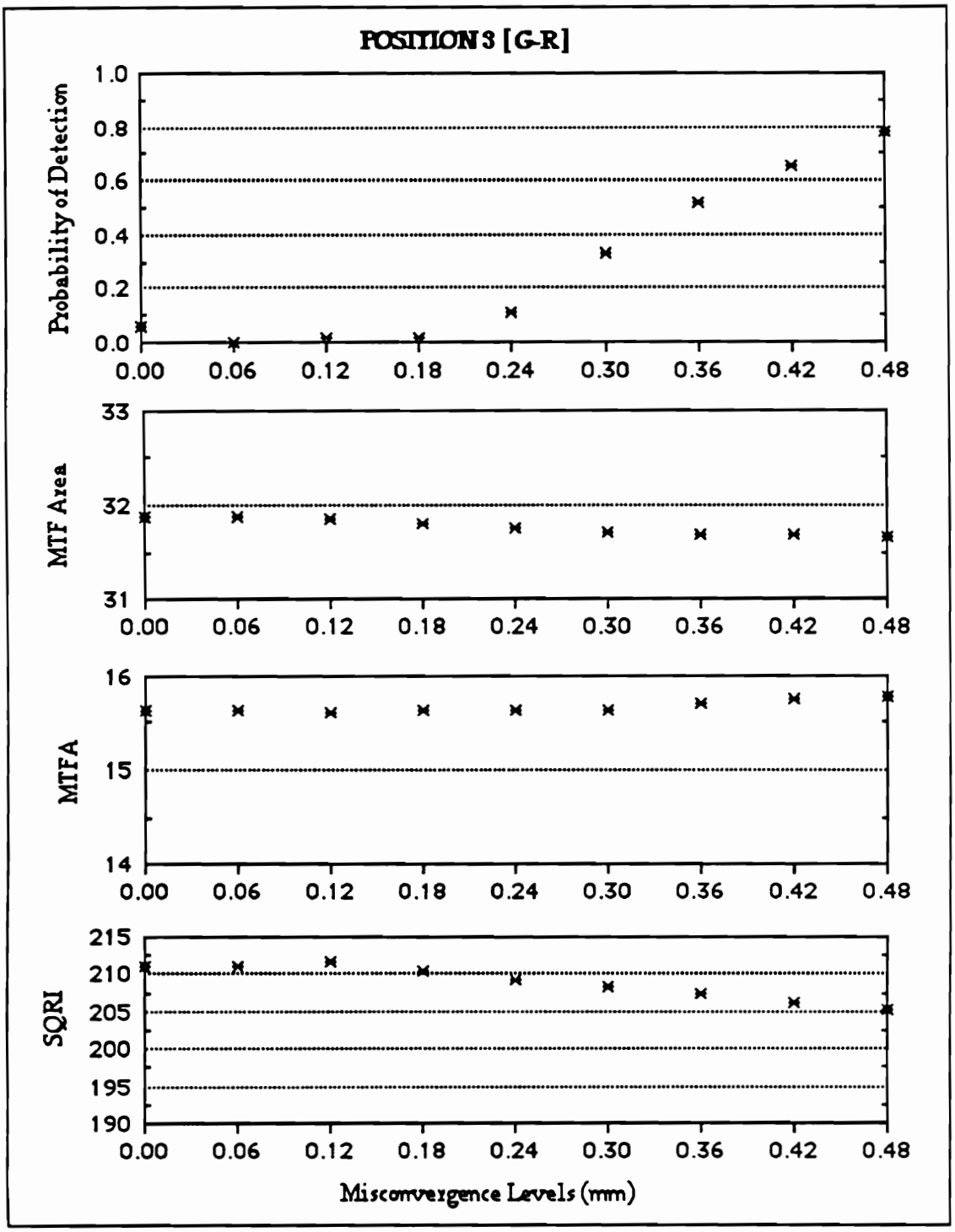

Figure 40. Probability of detection and MTF Area for Position 3 [G-R] at all levels of Misconvergence.

Table 8. Correlations between Image Quality Metrics and Reading Time.

Position Number	MTF Area	MTFA	SQRI
1 [B-G]	0.315	0.491	0.446
2 [B-R]	- 0.425	- 0.242	0.196
3 [G-R]	0.197	- 0.136	0.078
4 [R..G-B]	- 0.657	- 0.395	0.587
5 [R.G-B]	0.444	0.484	-0.499
6 [GR-B]	0.030	0.109	-0.082
7 [G.R-B]	- 0.240	- 0.298	0.275
8 [G..R-B]	0.180	0.178	-0.080
9 [B..G-R]	0.174	0.167	0.008
10 [B.G-R]	0.286	0.252	-0.179
11 [GB-R]	0.381	0.058	0.017
12 [G.B-R]	- 0.166	0.309	-0.463
13 [G..B-R]	- 0.494	- 0.087	-0.577

Table 9. Correlations between Image Quality Metrics and Subjective Ratings.

Position Number	MTF Area	MTFA	SQRI
1 [B-G]	- 0.136	0.312	0.921 **
2 [B-R]	- 0.025	- 0.058	0.929 **
3 [G-R]	0.959 **	0.771 *	0.993 **
4 [R..G-B]	- 0.816 **	- 0.933 **	0.940 **
5 [R.G-B]	- 0.837 **	- 0.982 **	0.928 **
6 [GR-B]	- 0.791 *	- 0.987 **	0.933 **
7 [G.R-B]	- 0.701 *	- 0.964 **	0.903 **
8 [G..R-B]	- 0.657	- 0.918 **	0.946 **
9 [B..G-R]	- 0.276	- 0.295	0.992 **
10 [B.G-R]	- 0.306	- 0.397	0.997 **
11 [GB-R]	- 0.367	- 0.511	0.992 **
12 [G.B-R]	- 0.174	- 0.394	0.985 **
13 [G..B-R]	0.075	- 0.243	0.991 **

* $p < 0.05$

** $p < 0.01$

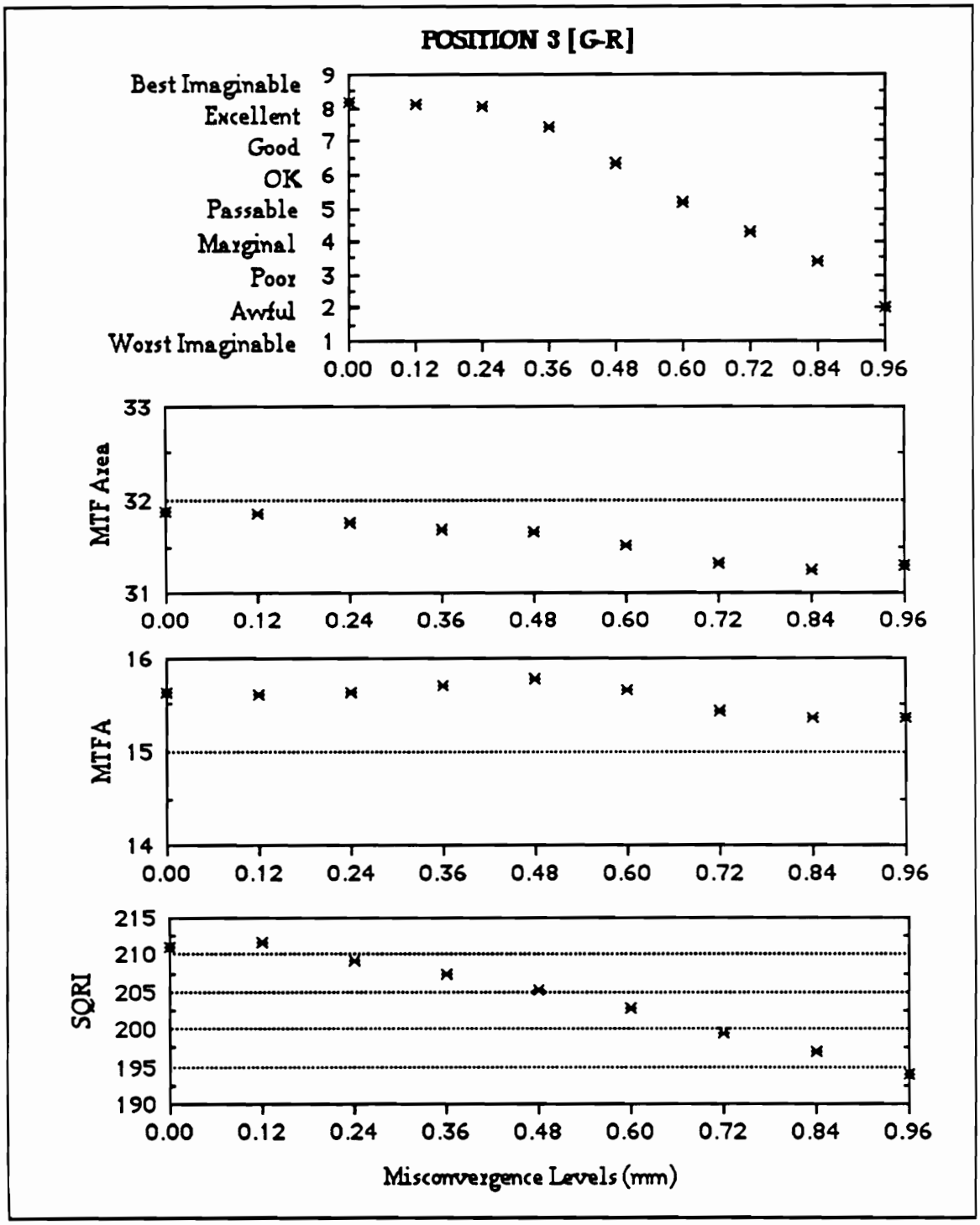

Figure 41. Subjective ratings and MTF Area for Position 3 [G-R] at all levels of Misconvergence.

41) illustrates the expanded range of the data. It further shows that the trends continue, but still can be considered minimal.

Positions 4 to 8 are the "white with blue varying" color combinations. In this group, all correlations, except MTF Area at Position 8, are significant between subjective ratings and the metrics. The results from this group are represented by the data for Position 6 [GR-B] in Figure 42. Notice that, as expected, the direction of correlation is reverse from the significant correlations seen with the detection data (Figure 38). This expanded view reveals the continued trends.

The last group, Positions 9 to 13, are the "white with red varying" color combinations. The correlations are *not* significant between the subjective ratings and the MTF Area and MTFA metrics. However, the SQRI metric continues to be significantly correlated. This group is illustrated with Position 11 [GB-R] in Figure 43.

Once again it can be noted while the correlations between the subjective ratings and the MTF metrics are significant for some positions, the variations are small and the direction is counter to what was expected. No explanation is readily available for this anomaly.

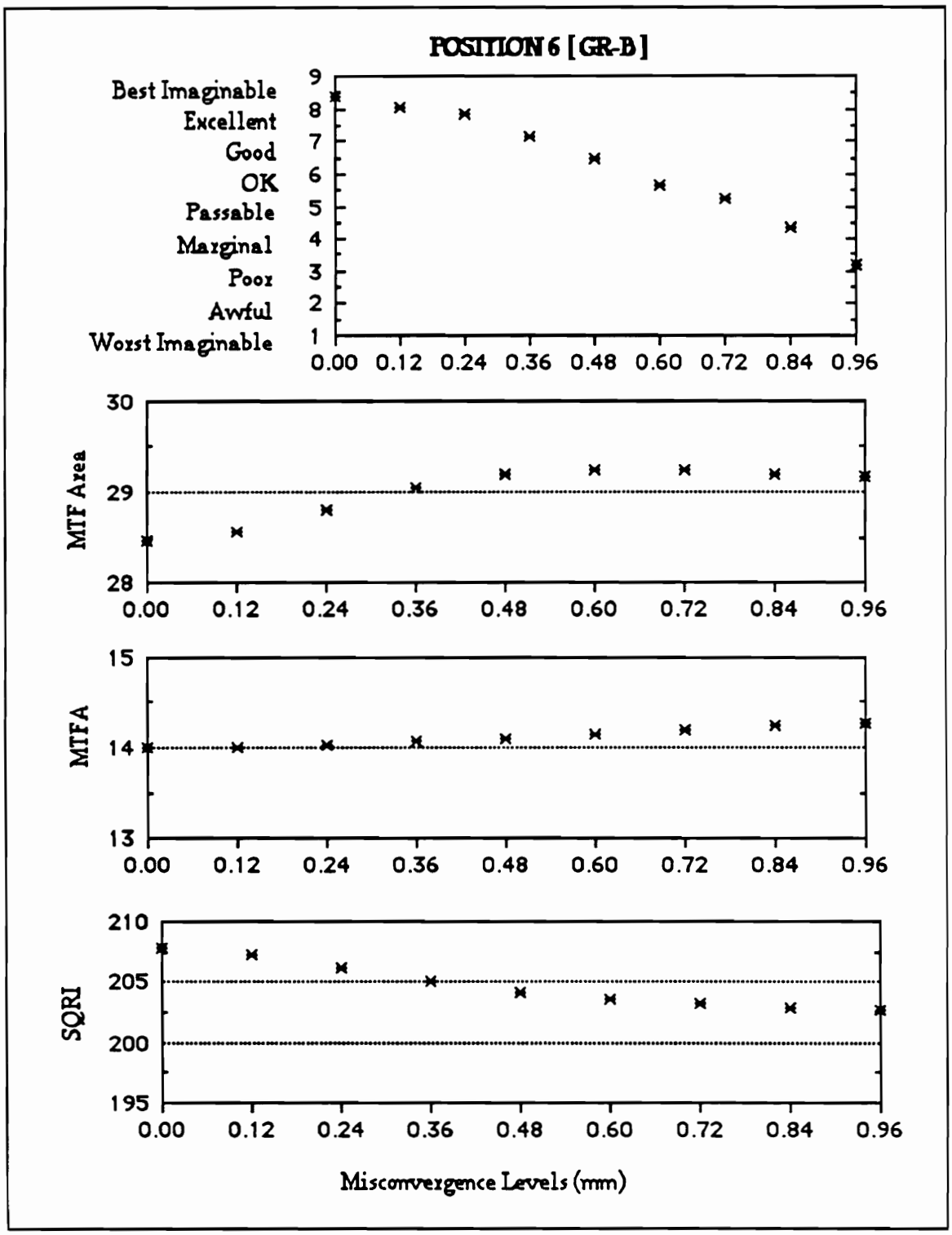

Figure 42. Subjective ratings and the computed metrics for Position 6 [GR-B] at all levels of Misconvergence.

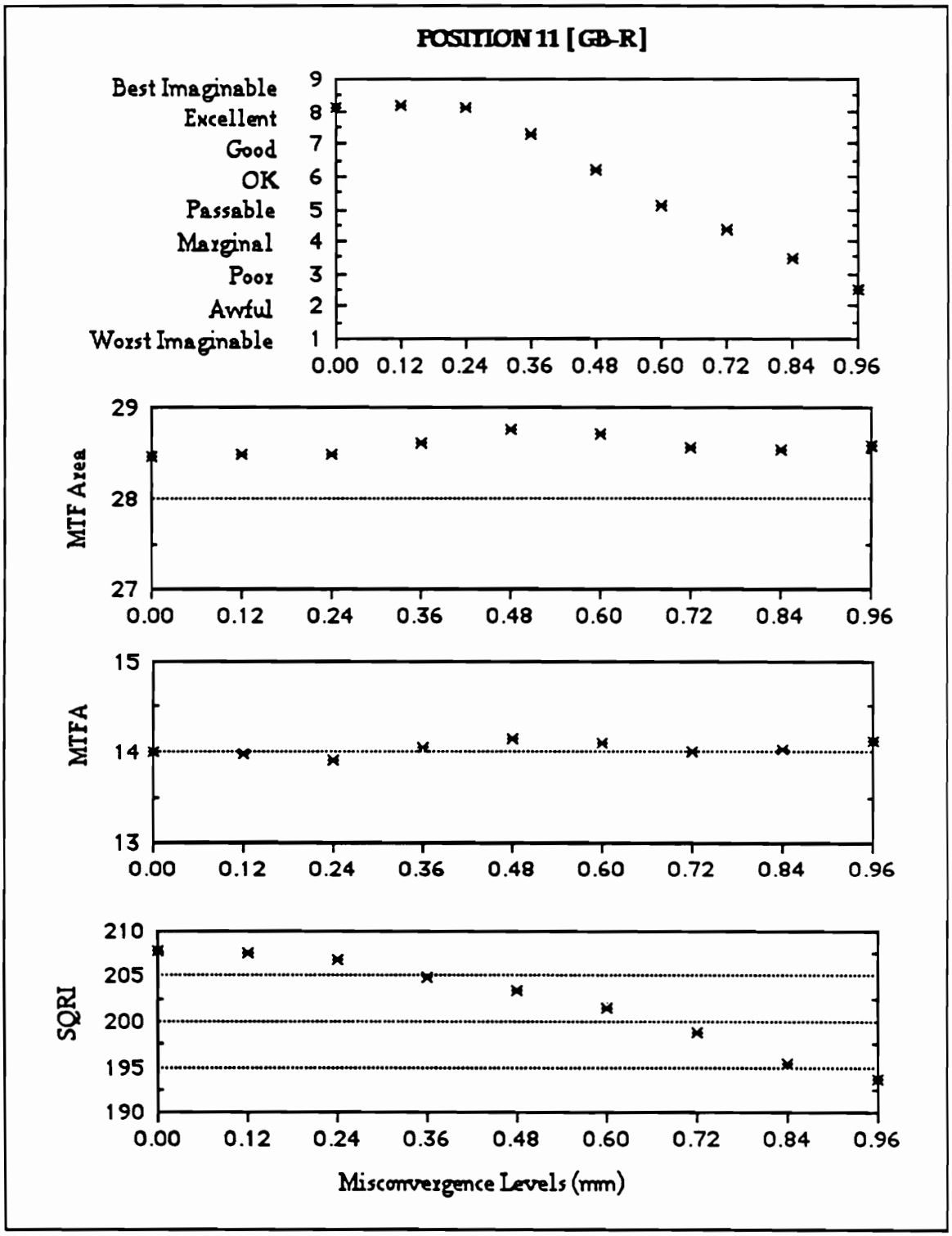

Figure 43. Subjective ratings and the computed metrics for Position 11 [GB-R] at all levels of Misconvergence.

DISCUSSION AND CONCLUSIONS

Comparisons Among Trials

In anticipation of finding varying sensitivities to misconvergence among visual tasks, the three selected tasks ranged from a threshold detection task (expected to be most sensitive to misconvergence) to a reading task (expected to be least sensitive). These expectations were fulfilled. Small differences in misconvergence patterns were significantly identified in the threshold detection task, while the reading task was totally insensitive to even the greatest amounts of misconvergence. The subjective quality ratings were also sensitive to positions and levels of misconvergence, generally as much as the threshold detection task.

Both the threshold detection task and the subjective rating task require the subject to examine and report small detectable differences in misconvergence; thus, responses on these two tasks are significantly correlated: increases in detection probability are correlated with decreases in subjective quality ratings (Table 6). Reading performance, on the other hand, was not significantly affected by Position, Misconvergence, or their combinations (Table 3). Clearly the inherent redundancy in the reading passages and the short duration (average reading time was 6.55 s) makes image quality less important, even though quality ratings for the "worst" misconvergence conditions were rated between "Awful" and "Worst Imaginable." As has been found previously (e.g., Snyder and Maddox, 1978), readability is much less sensitive to image quality degradation than is legibility of individual elements.

The results from the detection tasks are in agreement with past research which has shown that "misconvergence within the range of 1 to 2 arcmin separation between primary color images is required for acceptable color images" (Silverstein and Merrifield, 1985. p. 114). As can be seen by the lower horizontal axis on Figures 19, 20, and 21, these results fall in this range.

However, there are some individual differences with some of the previous research. First, Silverstein and Lepkowski (1986) results found detection threshold at higher levels (i.e., 2.5 to 5.9 arcmin). These higher levels resulted because the visual stimulus used in that study simulated a widening spot profile in the varying beam rather than a displaced profile as used in this study. Therefore, higher levels would be expected due to the continued overlap of the two primary colors.

The results from this study clearly indicate that [R-B] misconvergence is more detectable than [G-R] misconvergence (Figure 19). This finding is opposite to the Merrifield et al. (1979) results which showed that red-green misconvergence was more detectable than red-blue misconvergence. Possible explanations for this reversal lie in the stimulus which was used. Merrifield et al. used a "DH" symbol and presented vertical misconvergence in which the varying color could appear either above or below the stationary color. The present study used a single pixel vertical line and systematically varied horizontal misconvergence by progressing incrementally to the left. Therefore, in Position 3 [G-R], the red gun was varied from the original starting position (to the right of the green), toward the left (toward then past the green) as can be seen in Figures 30 and 32. The positional shift accounts for the lack of detectability at the 0.06 to 0.18 mm Misconvergence levels for the [G-R] combination.

These results are important in that they (1) agree with prior studies of detection of misconvergence, but (2) suggest that mere detection of misconvergence may have little to do with many forms of visual task performance. For safer generalization along these lines, future research should assess the effects of Position and Misconvergence on other typical visual tasks, such as single symbol search, target recognition, and target tracking.

While the threshold detection and subjective rating data appear equally sensitive to the effects of Position and Misconvergence, there are notable differences which limit their correlation (Table 6). For example, the probability of detection results, across levels of

misconvergence, are quite different for magenta [R-B] and yellow [G-R] (Figure 19), yet the subjective rating data for magenta and yellow, while statistically different, are quite similar (Figure 26). Also, the detection thresholds (Figure 20) for the "white with blue varying" color combinations (i.e., Positions 4 to 8) cluster somewhat differently than the subjective ratings for those combinations (Figure 27). A similar comparison can be made between the detection threshold data and subjective ratings for the "white with red varying" color combinations (Figures 21 and 28, respectively). On balance, however, it is striking that essentially three clusters of Position, seen as visual different, were identified: (1) the two-primary combinations, with some differences among them; (2) white with blue varying; and (3) white with red varying. No clues for explanation of this clustering appear to be reasonable from either the CRT Model effort or from an examination of the CRT image itself.

Model Validity

The Color CRT MTF model is geometrically based and mathematically defined to permit calculations using a variety of input variables. The model runs very efficiently, with a calculation time of less than 3 s on a Macintosh IIcx. In its present form, the Color CRT MTF model provides output in three data files. The first data file contains the parametes (Figure 12) used for the model. The second data file gprovies the luminance (cd/m^2) across the scanning distance. The third data file provides the luminance modulation as a function of spatial frequency (e.g., MTF) summed across all three beams. Figure 36 provides an example graph of these data files. Hence, this part of the model met the objectives and expectations.

The second part of the model is to compute MTF-based image quality metrics. As has been seen in the results (Figures 37 to 43), the MTF-based quality metrics (MTF Area, MTFA, and SQRI) have very little variability across the very wide range of misconvergence. That is,

while the luminance distributions of the resulting misconverged spot vary greatly across the Position and Misconvergence levels, the three integrated quality metrics are insensitive to these differences. As a result, the correlations between visual task measures and the model output, while statistically significant, are generally illogical and not useful.

Another noteworthy trend is the tendency for the SQRI metric to be consistently highly correlated with both the detection data and the subjective ratings. While the SQRI metric may appear to predict these data very well, differences in the order of 7 to 10 SQRI units are required for this metric to establish a practical significant just noticeable difference. The computed SQRI values for these data (Figures 37 to 43), however, only vary approximately 3 to 10 SQRI units across the entire range of misconvergence. This result would indicate that the entire range represented approximately one just-noticeable-difference. Clearly, this conclusion does not agree with the detection data which indicate detection will occur within the first quadrant of the full 0.96 mm range of Misconvergence.

One likely explanation for the failure of the model to predict properly the visual task data is that the model integrates *luminance* distributions from the three beams, disregarding chrominance interactions that likely affect visual perception. For example, two widely separated dots (e.g., R and B) are seen by the model as two separate spots, each with high frequency information or well resolved. The visual system, however, finds fault with these resolvable spots in that they do not integrate to form magenta, rather than red and blue separately. Thus, the model accounts for quantitative differences in the CRT image (in the luminance domain), but not qualitative differences (in the chrominance domain).

One reasonable conclusion from these results is that the MTF-based outputs of the model are simply not valid predictions of image quality for misconverged shadow-mask displays. Other metrics of image quality need to be developed and validated for the chrominance domain in which visual integration of chromatically different phosphor points is the key to perceived

image quality rather than simple luminance integration from these same points in the spatial frequency domain. Nonetheless, the formulation of the present model permits a computational facility and ease for calculation of any other quality metric which contain a spatial frequency or spatial distance component. The addition of chromatic weightings or chrominance filter functions to the present model can be accomplished easily to permit testing of other conceptual metrics of shadow-mask CRT image quality.

REFERENCES

Barten, P. G. J. (1984). Resolution of data display tubes. *Proceedings of the Society for Information Display, 25*(1), 35-42.

Barten, P. G. J. (1987). The SQRI method: A new method for the evaluation of visible resolution on a display. *Proceedings of the Society for Information Display, 28*(3), 253-262.

Barten, P. G. J. (1988). Effect of convergence errors on resolution. *Proceedings of the Society for Information Display*, 29(1), 3-5.

Barten, P. G. J. (1989). The square root integral (SQRI): a new metric to describe the effect of various display parameters on perceived image quality. *SPIE - Human vision, visual processing, and digital display, 1077*, 144-151.

Beaton, R. J. (1984). A human-performance based evaluation of quality metrics for hard-copy and soft-copy digital imagin systems. Unpublished doctoral dissertaion, Virginia Polytechnic Instituite and State University, Blacksburg, VA.

Beaton, R. J. (January 1988). Linear systems metrics of image quality for flat-panel displays. *SPIE - Image processing analysis, measurement, and quality, 901*, 144-151.

Benzschawel, T. and Watson, T. J. (1985). Human factors influence effective use of color in information displays. *Information Display, 1*(9), 16-34.

Christ, R. E. (1975). Review and analysis of color-coding research for visual displays. *Human Factors, 17,* 542-570.

Decker, J. J., Pigion, R. D., and Snyder, H. L. (1987). A literature review and experimental plan for research on the display of information on matrix-addressable displays. (Technical Memorandom 4-87). Aberdeen Proving Ground, Maryland: U. S. Army Human Engineering Laboratory.

Feldmann, S. C. (1972). Basic reading rate scale. *Journal of Reading, 15*(6), 451-452.

Feldt, L. S. (1959). Tinker speed of reading test. In O. K. Buros (Ed.) *The fifth mental measurements yearbook* (pp. 780-781). Highland Park, NJ: Gryphon Press.

Gaskill, J. D. (1978). *Linear systems, Fourier transforms, and optics.* New York, NY: Wiley.

Gregorie, T. G., and Driver, B. L. (1987). Analysis of ordinal data to detect population differences. *Psychological Bulletin, 101*(1), 159-165.

Hale, S. L. and Billmayer, H. J. (1988). Use of color CRTs in aircraft cockpits: A literature review. (Technical Note 3-88). Aberdeen Proving Ground, Maryland: U. S. Army Human Engineering Laboratory.

Infante, C. (1984). On the resolution of raster-scanned CRT displays. *SID Seminar Lecture Notes* , Session 2.2b. Playa del Rey, CA: Society for Information Display.

Johnson, N. L. (1949a) Systems of frequency curves generated by methods of translation. *Biometrica, 36,* 149-176.

Johnson, N. L. (1949b) Bivariate distributions based on simple translation systems. *Biometrica, 36,* 297.

Johnson, N. L, and Kotz, S. (1970). *Continuous univariate distributions. Vol 1* . New York, NY: Wiley.

Kendall, M. G., and Stuart, A. (1963). *The advanced theory of statistics. Vol 1. Distribution theory (2nd ed.).* London: Griffin and Company.

Kojima, A. (1983). An analysis of horizontal MTF in color CRTs. *SID 83 Digest of Technical Papers,* 66-67. Playa del Rey, CA: Society for Information Display.

Kubo, T. (1982). Development of high-definition TV displays. *IEEE Transaction on Broadcasting, BC-28* , (2), 51-64.

Matthews, M. L. (1987). The influence of colour on CRT reading performance and subjective comfort under operational conditions. *Applied Ergonomics, 18.4* , 323-328.

Merrifield, R. M. (1987). Visual parameters for color CRTs. In H. J. Durrett (Ed.), *Color and the computer* (pp. 63-81). Boston, MA: Academic Press.

Merrifield, R. M., Haakenstad, L., Ruggiero, F. T., and Lee, J. N. (1979). Electronic flight instrument system (EFIS) misconvergence testing (Technical Report SYST-B-8764-10-79-085). Seattle, WA: Boeing Commercial Airplane Company.

Murch, G. (1987). Color displays and color science. In H. J. Durrett (Ed.) *Color and the computer* (pp. 1-25). Boston, MA: Academic Press.

O'Callaghan, J. P., and Veron, H. (1987). Parametric MTF analysis for shadow-mask CRT monitor configurations. *SID 87 Digest of Technical Papers,* 214-217. Playa del Rey, CA: Society for Information Display.

Park, S. K., Schowengerdt, R., and Kaczynski, M. A. (1984). Modulation-transfer-function analysis for sampled image systems. *Applied Optics,* 23(15), 2572-2582.

Pearson, E. S. and Hartley, H. O.. (1970) *Biometrica tables for statisticians, Vol II.* Cambridge, England: University Press.

Read, C. (Ed.) (1983). *Encyclopedia of statistical science, Vol 3,* (pp. 212-225), New York, NY: Wiley.

Reising, J. M. and Aretz, A. J. (1987). Color computer graphics in military cockpits. In H. J. Durrett (Ed.), *Color and the computer* (pp. 151-169). Boston: Academic Press.

Robertson, P. J., and Jones, M. R. (1984). Subjective reactions to misconvergence on a colour display. *Displays,* 165-169.

Silverstein, L. D. (1987). Human factors for color display systems: Concepts, methods, and research. In H. J. Durrett (Ed.), *Color and the computer* (pp. 27-61). Boston, MA: Academic Press.

Silverstein, L. D., and Lepkowski, J. S. (1986). The perception of color primary spatial distribution in color information displays. *SID 86 Digest of Technical Papers*, 416-419. Playa del Rey, CA: Society for Information Display.

Silverstein, L. D. and Merrifield, R. M. (1985). The development and evaluation of color systems for airborne applications-Phase I: Fundamental visual, perceptual, and display system considerations . (Contract Final Report, Technical Document DOT/FAA/PM-85-19). Federal Aviation Administration and Naval Air Test Center.

Snadowsky, A. M., Rizy, E. F., and Elias, M. F. (1966). Symbol identification as a function of misregistration in color additive displays. *Perceptual and Motor Skills*, 22, 951-960.

Snyder, H. L. (1988). Toward the determination of electronic display image quality. *Advances in Man-Machine Systems Research, Vol 4*, . 1-68.

Snyder, H. L., and Maddox, M. E. (1978). Information transfer from computer-generated dot-matrix displays. Virginia Polytechnic Institute and State University Technical Report for U. S. Army Research Office (TR-78-1).

Tadikamalla, P. U. (1980). On simulating non-normal distributions. *Psychometrika*, 45 (2), pp. 273-279.

Task, H. L. (1979). *An evaluation and comparison of several measures of image quality for television displays.* Wright-Patterson Air Force Base, OH: Report AMRL-TR-79-7.

Veron, H. (1985). The measurement of resolution of shadow-mask CRTs. *Proceedings of the Society for Information Display, 26* (4), 299-303. Playa del Rey, CA: Society for Information Display.

Veron, H., and O'Callaghan, J. P. (1987). A technique for the automated measurement of the resolution of shadow-mask CRT displays. *SID 87 Digest of Technical Papers,* 211-213. Playa del Rey, CA: Society for Information Display.

Walraven, J. (1984). Perceptual artifacts that may interfere with colour coding on visual displays. In C. P. Gibson (Ed.), *Proceedings of the workshop on colour coded vs monochrome electronic displays* (pp. 13.1-13.11). Farnborough, England: Royal Aircraft Establishment.

Weast, R. C. (Ed.) (1978). *CRC handbook of chemistry and physics,* 58th Ed., Cleveland, OH: CRC Press.

APPENDIX A

DERIVATIONS OF MODULATION TRANSFER FUNCTIONS

In discussing the resolution of raster-scanned CRT displays, Infante (1984) defined two general modulation transfer functions, $M_C(u)$ and $M_V(u)$, to represent the contributions of the beam profile and the video amplifier, respectively. These functions include parameters which can be varied to enable one to investigate various display systems. With the assumption that the desired system is "linear enough", the MTF for the total system is expressed as a product of the two component MTFs

$$\text{MTF} = M_C(u) \text{ and } M_V(u) . \tag{A-1}$$

Following are the derivations of these two functions as presented by Infante. However, it should be noted that the expression for the Gaussian distribution (equation A-6) has been altered from the original publication to include a "2" which was omitted from the denominator. While this omission does affect the expression for the transform when expressed as a function of "σ" (equation A-11), it does *not* impact the end result (equation A-14) used in the published paper.

MTF of the Monochrome CRT ($M_C(u)$)

The modulation transfer function (MTF) for a monochrome CRT with a spot profile f (x) is expressed as

$$M(\omega) = | F(\omega) | \tag{A-2}$$

where F (ω) is the Fourier transform of f (x) and ω is 2 π times the spatial frequency (u) in cycles per arcminute. F (ω) is derived as follows

$$F(\omega) = \int_{-\infty}^{+\infty} f(x) \exp(-i\omega x)\, dx \tag{A-3}$$

$$F(\omega) = \int_{-\infty}^{+\infty} f(x) \cos(\omega x)\, dx + i \int_{-\infty}^{+\infty} f(x) \sin(\omega x)\, dx . \tag{A-4}$$

Since f (x) is an even function while cos (ω x) and sin (ω x) are even and odd functions, respectively, equation A-4 can be rewritten as

$$F(\omega) = \int_{0}^{+\infty} 2 f(x) \cos(\omega x)\, dx . \tag{A-5}$$

The spot profile f (x) is assumed to be a Gaussian distribution, therefore it can be expressed in a normalized form as

$$f(x) = \exp\left(\frac{-x^2}{2\sigma^2}\right). \tag{A-6}$$

Hence, the final expression for the Fourier transform of f (x) is

$$F(\omega) = \int_{0}^{+\infty} 2 \exp\left(\frac{-x^2}{2\sigma^2}\right) \cos(\omega x)\, dx . \tag{A-7}$$

It is noted that this standard integral expression (CRC, 1978) is evaluated as

$$\int_{0}^{+\infty} \exp(-a^2 x^2) \cos(b x)\, dx = \frac{\sqrt{\pi}}{2a} \exp\frac{-b^2}{4a^2} . \tag{A-8}$$

Substitutions for "a" and "b" are obtained from equation A-7 with the following result

$$F(\omega) = \sigma\sqrt{2\pi}\, \exp\left[\frac{-\sigma^2 \omega^2}{2}\right] dx \tag{A-9}$$

or

$$M(\omega) = |F(\omega)| = \sigma\sqrt{2\pi}\, \exp\left[\frac{-\sigma^2 \omega^2}{2}\right] dx . \tag{A-10}$$

Normalizing equation A-10 so that M (0) = 1 and expressing ω in terms of spatial frequency (i.e., $\omega = 2\pi u$) results in

$$M(u) = \exp\left[-2\pi\ \sigma^2\ u^2\right]. \tag{A-11}$$

This expression is valid for any Gaussian spot profile with a standard deviation of σ. Equation A-11 can further be expressed in terms of a spot profile defined as S = the full width at half of the maximum values. By this definition

$$S = f(x) = \exp\left(\frac{-x^2}{2\sigma^2}\right) = \frac{1}{2} \tag{A-12}$$

the relationship between the spot width (S) and the standard deviation (σ) is

$$\sigma = \frac{S}{2\sqrt{2\ln 2}}\ . \tag{A-13}$$

By substituting this value into equation A-8, one can express the modulation transfer function of the Gaussian spot profile as

$$M_c(u) = \exp\left(-\frac{\pi^2}{4\ln 2}\ S^2\ u^2\right) = \exp\left(-3.560\ \ S^2\ u^2\right) \tag{A-14}$$

where S is the beam diameter measured between the 50% points, and u is the spatial frequency in cycles per arcminute. This portion of the overall MTF can be evaluated for various spot sizes across the spatial frequency.

MTF of the Video Amplifier ($M_v(u)$)

If G (f) is the gain of the system in terms of the video frequency, in cycles per unit time, and u is the spatial frequency, the modulation transfer function for the video portion of the CRT system can be expressed as

$$M_v(u) = G[\,f(\,u\,)\,] \tag{A-15}$$

which is normalized so that M (0) = G (0) = 1. The frequency response of most amplifiers can be approximated with a simple two-pole transfer function stage with a given amount of peaking. Therefore, the amplifier's gain is given by

$$\left| G(f) \right| = \frac{1}{\sqrt{\left(1 - \left\{\frac{f}{f_o}\right\}^2\right)^2 + \left(2\zeta \frac{f}{f_o}\right)^2}} \qquad \text{(A-16)}$$

where f_o is the normalized bandwidth and ζ is the damping factor. With this expression, the effect of the video amplifier can be examined.

APPENDIX B

FAMILIES OF DISTRIBUTIONS

The normal, or Gaussian, distribution has played a dominant role in both theoretical and applied statistics since the time of Laplace. It was soon evident that the normal curve could not provide an adequate representation for the many distributions occurring in observational data. "Toward the end of the nineteenth century attempts were made to construct systems of frequency curves which should be capable of representing a wider variety of distributions" (Johnson, 1949a, p.149). One of the most successful systems was constructed by Karl Pearson in 1895. Further work published by Johnson in 1949 proposed an alternative system which employed the method of translation to transform variables into approximate normal variates.

Pearson System

Karl Pearson (Kendall and Stuart, 1963, pp. 148-156) developed a family of curves to represent a wide variety of possible distributions. Each member of the system has a probability density function p(x) which satisfies a differential equation of the form

$$\frac{1}{p}\frac{dp}{dx} = -\frac{(a + x)}{(c_0 + c_1x + c_2x^2)} . \qquad \text{(B-1)}$$

The shape of the distribution depends on the values of the four parameters: a, c_0, c_1, and c_2. The distributions are grouped into various "Types." Figure B-1 is a beta plane where the abscissa is β_1, a measure of the skewness of a distribution which is defined as

$$\beta_1 = \frac{\mu_3^2}{\mu_2^3} \qquad \text{(B-2)}$$

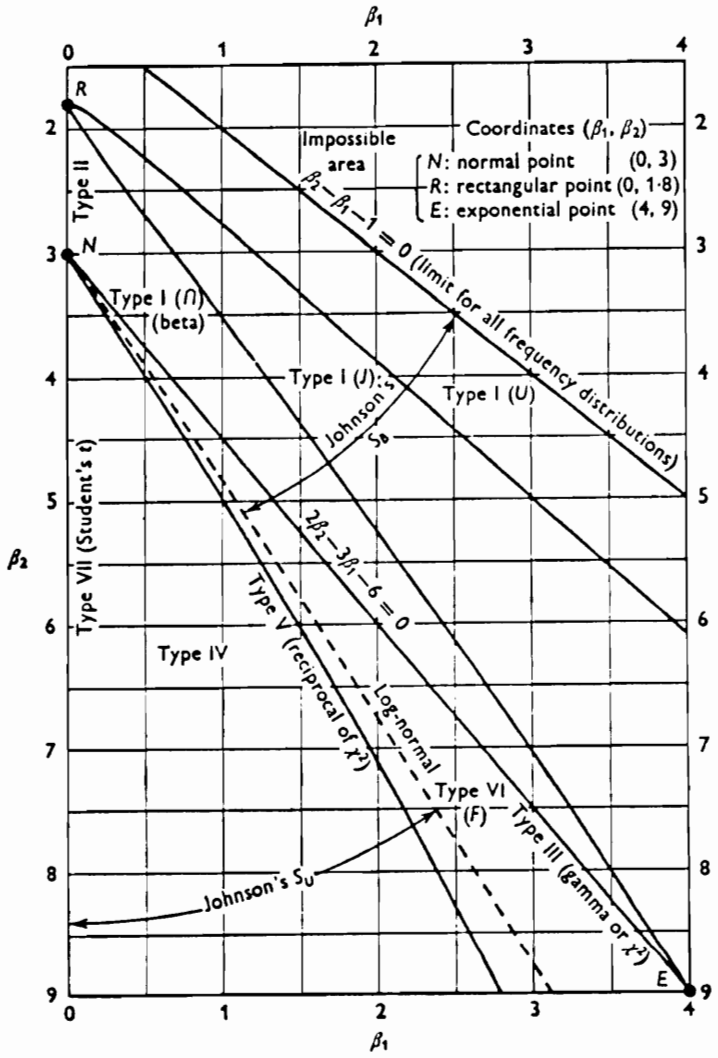

Figure B-1. Beta plane with major members of the Pearsonian and Johnson systems of distributions indicated. (Source: Pearson and Hartley, 1970, p. 78)

where μ_3^2 is the square of the third central moment of the distribution, and μ_2^3 is the cube of the second central moment. The ordinate of the beta plane is β_2, a measure of the kurtosis of a distribution which is defined as

$$\beta_2 = \frac{\mu_4}{\mu_2^2} \tag{B-2}$$

which is the ratio of the fourth central moment to the square of the second central moment. This type of beta plane is useful for comparison between families of distributions. The major members of the Pearson family of distributions can be located on Figure B-1 and are identified as follows:

Type I	(Beta distribution of the first kind)
Type II	(symmetrical form of Type I)
Type III	(Gamma distribution)
Type IV	(no common statistical distributions of this type)
Type V	(reciprocal of χ^2)
Type VI	(Beta distribution of the second kind)
Type VII	(Central t-distribution)

To model observational data with a Pearsonian distribution, the first four moments of the data set are calculated, providing observed values for β_1 and β_2 and Pearson's k criterion. This information is then combined and used to select an appropriate distribution Type. Following the Type selection, the four parameters (a, c_0, c_1, and c_2) are estimated with specified formulae and a mathematical expression is written to represent the distribution of the observational data.

While the Pearson family of distributions is of interest, its application is limited. Kendall and Stuart (1969, p. 152) summarized the usage of this system by stating "it has been found that Pearson distributions sometimes give a good representation of observational data.

Apart from this, they (and in particular Types I and III) are sometimes useful in approximation to theoretical distributions form their known moments." Because of the wide variety of distribution Types and expressions, the use of the Pearson system in simulation studies is limited (Tadikamalla, 1980).

Johnson System

In light of the important position occupied by the normal curve, it was natural to consider the possibility of relating observed distributions to the standard normal form. Johnson (1949a) employed the method of translation to transform variables into approximate normal variates. He defined a general function of the observed variable, f(x), which translated it to z, a unit normal variable. This is formally written as:

$$z = f(x). \tag{B-2}$$

Normal theory, therefore, can be applied to the transformed variable. In order to obtain a system of curves analogous to the Pearson system, Johnson defined three simple f(x) functions, each specified with four parameters (γ, δ, ζ, and λ) as follows:

$$z = \gamma + \delta f\left[\left(x - \zeta\right) / \lambda\right]. \tag{B-3}$$

The parameters γ and δ determine the shape of the distribution, while λ provides a scale factor and ζ provides a location factor. Since the parameters λ and ζ affect the distribution in a straightforward manner, attention is concentrated on the relationship between γ and δ and the distribution of x. A common practice is to express equation (B-3) as:

$$z = \gamma + \delta f(y) \tag{B-4}$$

$$\text{where} \quad y = \left(x - \zeta\right) / \lambda$$

Three general functions are defined in the Johnson system of distributions to cover the same area of the beta plane as does the Pearson distributions. Johnson defined his three systems are as follows:

(1) S_L -- the "log-normal" system, where $f(y) = \ln(y)$. This is the most common transformation and has proved useful in a number of applications. However, the system has limited flexibility and is restricted to specific values of β_1 and β_2, that is, to lie on the dotted-line on the beta plane.

(2) S_U -- the "unbounded" system, where $f(y) = \sinh^{-1}(y)$. This system is unbounded in the extremities and covers the area below the "log-normal" system on the beta plane. Therefore, all of the members of this system of distributions are leptokurtic.

(3) S_B -- the "bounded" system, where $f(y) = \ln\left(\frac{y}{(1-y)}\right)$. This system is bounded in both extremities ($0 < y < 1$) or ($\zeta < x < \zeta + \lambda$) and lies within the area above the "log-normal" system on the beta plane but below the limiting line for all distributions ($\beta_2 - \beta_1 - 1 = 0$).

As noted, the Johnson "bounded" system (S_B) takes the X variable of interest, ranging from ζ to $\zeta+\lambda$, scales it into a Y variable ranging from 0 to 1, and translates it into a z variable, a standard normal, as follows:

$$z = \gamma + \delta \ln\left(\frac{y}{(1-y)}\right) \qquad \text{(B-5)}$$

where $y = (x - \zeta) / \lambda$. This relationship is used to illustrate the translation method in a diagram prepared by Johnson (1949a) and reproduced as Figure B-2. Note that this figure includes Johnson's explanation of the process.

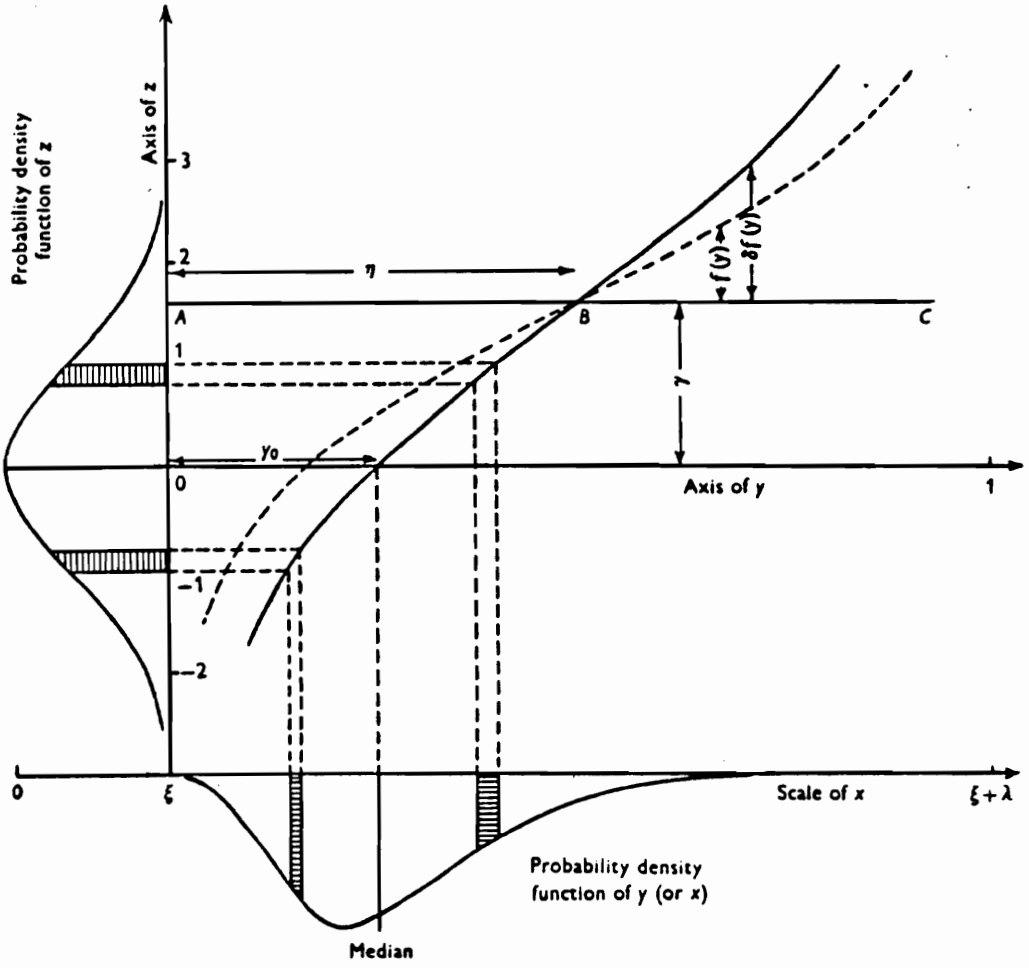

Figure B-2. General properties of the translation system used in the Johnson system. Relative to the baseline ABC, the dotted curve has been plotted with ordinate f(y) and abscissa y such that $f(y) = \ln\left[\frac{y}{(1-y)}\right]$. The baseline ABC is parallel to and a distance γ from the "axis of y". For the solid line curve the ordinates, measured from ABC, have been multiplied by δ. As a result, when referred to the axis of y and z, the solid line curve represents the functional relationship between y and z. (Source: Johnson, 1949a, p. 153).

Application of the Johnson System

To use this translation system to express the beam profile, one must first express the system in terms of its probability density function. This approach will provide the basic shape of the distribution and can be appropriately scaled to the desired amplitude. The expression for the basic density functions in Johnson translation system is given as:

$$f(y) = \frac{1}{\sqrt{2\pi}} \exp\left(-\frac{1}{2}\left\{\gamma + \delta\, g(y)\right\}^2\right) \delta\, g'(y) \qquad \text{(B-6)}$$

where the functions $g(y)$ and $g'(y)$ are defined for each of the three systems, as follows:

Bounded System (for $0 < y < 1$):

$$g(y) = \ln\left(\frac{y}{(1-y)}\right) \quad \text{and} \quad g'(y) = \frac{1}{[\,y\,(1-y)\,]} \qquad \text{(B-7)}$$

Lognormal System (for $0 \le y \le \infty$):

$$g(y) = \ln(y) \quad \text{and} \quad g'(y) = \frac{1}{y} \qquad \text{(B-8)}$$

Unbounded System (for $-\infty \le y \le \infty$):

$$g(y) = \ln\left(y + \sqrt{y^2 + 1}\right) \quad \text{and} \quad g'(y) = \frac{1}{\sqrt{y^2 + 1}}. \qquad \text{(B-9)}$$

These relationships between the non-normal variate, i.e., X scaled to Y, and the normal variate, Z, provide the ability to determine the bounds within which a given proportion of the non-normal variate will lie. For example, the values of X at which the spot profile has reached 50% of its maximum height are determined by working backwards from the value of p(z) which is 50% of its maximum ordinate (i.e., 50% of 0.3989). The resulting values of Y are associated with that particular curve (i.e., for a given γ and δ) and can then be translated backed to the original X scale. These 50% values are included in the data base for each of the distributions being used.

APPENDIX C

SHADOW-MASK / PHOSPHOR-DOT FILTER

The sampling filter used in the modulation transfer model for a color CRT was created to represent the combined shadow mask and phosphor dot structure. The expression was developed from the general equation for a circle. Other parameters were included to expand the general equation into an expression for the combined structure.

Basic Formulation

First, consider the basic element in the shadow-mask phosphor dot structure. This can be expressed as a circle centered at (0,0) using a (x*,y*) coordinate system in which "x*" and "y*" describe horizontal and vertical distances, respectively (see Figure C-1a). To represent the beam energy which will pass through this circle, the function f(x*, y*) will take on the value of 1 within the circle to indicate all incident beam energy is transmitted through the aperture, and a value of 0 outside the circle to represent the blocking effect such that

$$f(x^*,y^*) = \begin{cases} 1 \text{ for } \begin{cases} -r < y^* < r \text{ and} \\ -\sqrt{r^2-y^{*2}} < x^* < \sqrt{r^2-y^{*2}} \end{cases} \\ 0 \text{ otherwise} \end{cases} \qquad \text{(C-1)}$$

If the shadow-mask structure included only one aperture or the phosphor screen contained only one dot, the sampling effect provided by this function would be adequate. However, the complex nature of the phosphor dot screen and the shadow-mask structure must be described together to obtain an adequate representation.

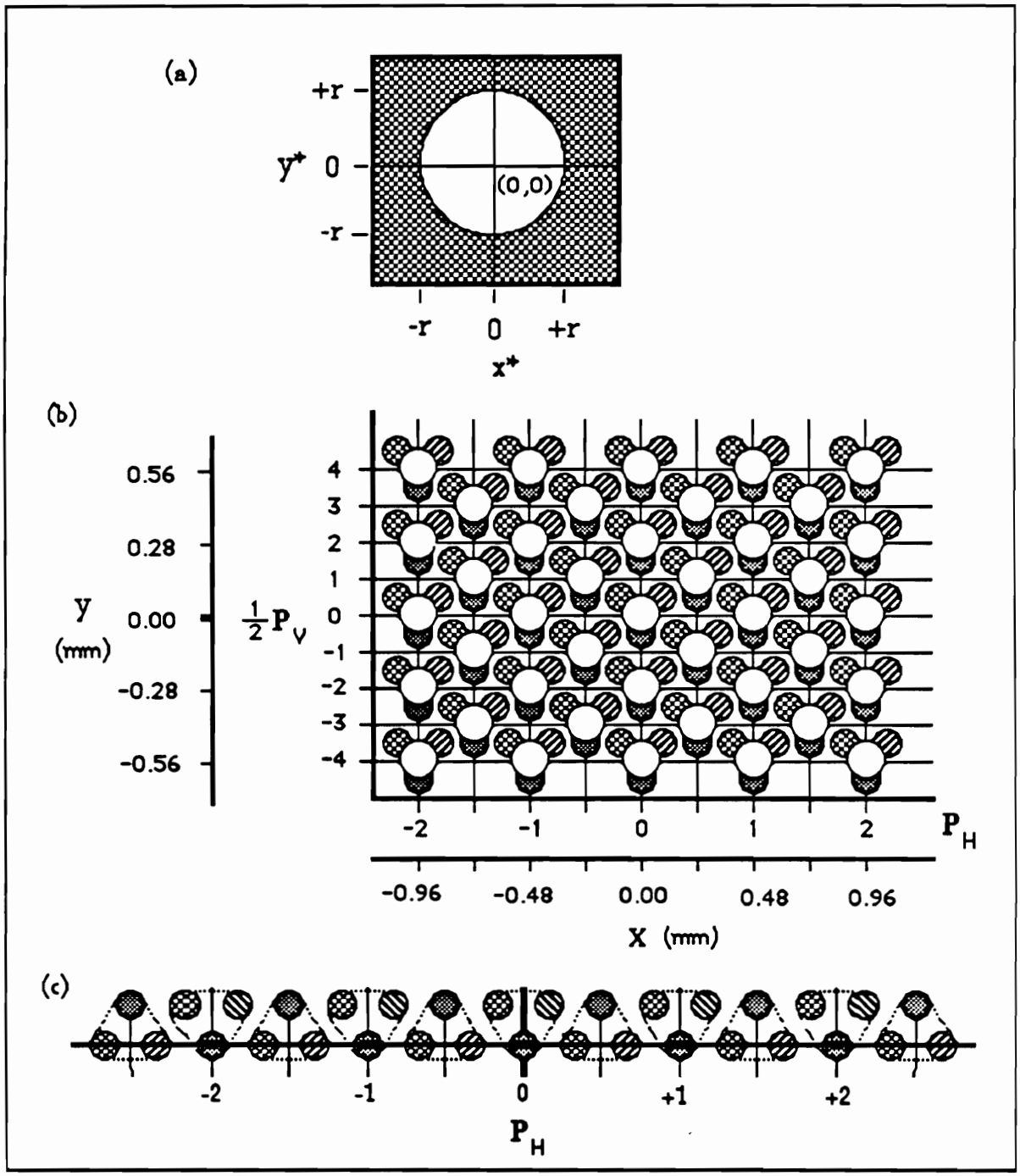

Figure C-1. Examples of the phosphor-dot and shadow-mask structures of a color CRT.

Phosphor Dot and Shadow-Mask Structure

The screen of a color CRT is coated with red, blue, and green phosphor dots, arranged in a standard delta triad configuration (refer back to Figure 9). In this delta configuration, phosphor dots of any one primary color are arranged in an equilateral hexagon pattern. The overall pattern is described by the vertical pitch (P_V), which is the vertical separation between consecutive phosphor dots of the same color. The horizontal pitch (P_H) is the distance between consecutive phosphor dots of the same color in the horizontal direction. The vertical pitch is generally specified, and the horizontal pitch is derived from it as follows:

$$P_H = \sqrt{3}\, P_V \tag{C-2}$$

The apertures of the shadow-mask are aligned with the phosphor dot triads and designed to direct each of the three electron beams toward its specific phosphor dot. Thus, the shadow mask allows beam energy to pass through the aperture (each at a different angle) and excite only the appropriate phosphor dot. This shadow-mask structure can be described with the inclusion of two indices as follows

$$\begin{aligned} X &= x^* + n\, P_H \\ y &= y^* + m\, P_V \end{aligned} \quad \text{where} \quad \begin{cases} n = 0, \pm1, \pm2, \ldots & \text{for } -r < x^* < r \\ m = 0, \pm1, \pm2, \ldots & \text{for } -r < y^* < r \end{cases} \tag{C-3}$$

The first index "n" references the horizontal distance "x" across the display and takes on integer values (i.e., n = 0, ±1, ±2, ...). Similarly, the second index "m" references "y", the vertical distance, and only takes on integer values (i.e., m = 0, ±1, ±2, ...) to reference one-half steps in the vertical pitch. An example of this referencing system is presented as Figure C-1b.

Shadow-Mask Filter

A two-dimensional filter, f(x,y), can be described for the sampling effect of the shadow-mask as follows

$$f(x,y)=\begin{cases}1 \text{ for } \begin{cases} mP_V - r_m < y < mP_V + r_m \text{ and} \\ nP_H + k - \sqrt{r_m^2-(y-mP_V)^2} < X < nP_H + k + \sqrt{r_m^2-(y-mP_V)^2} \end{cases} \\ 0 \text{ otherwise}\end{cases} \quad \text{(C-4)}$$

where x and y are the horizontal and vertical distances across the display, respectively. P_V is the vertical pitch of the display, n and m are integer values (i.e., 0 ±1, ±2, etc.), k is a shift variable which equal $\frac{1}{2}P_H$ when $(-1)^m$ is negative and 0 otherwise. $P_H = \sqrt{3}\,P_V$ is the horizontal pitch of the display, andr is the radius of a shadow-mask aperture. The horizontal and vertical dimensions (in mm) of the screen area to be sampled can be expressed in terms of the sampling function of a single aperture, f(x*,y*) and the number of sampled apertures, that is, n P_H and m P_V. The function f(x,y) requires information only about the vertical pitch (P_V) of the display system under investigation and the radius (r_m) of the shadow-mask aperture. Notice that this filter describes the sampling effect of the SM apertures only. Therefore, when an electron beam falls upon one aperture, the function indicates that all three phosphor dots are excited. This may be sufficient for a converged white spot, but it does not allow each of the primary beams to be independently sampled.

Phosphor-Row Filter

The sampling effect from a single row of phosphor dots (Figure C-1c) can be represented as

$$f(x,y)=\begin{cases}1 \text{ for } \begin{cases} -r_p < y < r_p \text{ and} \\ -\sqrt{r_p^2-y^2} < [x + nP_H + h] < \sqrt{r_p^2-y^2} \end{cases} \\ 0 \text{ otherwise}\end{cases} \quad \text{(C-5)}$$

where h = 0 for the green beam, $\frac{-1}{3}P_H$ for the red beam, and $\frac{+1}{3}P_H$ for the blue beam. This effect can be a one-dimensional function by specifying a specific "y" value, for example, centered at the widest part, for each of the three primary beams. This function alone is

obviously not sufficient to describe the desired sampling effect because two phosphor rows are addressed by one aperture row.

Shadow-Mask-Phosphor Filter

Incorporating the features of both the Shadow-Mask Filter and the Phosphor-Row Filter yields a combined Shadow-Mask-Phosphor Filter. The mathematical expression for this filter is as follows

$$f(x,y) = \begin{cases} 1 \text{ for } \begin{cases} -r < \left[y + m P_V + k\right] < r \text{ and} \\ -\sqrt{r^2 - (y + m P_V + k)^2} \\ \qquad < \left[x + n P_H + h\right] < \\ \qquad\qquad \sqrt{r^2 - (y + m P_V + k)^2} \end{cases} \\ 0 \text{ otherwise} \end{cases} \tag{C-6}$$

where h = 0 for the green beam, $\frac{-1}{3} P_H$ for the red beam, and $\frac{+1}{3} P_H$ for the blue beam. The value of p is equal to $|n|$ for the read and blue beams and $|n+1|$ for the green beam. The value of p is used to provide alternate signs for "k" in the expression

$$k = (-1)^p \frac{1}{4} P_V. \tag{C-7}$$

In the model, each primary beam is sampled independently with this function. The three results are then summed to produce the total effect of the three primary beams and the CRT structure.

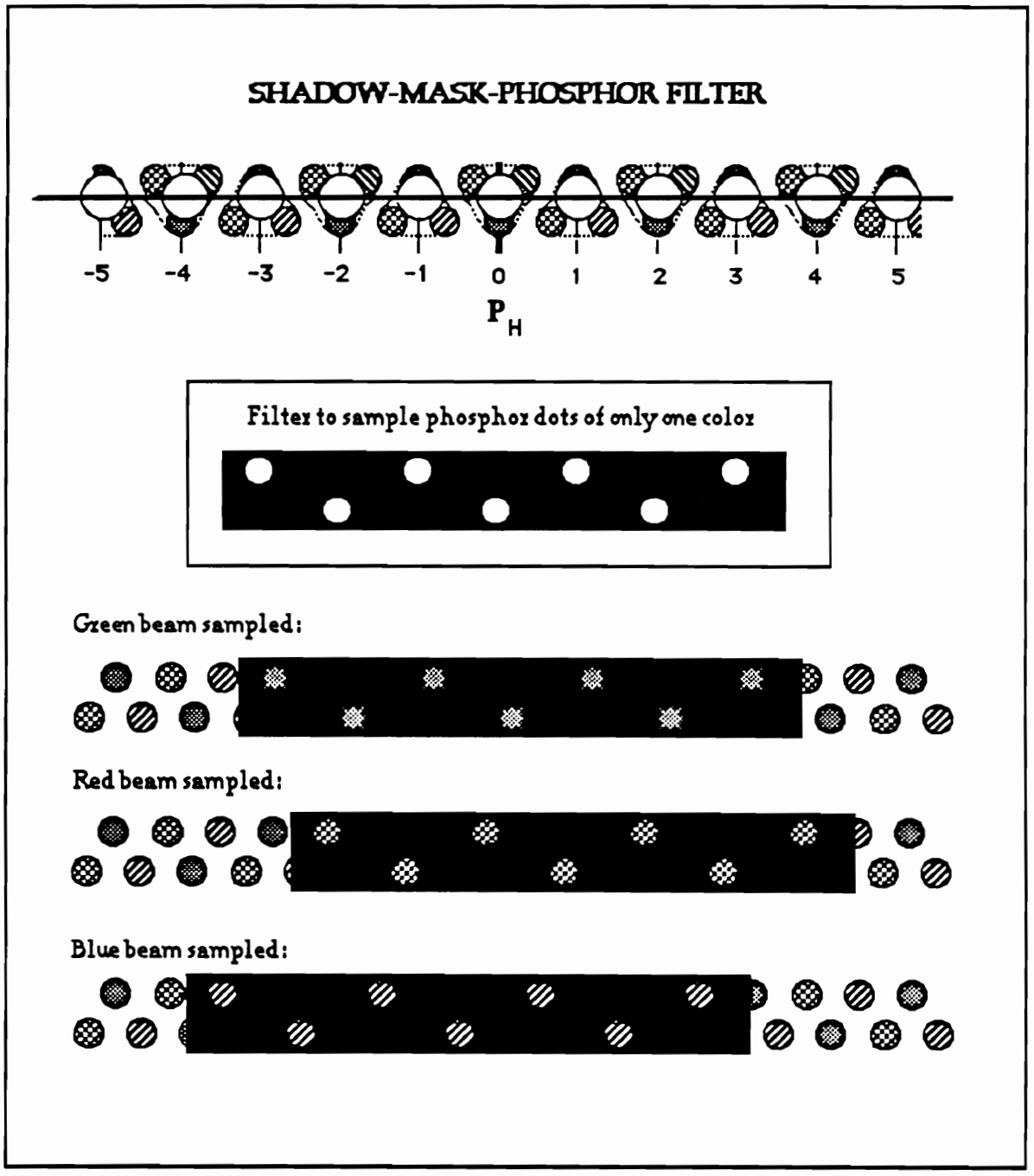

Figure C-2. Illustration of the effect of the combined filter in sampling one beam at a time.

VITA

Carita Allene DeVilbiss

Carita Allene DeVilbiss was born in Jennings, Louisiana, on February 10, 1945. She obtained her B. S. in psychology from Lamar University, Beaumont, Texas, in May 1977. Following that she attended Southern Methodist University in Dallas, Texas, and obtained an M. S. in statistics. Upon completion of this degree, she began work as a civilian member of the United States Air Force with the Air Force Management Engineering Agency, Randolph AFB, Texas, where she worked with the Technical Guidance branch for management engineering teams throughout the Air Force. In July, 1982, she transferred to a position as a consulting statistician at the School of Aerospace Medicine at Brooks AFB, Texas, where she provided statistical guidance to researchers and taught introductory computer courses. In May, 1984, she was promoted to a program analyst position in the Commanders Action Group of the Human Systems Division where she provided support for the Commander.

In August, 1987, Carita began her academic studies at Virginia Polytechnic Institute and State University, Blacksburg, Virginia, with Air Force support for her long-term full-time training program. For her dissertation, she develop an analytic model for the luminance distribution from a color CRT and collected human performance data for the detection of misconvergence on a color CRT, the performance of a visual task under varying levels of misconvergence, and subjective evaluation of image quality. Upon completion of her dissertation, she will be assigned as a research psychologist to the Operations Training Division of the USAF Human Resources Laboratory at Williams AFB, Arizona.

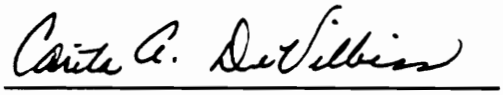

Carita A. DeVilbiss